12-2022

Development of a Tissue Engineered Cardiac Patch

Howard Herbert
hdherbe@g.clemson.edu

DEVELOPMENT OF A TISSUE ENGINEERED CARDIAC PATCH

A Dissertation
Presented to
the Graduate School of
Clemson University

In Partial Fulfillment
of the Requirements for the Degree
Doctor of Philosophy
Bioengineering

---

by
Howard D Herbert IV
December 2022

Accepted by:
Agneta Simionescu, Ph.D., Committee Chair
Dan Simionescu, Ph.D.
Jeremy Mercuri, Ph.D
Christopher Wright, M.D.

Abstract

Cardiovascular Disease(CVD) is the leading cause of mortality in the developed world. CVD is most commmonly manifested as atherosclerosis of the coronary arteries leading to Myocardial Infarction(MI). After MI, fibrosis of the ventricular wall leads to heart failure(HF), a pandemic affecting 26 million people globally. Whille therapies are continuoully developed to combat HF, the treatment of choice, whole heart transplamt, is limited by the availability of donor hearts. It is clear that there is a need to develop a long term solution to combat HF and its enormous economic burden. Tissue Engineerig and Regnerative Medicine holds promise as possible solution by the developemt of cardiac grafts capable of retunring the function lost from MI.

Current efforts in the development of cardiac tissues have been plagued by inability to generate tissues of sufficient thickness(>100μm) or contractility of mature tissue, resulting in low engraftnent rates or lacking in efficacy. This leads to the focus of this research being the generation of a thick vascularized cardiac patch capable of long term survival.

First we decelled whole porcine hearts for the production of ventricular flap and myocardial scaffolds. Scaffolds showed now evidence of retained cellular content or DNA, but retained key characteristics of the extracellular matrix and maintained the same mechanical properties as native tissue. We then performed a combined cell seeding to reendothelialize the vasculature of the ventricle wall and repopulate the myocardium. Finally we developed a custom perfusion electromechanical bioreactor for the purpose of conditioning and maitainting the viability of our patch long term.

We expect that this research will result in the developmetn of cardiac grafts with long term implications of a therapy to solve MI related HF.

Dedication

To my Family and Friends

Acknowledgement

I would like to acknowledge my advisor and Committee Chair, Agneta Simionescu PhD, without whose patience, support, and guidance I would not have reached this goal. To the rest of my committee, Dan Simionescu PhD, Chris Wright MD, and Jermery Mercuri PhD for the aid and support in and out of this project. To all my former and current lab members, especially Spencer Marsh PhD, Bethany Lefeber PhD, and Collin Owens PhD. To the support of all the technical staff at Clemson Bioengineering including Cassie Gregory, Trish Nigro, Maria Torres and many more. To Snow Creek Meat Processing for the constant supply of fresh hearts. Finally, to my mother, Teresa, father, Howie, for the constant and unwavering support, my sisters, Katie and Sally, for breeding a mostly healthy competitive spirit, and all my close friends, especially Benjamin Levy, MD, whose friendship of the last 12 years has helped mold me into the man I am today, and Cason Collins who gave me and job, a place to live, and a nice kick in the pants to get back into school.

Table of Contents

List of Figures

List of Abbreviations

Cardiomyocyte (CM)

Sino Atrial (SA)

Adenosine triphosphate (ATP)

Matrix-metalloproteinases (MMP)

α-smooth muscle actin(α-SMA)

Cardiac Fibroblast (CFs)

Extracellular matrix (ECM)

Damage-associated particles (DAMPs)

Coronary artery disease (CAD)

Finite element analysis (FEA)

Reperfusion injury (RI)

Myocardial Infarction (MI)

Heart Failure (HF)

Induced pluripotent stem cells (iPSC)

Cardiac Troponin (cTnT)

Myosin Heavy Chain (MHC)

Connexin 43 (CX-43)

Endothelial Cell (EC)

Platelet and endothelial cell adhesion molecule-1 (CD31)

Beta integrin 1 (β-int)

Immunohistochemistry (IHC)

Immunofluorescence (IF)

Decellularize/decellularization (decell)

Sodium Dodecyl Sulfate (SDS)

Phosphate Buffered Saline (PBS)

Tris Buffered Saline (TBS)

Left Ventricular Assist Device (LVAD)

Chapter 1: Review of the Literature

1.1.1 Cardiac Anatomy and Physiology

The human heart is a complex muscular blood pump characterized by its four main chambers capable of contractions approximately every second for an entire lifetime.[1] The mammalian heart is divided into two sides, the left, and the right, with each side having an atrial and ventricular chamber. De-oxygenated blood flows from the superior and inferior vena cava into the right atrium. During atrial systole, the blood flows through the tricuspid valve into the right ventricle, where it is ejected through the pulmonary valve into the pulmonary artery. Oxygenated blood returns to the left side of the heart via the pulmonary vein, which flows from the left atrium through the mitral valve into the left ventricle and out to the aorta via the aortic

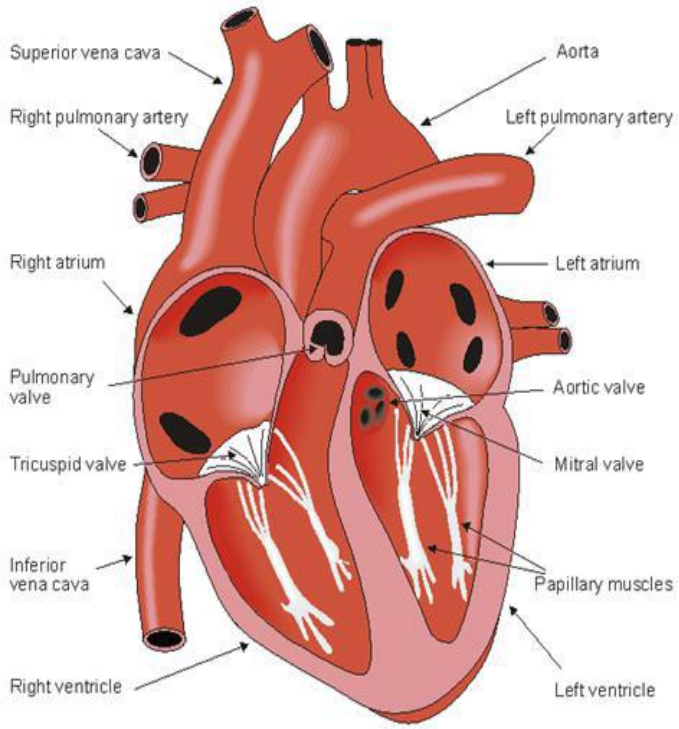

Figure 1-1: The gross anatomy of the human heart.
Malmivuo, et al. Bioelectromagnetism: principles and applications of bioelectric and biomagnetic fields. Oxford University Press, USA, 1995.

valve (**FIG 1.1)**. The pressure produced in each ventricle is approximately 20mmHG in the right and 120mmHg in the left for healthy organs, but under hypertensive conditions, this peak pressure will be elevated.[2] This pressure difference is signified by the requirements of each ventricle to allow blood flow to complete its respective circuit. The right ventricular pressure is only required to complete flow through the lungs and return to the heart. In contrast, the left ventricular pressure is more significant to accommodate the complete perfusion of blood to the cranium and outer extremities. Because of these pressure differences, the thickness of the cardiac muscle varies in each chamber. The right ventricular wall thickness is approximately 3-5mm thick, while the left ventricle can be 7-9mm thick under normal conditions.[3, 4]

The heart is found posterior to the sternum in the chest cavity encased by the pericardium, a fibrous sac that secretes a serous fluid. The pericardial sac serves to protect the heart via immersion in the low friction serous fluid. The ventricular wall is composed of three main layers, the epicardium, myocardium, and endocardium.[5] The epicardium comprises thin mesothelium in contact with the serous fluid of the pericardium. The epicardial layer contains adipose tissue deposits and is the primary layer of travel for the coronary arteries. The myocardium composes the heart's musculature and is commonly the thickest layer of the seats. This myocardial layer is highly vascularized compared to other muscle tissue in the body and contains connective tissue for mechanical support. The endocardium is the blood contacting layer of the heart composed of a specialized epithelium **(FIG 1.2)**.

The cardiac skeleton refers to the fibrous rings of connective tissue mainly composed of collagen that encircles and provides an anchor for the heart valves. In addition to the anchoring effect, the fibrous ring also forms an electroconductive barrier between the atria and ventricles, allowing the asynchronous propagation of the cardiac contraction signal.[6] The fibrous network

of the cardiac skeleton is developed by cardiac fibroblasts derived from migrating epicardial cells during embryonic development. Along with the gross fibrous skeleton of the heart, there is also

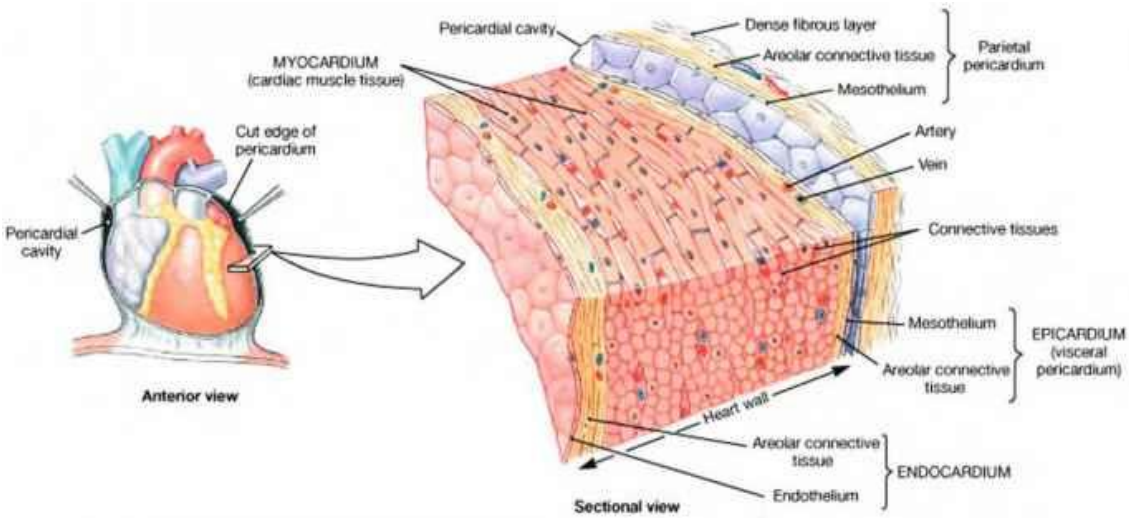

Figure 1-2: The layers of heart wall

Iaizzo, P.A., ed. *Handbook of the cardiac anatomy, physiology, and devices, third edition*. 2015.

a collagen network that allows for anchoring the cardiomyocytes within the extracellular matrix (ECM).

1.2.1 Cardiac Cell Populations

The five major cell types found in the adult human heart are cardiomyocytes (CM), cardiac fibroblasts (CF), endothelial cells (EC), vascular smooth muscle cells, and immune cells. Of these, the CM's make up the most significant volume of the heart wall at 75%; however, the overall percentage of CM's in the heart has been a debated topic.[7] Most recently, an extensive study using adult donor hearts determined that CM's comprised 49% of the overall cell population in the ventricular wall.[8] In this comprehensive study completed by Litvinukova et

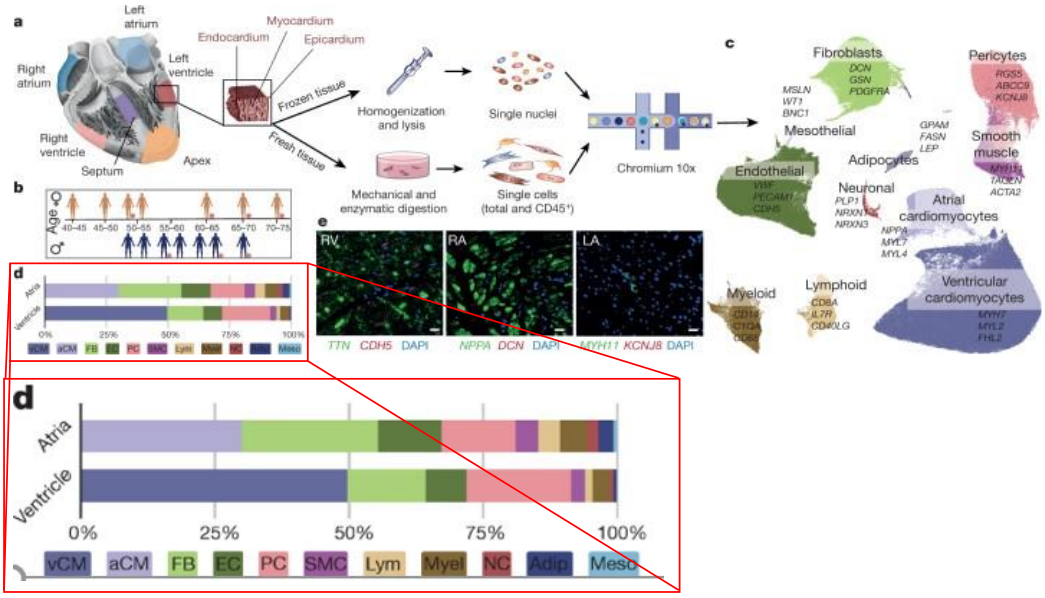

Figure 1-3: The major cells of the heart have been isolated and categorized to discover that the ventricular cell population is approximately 50% CM.

Litvinukova, M., et al., Cells of the adult human heart. Nature, 2020. 588(7838): p. 466-472.

al., cells were isolated from each atrium and ventricle as well as the septum and apex and processed for either whole cell or single nuclei counting. After sequencing, a neural network was used to sequence the cells into their various populations, where the ratios of the cells were determined. The results of this sequencing are illustrated in **(FIG 1-3)**

1.2.2 Cardiomyocytes

In histological analysis, cardiomyocytes can be defined by their flat rod-like structure, sarcomeric striations, and unlike organized bundles of fibers found in skeletal muscle, intercalated discs, which are irregular branches off the fiber. CM's can be characterized by specific proteins for gap junctions (CX-43), calcium handling (SERCA), myosin heavy chain (MHC), troponin (cTnT), as well as many others.[9-13] The propagation of an electrical signal commencing at the SA node travels through the Purkinje fibers that effects the synchronous

contraction of the CM's to conduct the heartbeat. In prenatal hearts, the CMs are poorly developed and undergo hyperplasia; as the heart matures, the CMs become more specialized, form the myofibrils, and experience hypertrophic growth**(Fig 1-4)**.[14, 15] As CMs are terminally differentiated cells, they exhibit low turnover in the adult heart, where regeneration is approximately 1% annually.[16] Many specialized cells, such as CMs, exhibit a slight ability to proliferate due to the inhibition of cyclin and cyclin-dependent kinase signaling, preventing cell division.[17] Specialized pacemaker cells which do not contract in the Sino Atrial (SA) node initiate an action potential. This electrical impulse causes depolarization of the atrial wall resulting in the contraction of the atrial musculature. The electrical impulse is carried through the pacemaker cells to the atrioventricular node, where the signal is relayed to the ventricular musculature by the bundle of His and Purkinje fibers residing in the endocardium to initiate depolarization and contraction of the ventricular wall. The sequential signaling of the cardiac action potential leads to asynchronous systole and diastole of the atrial and ventricular chambers, allowing for efficient blood flow through the heart.

At the cell level, the functional unit of cardiac contraction is the sarcomere. The sarcomere is comprised of thick, myosin, and thin actin filaments crosslinked by a z line**(Fig 1-5)**.[18] Upon depolarization of the cell membrane, calcium channels are opened in the T-tubules, which release calcium ions into the cytoplasm. Cardiac troponins blocking actin binding sites bind to the calcium ions, removing the troponin complex from the sites.[19] Adenosine triphosphate (ATP) binds to myosin, imparting the chemical energy required for myosin to pull the thin filament actin towards the center of the sarcomere resulting in contraction. Upon

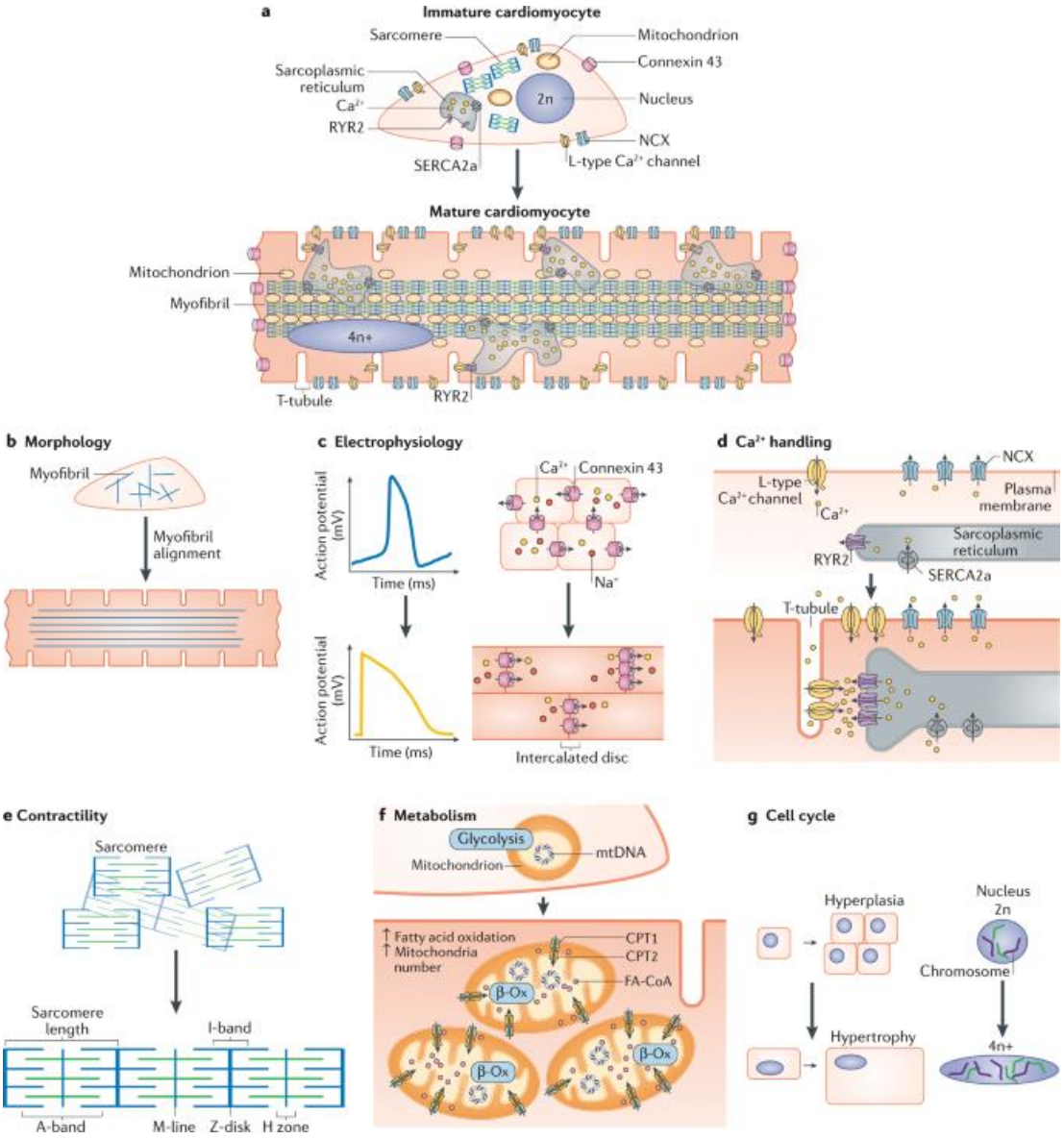

Figure 1-4: The cardiomyocyte has various phenotypical changes as it matures from a fetal type cell including a)Cell Size and Organization Morphology C) Electrophysiology D) Ca^{2+} Handling E) Contractility F) Metabolism and G) Cell Cycle .

Karbassi, E., et al., *Cardiomyocyte maturation: advances in knowledge and implications for regenerative medicine.* Nat Rev Cardiol, 2020. 17(6): p. 341-359.

release of calcium ions into the sarcoplasmic reticulum, the troponin binding complex returns to its inhibition state of actin, leading to sarcomere relaxation. Because of the massive amounts of

ATP needed to keep the heart beating approximately once a second, mitochondria comprise a significant volume of the CM cell.[20]

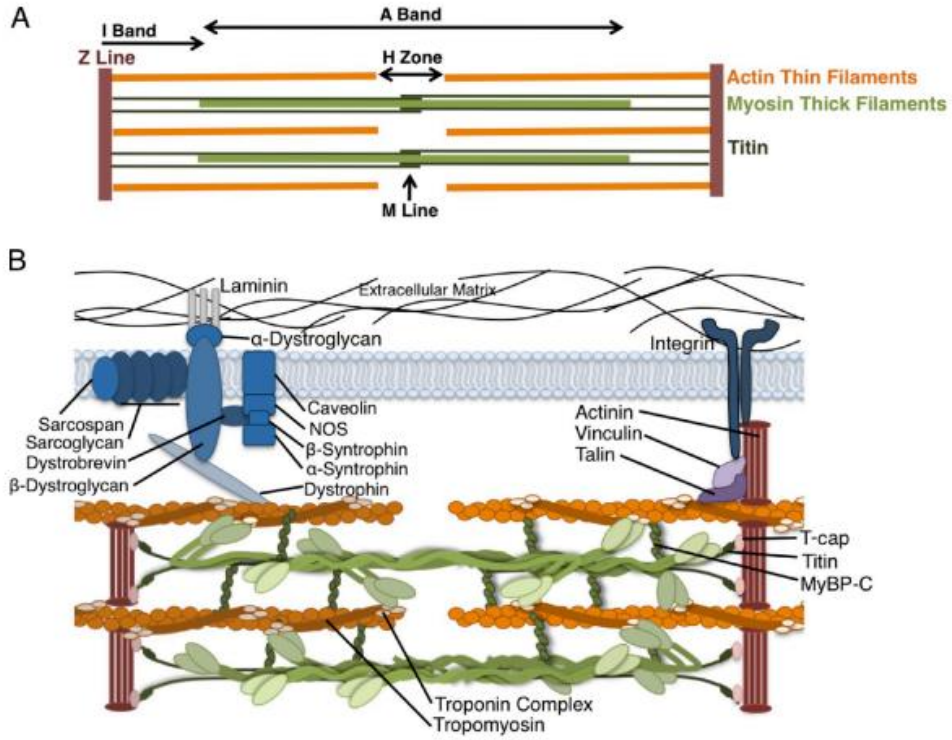

Figure 1-5: Specific organization of the cardiac sarcomere.

Harvey, P.A. and L.A. Leinwand, The cell biology of disease: cellular mechanisms of cardiomyopathy. J Cell Biol, 2011. 194(3): p. 355-65

1.2.3 Cardiac Fibroblasts

Cardiac Fibroblasts(CFs) are support cells of mesenchymal origin responsible for much of the homeostatic mechanisms of the ECM.[21] These mechanisms are predominantly a secretory role as they produce the connective tissue found within the heart. They are also responsible for matrix remodeling through the production of matrix degrading matrix-metalloproteinases

(MMP).[22] The primary structural components of the CF secretion are fibrillar collagens(type I and III), proteoglycans(fibronectin and laminin), and glycosaminoglycans(hyaluronan). CFs are also responsible for secreting a host of growth and transcription factors essential for cardiac development and cell signaling processes. Normally quiescent, the CFs can be activated upon injury and perform a morphological change into a myofibroblast, a semi-contractile cell characterized by its expression of α-smooth muscle actin(α-SMA).[23] It is hypothesized that other cells, such as pericytes or smooth muscle cells, may also differentiate into myofibroblasts, but this has not yet been confirmed**(FIG 1-6).**[24]

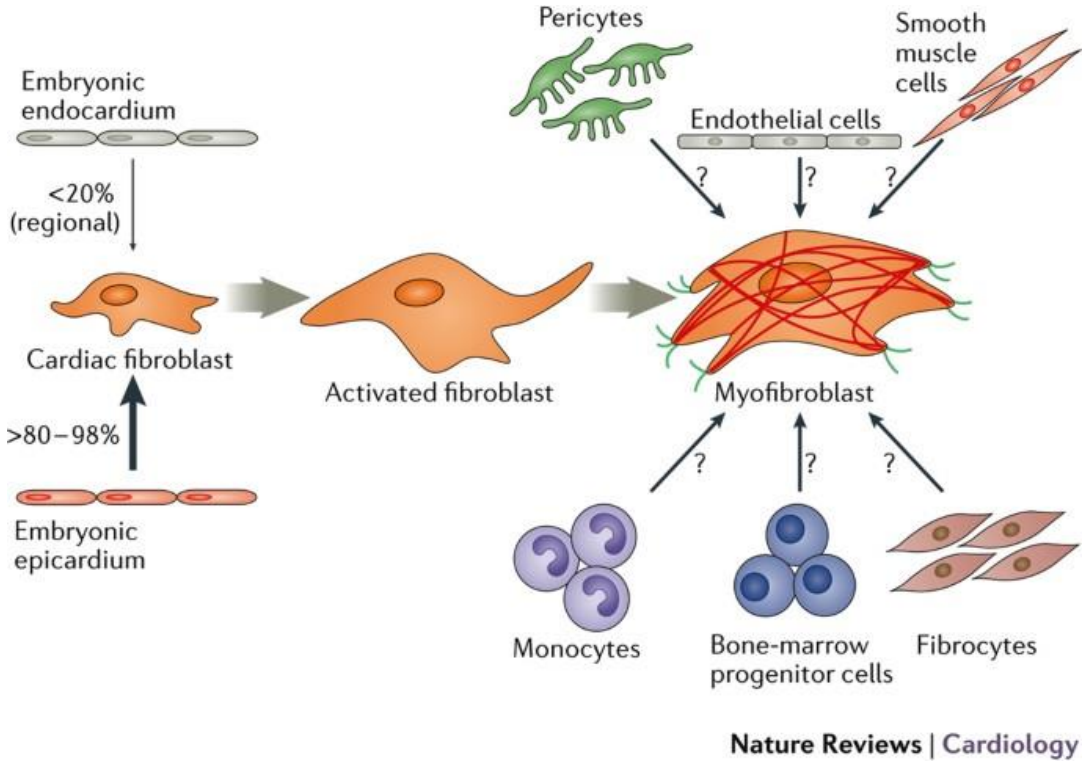

Figure 1-6: Cardiac fibroblast are mesenchymal cells originating from the endocardium and the epicardium

Tallquist, M.D. and J.D. Molkentin, Redefining the identity of cardiac fibroblasts. 2017.

1.2.4 Endothelial cells

As previously mentioned, the heart wall is highly vascularized to allow for the high nutrient demands of a constantly contracting tissue. Various cell groups can be categorized in these vessels, but the most significant is the blood contacting endothelial cells. The endothelial cells comprise the tunica intima of the larger vessels in the myocardium and are the sole contributor to the capillary walls where nutrient exchange occurs.[25] These cells have multiple roles, primarily in regulating vascular homeostasis, but they are also essential in cell communication roles for angiogenesis and cardiomyocyte development.[26] One of the most critical roles for

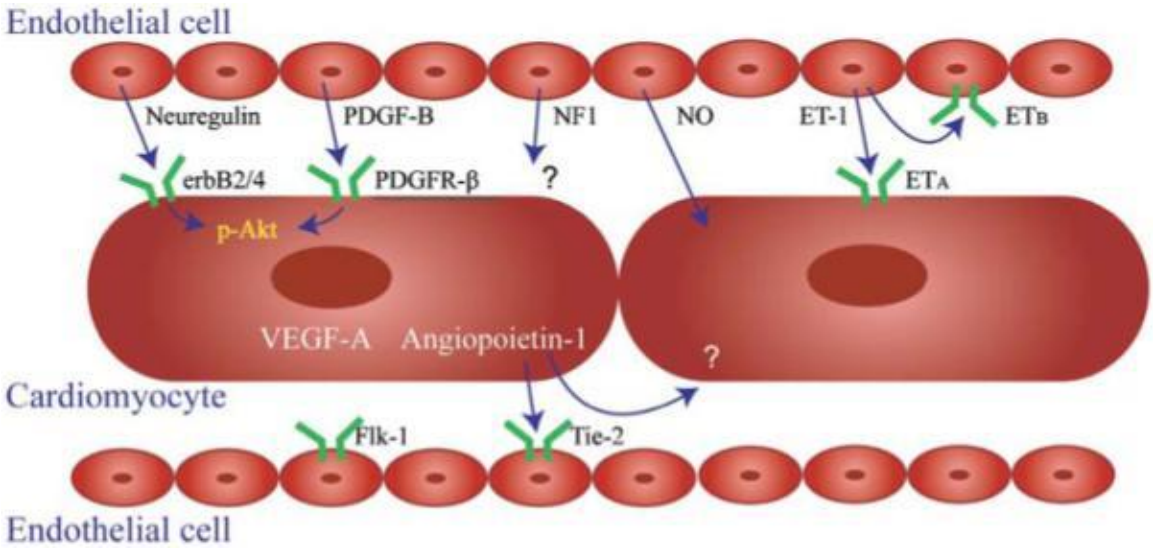

Figure 1-7 Endothelial cells and cardiomyocytes have various communication pathways

Hsieh, P.C., et al., *Endothelial-cardiomyocyte interactions in cardiac development and repair.* Annu Rev Physiol, 2006. 68: p. 51-66.

ECs is the regulation of nitric oxide, which plays a crucial role in vascular homeostasis. These cells are also responsible for secretions of vasodilators such as prostacyclin, and endothelin 1, a

vasoconstrictor. [27, 28] Due to the high capillary density of the myocardium, the ECs role in cell signaling is increased in this tissue compared to those less vascularized**(FIG 1-7)**.

1.2.5 Cardiac Extracellular Matrix

The ECM of the myocardium is a complex network of molecules mainly composed of fibrillar collagens and non-fibrillar molecules that comprise the structural and nonstructural elements.[29] The structural elements of the ECM are typically within the interstitial matrix, while the basement membrane is home to many of the regulatory molecules. The molecules found within the ECM are predominantly proteins bound to polysaccharides as proteoglycans or glycoproteins.[29] Glycosylation, the process in which these molecules are formed, is a post-translational modification performed within the cell's endoplasmic reticulum and Golgi apparatus **(FIG 1-8:A)**.

Within the interstitial matrix, Collagen types 1 and 3, as well as Elastin, are the primary structural proteins. Collagen is a trimer formed by the helix of a chain of alpha helices arranged in a Gly-X-Y orientation that includes the subunit of collagen known as tropocollagen.[30] Collagen has several subtypes, the most common of them being fibrillar in nature that serve as structural components of the ECM. The other main structural protein of the cardiac ECM is elastin, which provides elasticity and keeps the heart wall's tensile integrity.[31] The other glycoproteins and proteoglycans can also serve structural purposes but are vital in regulating the ECM**(FIG 1-8:B)**.

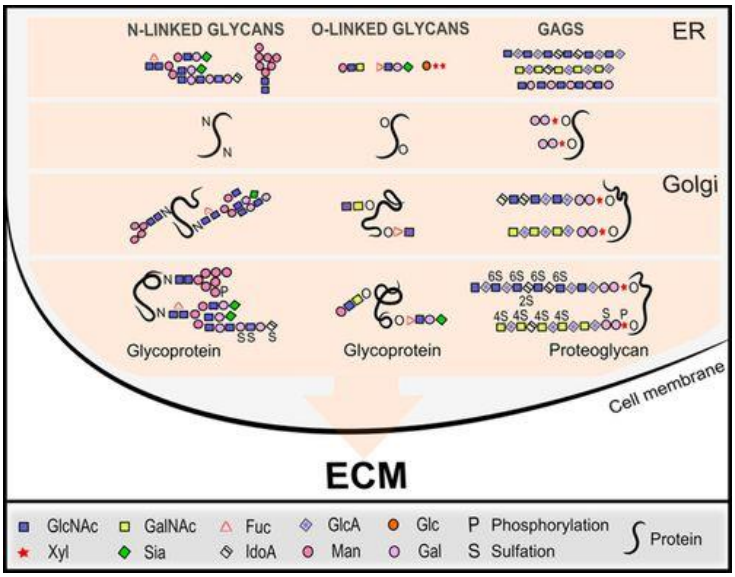

(A)

Cardiac Extracellular Matrix

GLYCOPROTEINS			GAGS	PROTEOGLYCANS			
Prototypical matricellular proteins	Fibers	Others	Hyaluronan	Hyalectans	Basement Membrane proteoglycans	Cell Surface proteoglycans	Small Leucine Rich Proteoglycans
Thrombospondin	Collagens	Fibronectin		Versican	Perlecan	Syndecan	Class I Biglycan, Decorin, Asporin
SPARC	Elastins (not glycosylated)	Laminin		Neurocan	Collagen XVIII	Glypican	Class II Lumican, Fibromodulin, PRELP, Keratocan, Osteoadherin
Tenascin				Brevican	Agrin		Class III Osteoglycin, Epiphycan, Optican
Osteopontin				Aggrecan			Class IV Chondroadherin, Nyctalopin, Tsukushi
Periostin							Class V Podocan, Podocan-like protein 1
CCN							

(B)

Figure 1-8: Glycosylation and ECM proteins (A) Glycosylation is a post translational modification of ECM proteins performed in the ER and Golgi apparatus. (B) Some proteins are non structural such as the column in pink. Others are purely structural in Blue, and those in Purple columns are a combination of both.

Rienks, M., et al., Myocardial extracellular matrix: an ever-changing and diverse entity. Circ Res, 2014. 114(5): p. 872-88.

Proteoglycans consist of a protein core bounds to chains of glycosaminoglycans.

Glycosaminoglycans or GAGs are negatively charged polysaccharide chains, of which the primary

of these, hyaluronic acid, is the only GAG found in the cardiac ECM not bound to a protein core.

However, it may form noncovalent bonds with other groups of proteoglycans. Transmembrane proteins known as integrins are the primary anchoring point of the cells to the ECM. These anchoring molecule groups consist of heparan sulfate, chondroitin sulfate, keratin sulfate, and hyaluronic acid.[32]

Any tissue engineered device must make an effort to effectively reproduce this complicated matrix; otherwise, cellular engraftment and survivability will be in question.

1.3.1 Cardiac Mechanics

As discussed, the heart is a complicated organ whose sole purpose is to efficiently and continually pump the blood for an entire lifetime. Physical and electrical mechanics govern the successful contraction of the cardiac wall to achieve this goal.

1.2.2 Mechanical Properties

Physically the contraction of the heart wall is complicated as it follows a different purpose than a normal striated muscle used for locomotion. Specifically, the contraction of the cardiac wall results in a reduced volume of the chamber, increased chamber pressure, and ejection of the blood. Parameters that govern the mechanics of these tissues include wall stress, longitudinal/radial strain, tissue stiffness, and stroke volume/ejection fraction, where changes within these metrics can be used as a sign of pathological remodeling or heart failure.

At its most straightforward, wall stress is governed by Laplace's Law, where the wall stress is directly proportional to the radius of the muscle wall but inversely proportional to the thickness of the wall.[33, 34] Early models of wall stress were limited by technology and computing power. Still, with improved imaging and the advancement of computing in finite element analysis (FEA) and other predictive models, estimates of wall stress are much improved

compared to just a few decades ago. Such FEA models have determined that peak wall stress can be approximated at 100kPa.[35] Typically higher wall stress can be associated with lower ejection fraction, which is a simple measurement to determine the volume of blood pumped by the ventricle, an important indicator of heart failure.

Stiffness of the myocardium is another critical metric to consider as the mechanosensitive cells will adapt to changes in substrate stiffness, bringing about important considerations for understanding cells in healthy and pathological states and determining proper scaffolding techniques in the regenerative medicine context that will be discussed later. Because the myocardium is anisotropic in nature, the analysis of the stiffness of the heart, usually expressed as Young's Modulus or E can have widespread values depending on the measurement method**(FIG1-9)**.[36] It is widely accepted that as the heart ages and with the rise of fibrosis, its substrate will become stiffer with time. Also, the stiffness of the heart changes throughout the cardiac cycle, as during diastole in the adult human left ventricle ranges of 8-15kPa are accepted. In contrast, during systole, the stiffness can increase up to 500kPa.[37]

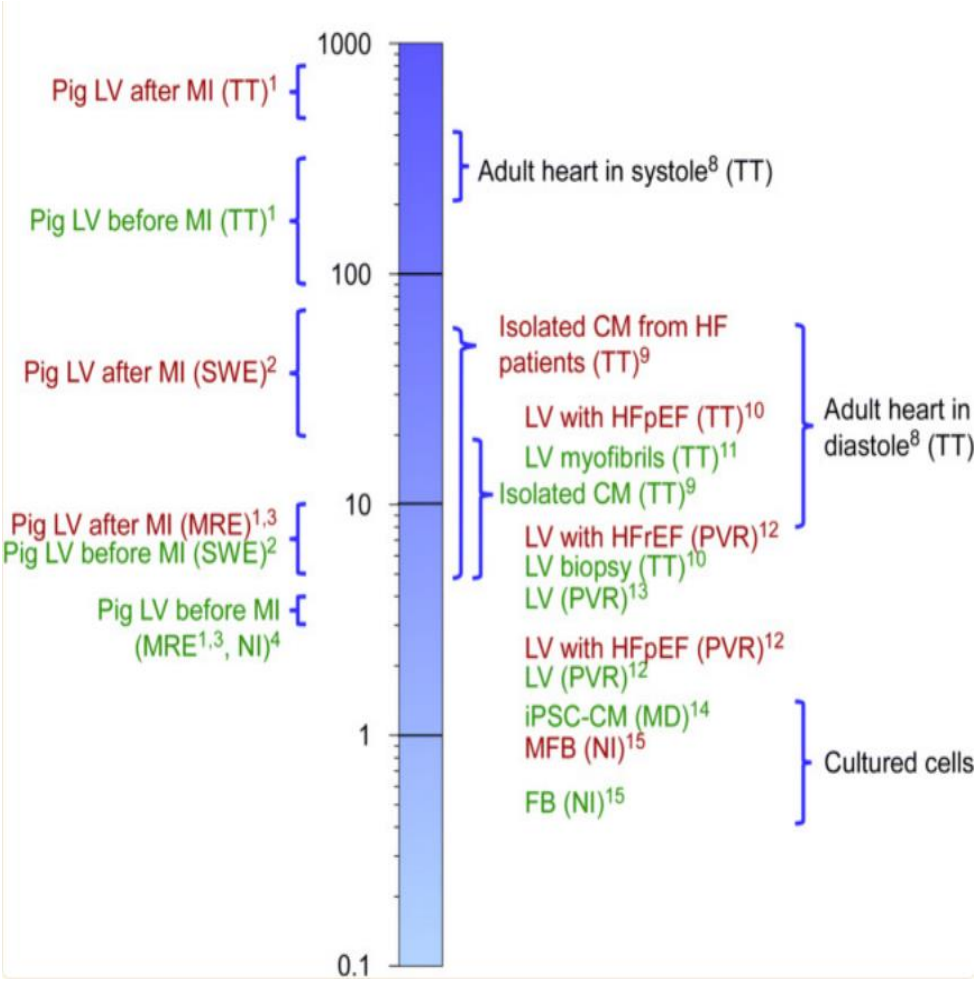

Figure 1-9: Associated stiffness of cardiac tissue varies from species, condition, and measurement method

Emig, R., et al., *Passive myocardial mechanical properties: meaning, measurement, models.* Biophys Rev, 2021. 13(5): p. 587-610

The heart contracts uniquely in the body compared with other striated muscles used for locomotion, where the contraction results in blood pumping. To achieve this result, the heart contraction results in a twisting shortening motion where the base contracts towards the apex, which visually remains relatively in place.[38] At the same time, this movement is happening,

the ventricle walls contract inward, and the apex and the base have opposite rotation paths.[39, 40]. The path of rotation can be shown through echocardiography strain imaging, as seen in **(FIG 1-10)**. From this imaging, it can be deduced that despite a shortening of 15% in longitudinal fibers, the resultant contraction results in a thickening of the wall by 40%.[41]

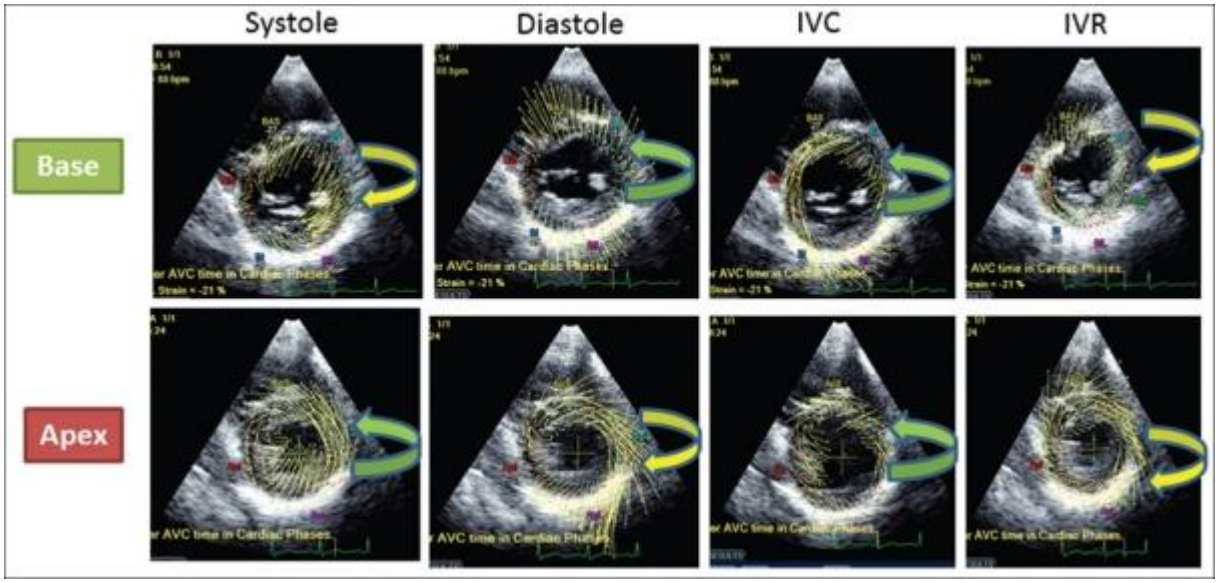

Figure 1-10: Echocardiography is used to display the twisting of the cardiac wall during contraction. Salvo, G.D., et al., Strain Echocardiography and Myocardial Mechanics: From Basics to Clinical Applications. J Cardiovasc Echogr, 2015. 25(1): p. 1-8.

1.3.3 Electrical Properties

From an electrophysiology standpoint, the heart contracts based on the propagation of an action potential dependent on changes in ion concentrations throughout the cardiac cycle. This action potential consists of 5 numbered phases from 0-4.[42] At phase 0, depolarization begins. The resting membrane potential of -90mV rises as an action potential from another cardiomyocyte or pacemaker is detected. From this point, Na^+ begins to transfer through the membrane until the transmembrane potential rises over the threshold(-70mV). This leads to an

increase in Na^+ while also opening L-type Ca^{2+} channels when the transmembrane potential rises over -40mV. The transmembrane potential is briefly positive due to a massive influx of Na^+ where the open Na^+ channels then close, leading to Phase 1. Phase 1 begins with the opening of K^+ channels which brings the transmembrane potential back to 0mV, then leads into Phase 2, or the plateau phase. The plateau occurs as the L-type Ca^{2+} channels remain open, resulting in an influx of Ca^{2+} while K^+ passes out of the cellular space. This results in a rough equilibrium of charge, which causes the plateau to form just below 0mV. Once Ca^{2+} channels are inactivated, the more significant outflow of K^+ results in the falling of the transmembrane potential back to its resting potential of -90mV; this is the 3rd phase of the action potential known as repolarization. Once repolarization is achieved, the only movement of ions are those of potassium, leaving the transmembrane possibility around -90mV until the process is repeated. The full cardiac action potential is outlined in **(FIG 1-11)**. The resting membrane potential of the cardiomyocyte is slightly higher than the ideal equilibrium potential of K^+ that the Nernst Equation can describe:

$$E_K = \frac{RT}{zF} \ln \frac{[K]_o}{[K]_i}$$

Where R is the universal gas constant, T is the temperature in Kelvin, z is the number of ion charges, and F is Faraday's constant.[43]

The cell converts the energy generated by the rising action potential into muscular movement through a process known as excitation-contraction coupling. This process is detailed above in the function of CMs. Typically, the cells pass action potentials through gap junctions binding the membranes together; however, it has been discovered that electrical activation can all pass through the extracellular matrix, known as field coupling or ephaptic coupling.[44] This

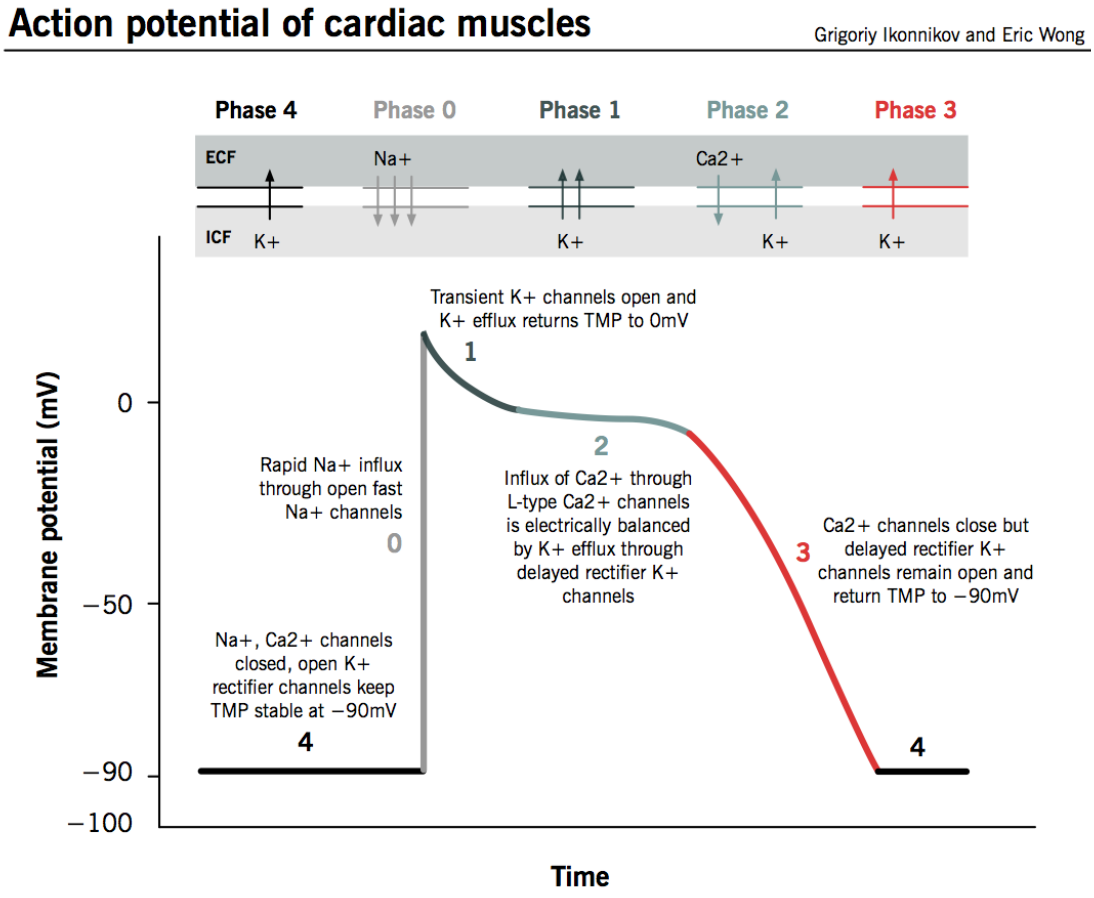

Figure 1-11: The phases of the cardiac action potential.

Nerbonne, J.M. and R.S. Kass,* Molecular physiology of cardiac repolarization. *Physiol Rev, 2005. 85(4): p. 1205-53.l

characteristic could be invaluable in studying cardiac contraction in the fibrotic heart, where action potentials do not easily pass through fibrotic spaces.

1.4 Pathology

1.4.1 Initiation of infarction and cell death

The collective group of cardiovascular diseases is the main contributing factor to death worldwide. Coronary artery disease (CAD), resulting in myocardial infarction, is the leading cause of these fatalities. CAD is characterized by atherosclerotic buildup in the main coronary arteries supplying nutrients to the heart wall. Atherosclerosis occurs disproportionately in those with contributing risk factors such as hypertension and hypercholesterolemia but can also be due to inflammatory responses after infection or other causes.[45] When these atherosclerotic lesions expand, they occlude the artery and obstruct patency or may be susceptible to thrombosis, which causes downstream embolism. The resultant ischemic event in the myocardium causes cell injury that, while at first reversible, can quickly lead to cell death if nutrients are not returned quickly. Specifically, it has been determined that cells may survive in a hypoxic to the anoxic environment for some time. Still, without a source of glucose to produce ATP through oxidative phosphorylation, the opening of the mitochondrial membrane is unavoidable, leading to necrosis.[46, 47] Necrosis is characterized by the breakdown of the plasma membrane releasing the cell's contents into the extracellular space where damage-associated molecular patterns (DAMPs) set off a cascade leading to a massive inflammatory response.[48]

The other primary form of cell death, known as apoptosis, was through either the intrinsic or extrinsic pathway, the cell fragments in a way that the body can process without

producing the same molecules leading to an inflammatory response. In the extrinsic pathway, a condition occurs outside the cell, causing a cascade into apoptosis. Cell surface receptors are death receptors, the most well-known of which are Fas and Tumor Necrosis Factor Receptor-1.[49, 50] Upon binding to these receptors, a sequence is set off, leading to the activation of Caspase 8, which activates other downstream Caspases 3 and 7, which will result in condensation of the chromatin in the nucleus and apoptosis. On the other hand, the intrinsic pathway is a response to intracellular cell stresses, typically associated with hypoxia in the case of infarction. The Bcl family of proteins are critical modulators of the intrinsic pathway. Molecules such as Bcl-2 are anti-apoptotic, while Bax is pro-apoptotic. Activation of Bax results in perturbation of the mitochondrial membrane. Once the mitochondria are compromised, it releases cytochrome c, leading to the activation of Caspase-9 and then Caspase-3, resulting in

chromatin condensation and apoptosis. The pathways of necrosis and apoptosis can be visualized in **(FIG 1-12)**

When blood flow returns to the infarcted area through natural clot breakup or medical intervention, there is a risk of reperfusion injury (RI). RI is caused by the quick return of blood flow to the damaged area where surviving cells experience high levels of oxidative stress from free radicals, leading to mitochondrial collapse. It is believed that a significant portion of all cell death in patients surviving an infarct occurs from RI (**FIG 1-13)**.[51]

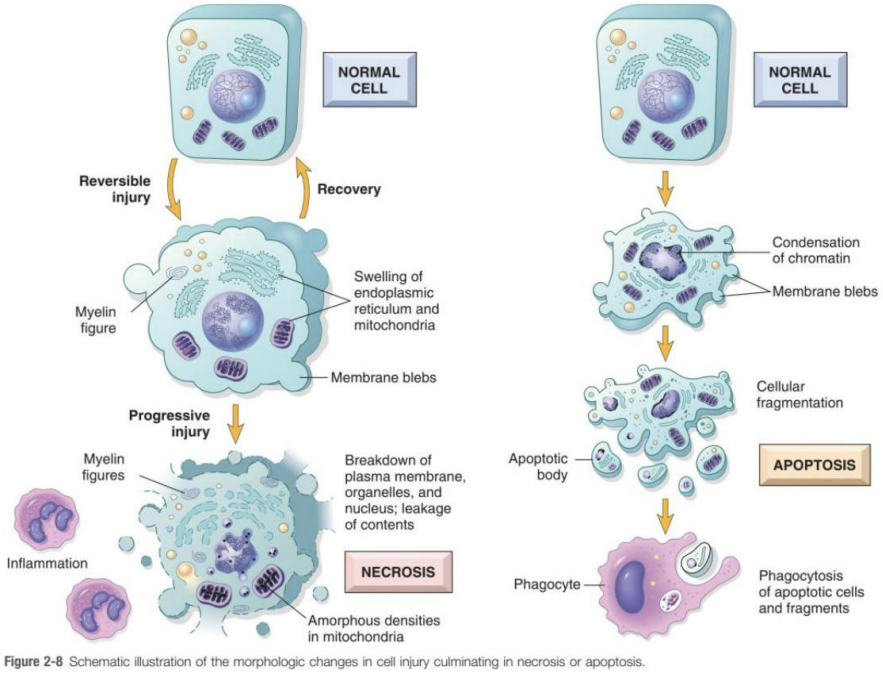

Figure 2-8 Schematic illustration of the morphologic changes in cell injury culminating in necrosis or apoptosis.

Figure 1-12: Characteristics of cell death mechanisms of necrosis and apoptosis.

Kumar, V., A.K. Abbas, and J.C. Aster, *Robbins & Cotran Pathologic Basis of Disease*. 2014: Elsevier Health Sciences

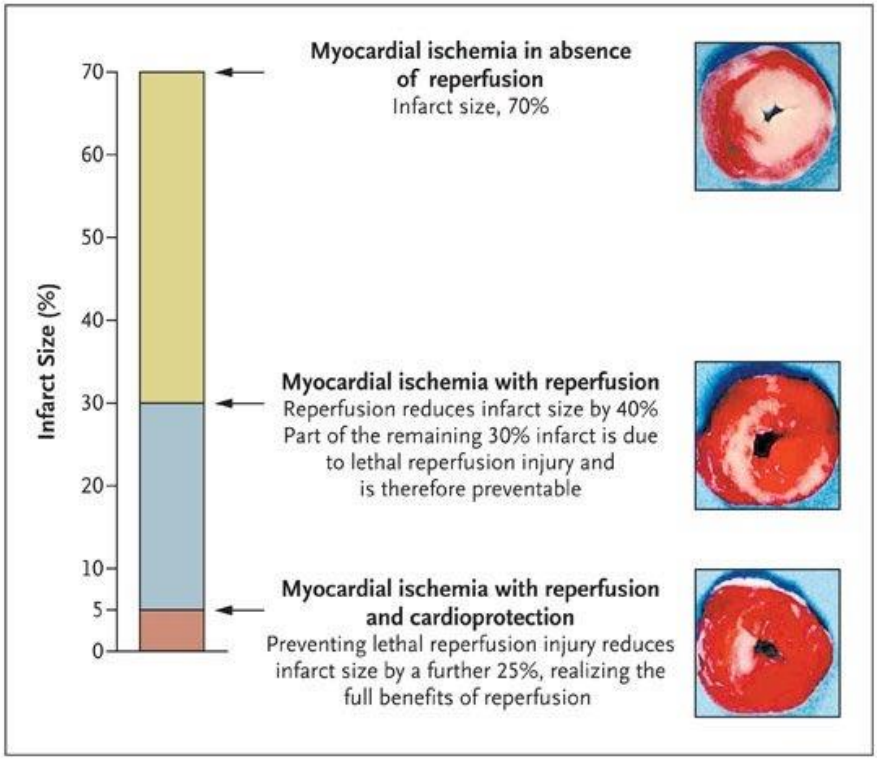

Figure 1-13: Myocardial reperfusion results in a significant portion of the total infarct area.

Yellon, D.M. and D.J. Hausenloy, **Myocardial Reperfusion Injury.** ***New England Journal of Medicine, 2007***

1.3.3 Inflammation and Remodeling

After initiating the inflammatory response, neutrophils are the first responder cells to arrive at the infarction site, where they begin removing cellular debris. Several factors lead to neutrophil activation and migration, starting with DAMPs which promote the release of Hydrogen Peroxide and then the activation of the CXCL8 family of chemokines and leukotrienes.[52] Once activated, the neutrophils will upregulate these signals and drive even further neutrophil migration. Monocytes then move into the area and mature into macrophages, responsible for many processes that contribute to wound repair but can also lead

to a persistent inflammatory response. One of the critical processes of the macrophages is to secrete growth factors such as transforming growth factor-beta(TGF-B), which allows for the transformation of fibroblasts into the previously mentioned myofibroblasts **(FIG 1-14)**.[53] The myofibroblasts begin degradation of the damaged ECM via MMP secretion and start producing the collagen that will make up the patch protecting the heart wall from failure. This patch is the method in which the body can repair the damaged area as complete regeneration is impossible due to the previously mentioned lot turnover of the native cardiomyocyte population. Myofibroblasts have limited contractile ability but will not replace the lost contraction forces of the native CMs and cannot contract synchronously with the healthy tissue.[54] Over time the myofibroblasts will crosslink the patch will eventually become a fibrous scar. Depending on the size of the spot, the rest of the ventricle may begin to undergo hypertrophy to preserve the ejection fraction, which may lead to dilated cardiomyopathy. With time downstream signaling of TGF-B may also lead to persistent myofibroblast activation and fibrosis at sites remote to the infarction site throughout the rest of the heart, leading to overall tissue stiffening and decreased ejection fraction.[55, 56]

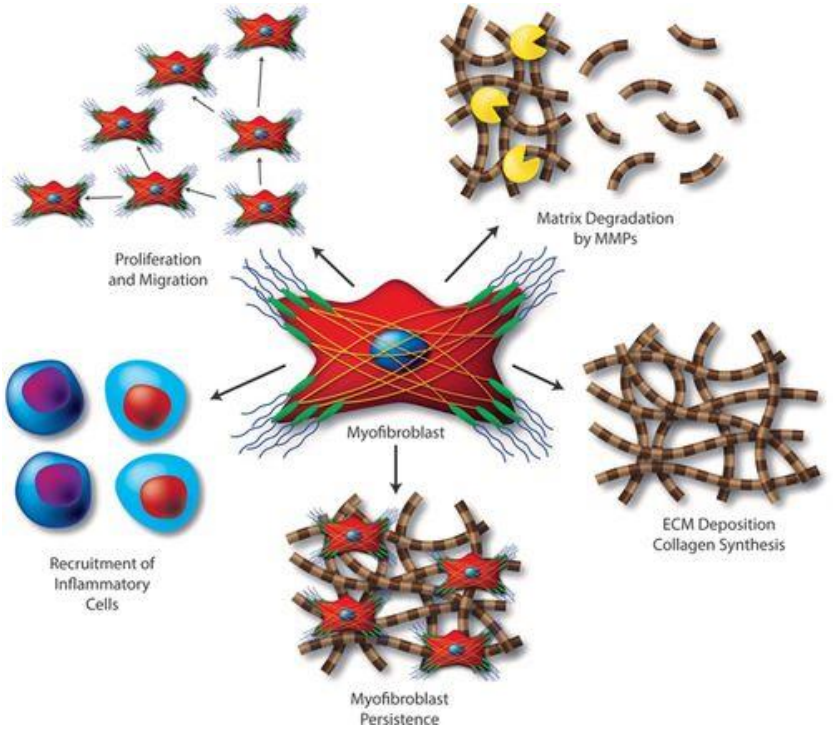

Figure 1-14: The activated myofibroblast plays an essential role in the ecm deposition and scar formation after MI

Travers, J.G., et al., *Cardiac Fibrosis: The Fibroblast Awakens.* Circ Res, 2016. 118(6): p. 1021-40.

1.4.3 Current Therapies

Therapies for MI and HF depend on the injury's response time. Quick treatment can limit the damage done and overall infarct size, leading to lower mortality. The first treatment after the onset of MI is typically the use of antiplatelet therapy, commonly oral administration of aspirin, which can be used to begin the thrombolysis. Aspirin treatment has also been shown to help prevent the onset of infarction; however, it is no longer advised to be taken daily unless a patient has already suffered one MI. Other thrombolytic agents are also commonly used to treat infarction in non-ST segment elevated MI.

In ST-segment elevated MI, the gold standard of treatment has moved towards revascularizing the heart wall. The two most common methods used in this treatment are

coronary artery bypass grafting (CABG) and percutaneous coronary intervention (PCI). CABG is a surgical procedure where the patient's heart is temporarily stopped, and the entire chest cavity is opened. An autograft is typically taken from the saphenous vein or mammary artery and grafted from the aorta to bypass the occlusion. The mammary artery is the preferred graft as they have better 10-year patency rates than those harvested from the saphenous vein.[57]

On the other hand, PCI is a balloon angioplasty that has become more common than CABG because of the relatively more straightforward catheterization procedure associated with it as opposed to the open-heart surgery required for CABG. PCI was limited in the past to the availability of catheterization labs; however, the number of clinics has grown over the last several decades where at least in the United States a majority of the population lives within a distance of one of these treatment centers. CABG is still an appropriate treatment as it has improved outcomes in patients with multiple coronary artery occlusions or those with heightened disease states such as diabetes **(FIG 1-15)**.[58]

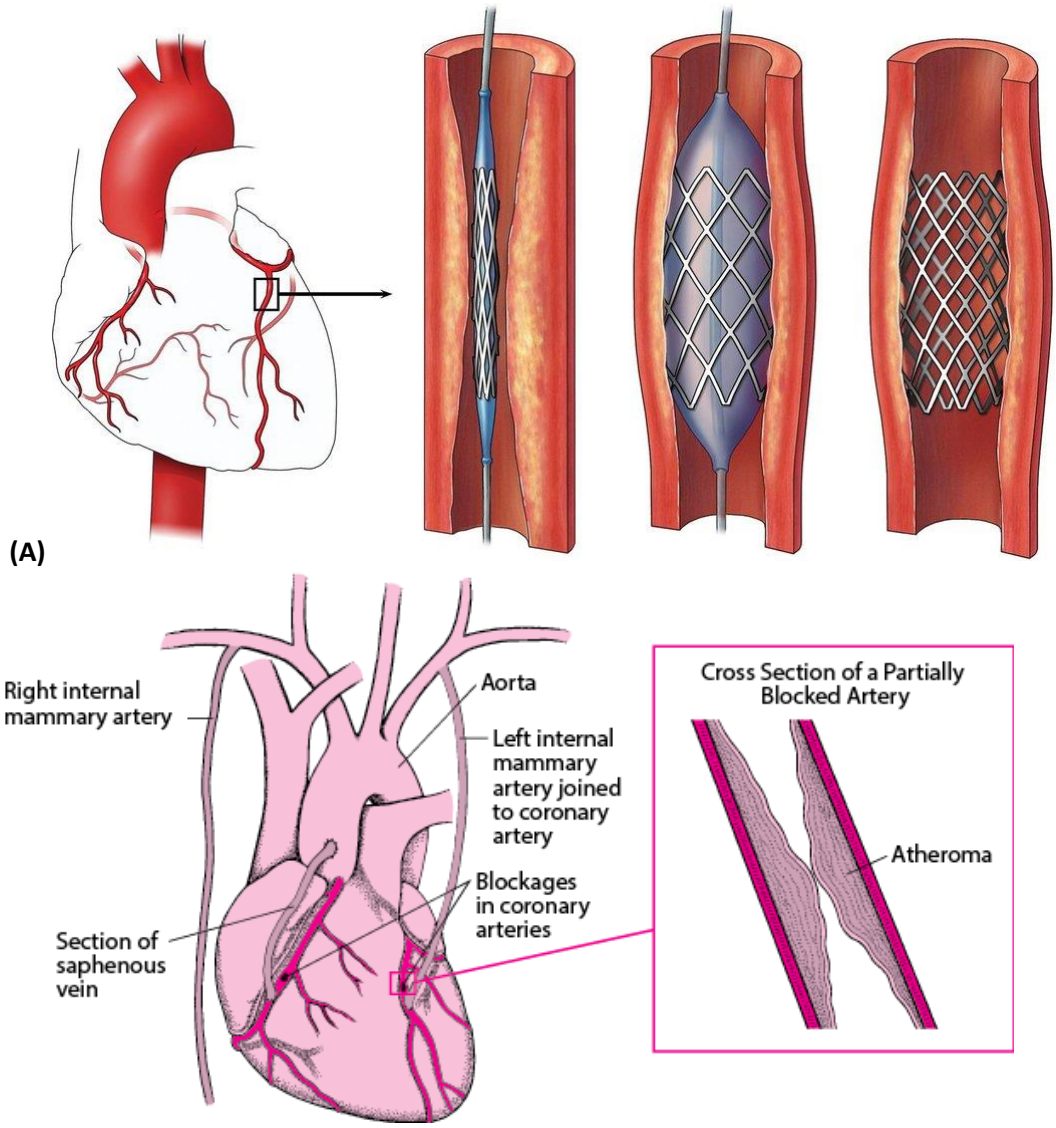

Figure 1- 15: Revascularization Techniques A) PCI, B) CABG

While revascularization is essential in patient survival and can lead to reduced infarct size, it is not a perfect treatment as it is not ordinarily possible to revascularize the tissue in time to prevent cell necrosis. Irreversible damage is done to the heart wall in the first 20-40 minutes after the onset of infarction, with coagulative necrosis occurring in the first 30 minutes. Notably, the revascularization of the heart wall leads to reperfusion injury, as previously discussed. No

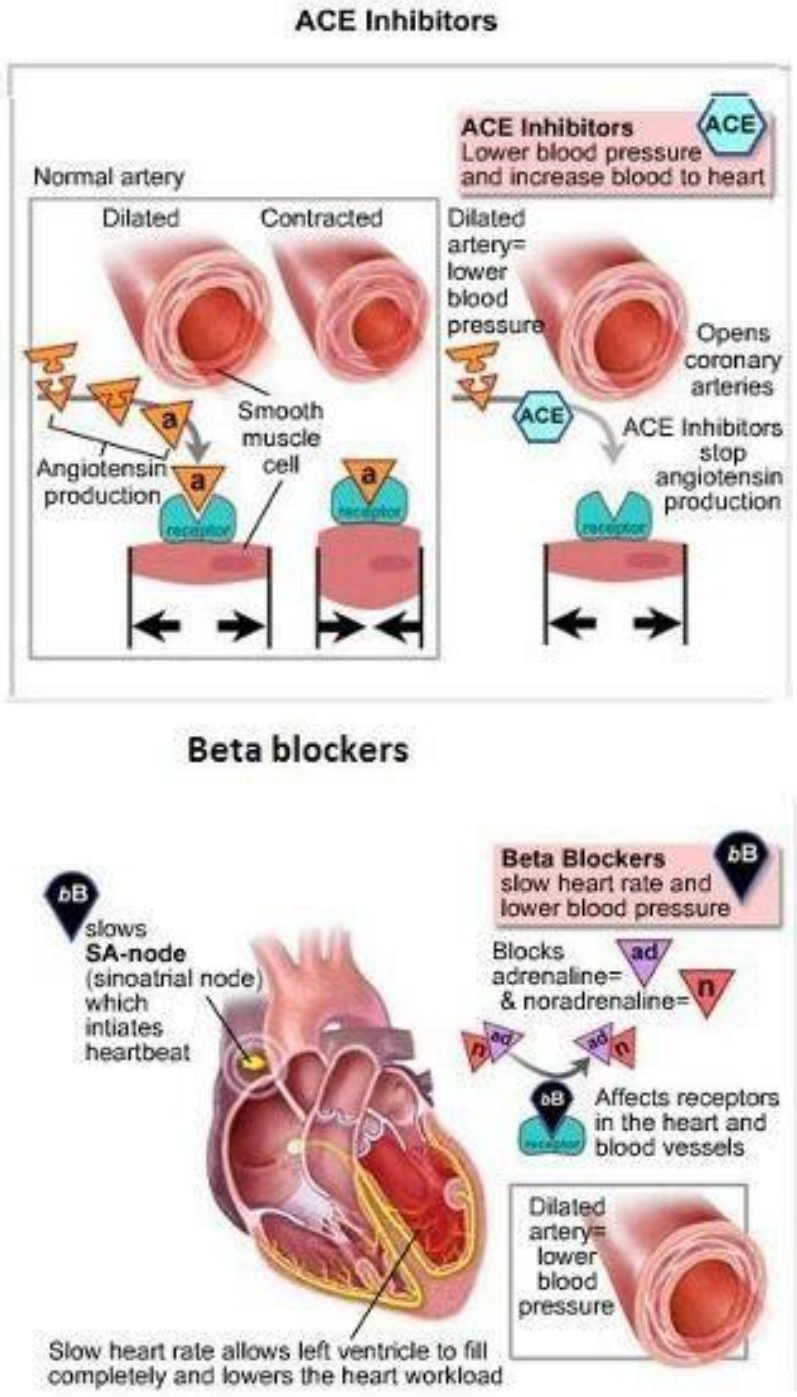

Figure 1-16: Beta Blockers and Ace Inhibitors work to decrease the load on the heart to prevent heart failure

current therapy can prevent the loss of cells despite some promising results in animals with techniques such as ischemic preconditioning, wherein the tissue is treated with short periods of ischemia to avoid more extended periods from resulting in cell death. While treatment does lead to more minor infarct scars and lower mortality rates, it cannot preclude that any damage and cell death in the ventricular wall, regardless of the size, can lead to scarring and interstitial fibrosis.

Treatments to treat the advent of fibrosis and dilated cardiomyopathy usually begin with pharmacological agents to reduce the load on the heart. Both ACE (angiotensin-converting enzyme) inhibitors and beta blockers work by reducing overall blood pressure to help lessen the load on the heart and prevent the onset of hypertrophy **(FIG 1-16)**. While these treatments have been proven to reduce mortality after infarction, they come with their side effects and once again do not treat the underlying scar. Despite some potential in animal studies, no known pharmacological cure has been demonstrated to minimize human fibrosis.[59-61]

After pharmaceutical intervention, there are other surgical options depending on the time after MI and the progression of HF. One of these methods is known as ventricular restoration. This procedure is used to reverse the morphological changes associated with ventricular remodeling in patients who have severely reduced ejection fraction(<20%).[62] While this procedure results in higher mortality in advanced heart failure patients when compared to more mild HF, it has been found to result in better outcomes than medically managed patients alone. Another method to attempt to reduce EF is the use of a ventricular restraint device. These devices are usually in the form of a mesh that is surgically wrapped around the heart to provide passive pressure that alleviates symptoms of heart failure. While

these have shown promise in certain animal models, they have not been associated with higher survivability in humans and do not appear to be currently marketed for therapy.[63, 64]

While all these therapies have their own merits when end-stage heart failure occurs, one therapy has remained the gold standard: the heart transplant. The heart transplant was first successful in the 1960s and has been associated with the most favorable outcomes of HF therapy with 1 year and 3 year survival rates at 85-90% and 75%, respectively.[65, 66] The limiting factor in heart transplantation has been the paucity of available donor hearts, with just over 3000 hearts transplanted per year, leaving many on a waiting list.[67] To combat this issue, ventricular assist devices were developed as a bridge to transplantation therapy. The success of these devices with suitable 5-year survival, when compared with drug therapy alone, has led to their use as a destination therapy, especially, in those who cannot receive a transplant.[68, 69] I

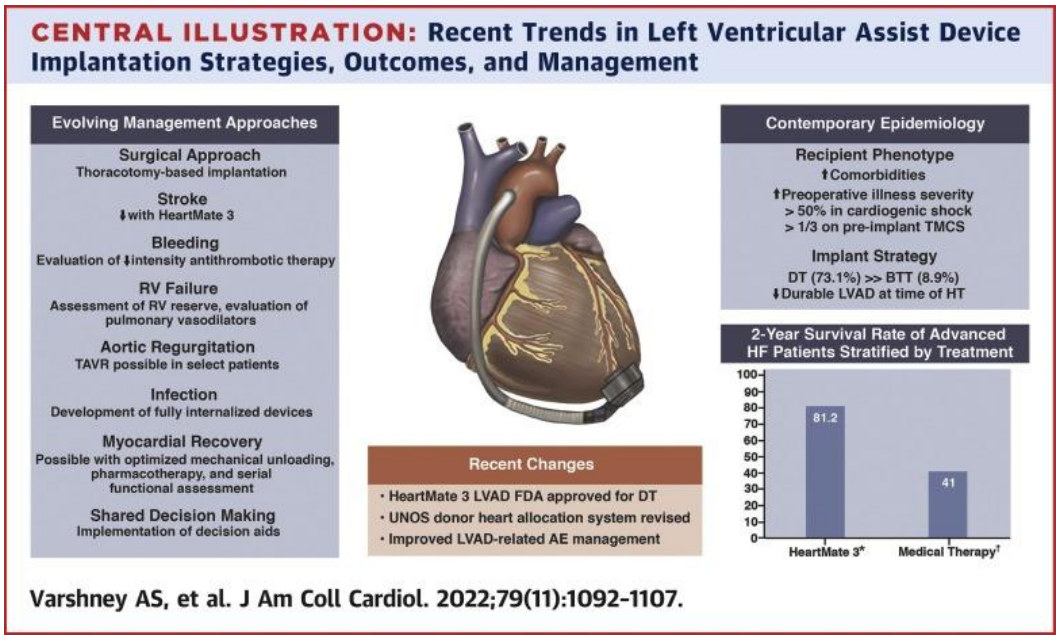

Figure 1-17: Safety of LVADs and their promise as a destination therapy

Varshney, A.S., et al., *Trends and Outcomes of Left Ventricular Assist Device Therapy.* Journal of the American College of Cardiology, 2022. 79(11): p. 1092-1107.

has to be noted that the use of a mechanical device comes at risk of its own complications, but

new devices such as the Heartmate 3 have significantly reduced these outcomes.[70] Finally, it should be noted that one trend in research that, while not currently available, could be a possible therapy in the future is that of xenogeneic grafts.[71] While all therapies related to HF have promise in treating affected patients, it is clear that there still exists a gap in which novel therapies for the treatment of cardiac fibrosis and HF are needed.

1.5 Cardiac Tissue Engineering

1.5.1 Tissue Engineering

Tissue engineering as a paradigm evolved from biomaterials research in the early 1990s when Langer and Vacanti defined the concept as "an interdisciplinary field that applies the principles of engineering and life sciences toward the development of biological substitutes that restore, maintain, or improve tissue function or a whole organ."[72] In practice, three main characteristics combine to produce tissue engineering products: A) the use of primary or stem

cells, B) combined into a naturally occurring or synthetic scaffold, C) conditioned using bio stimuli or bioactive molecules in a bioreactor to produce a functional tissue**(FIG 1-18)**.

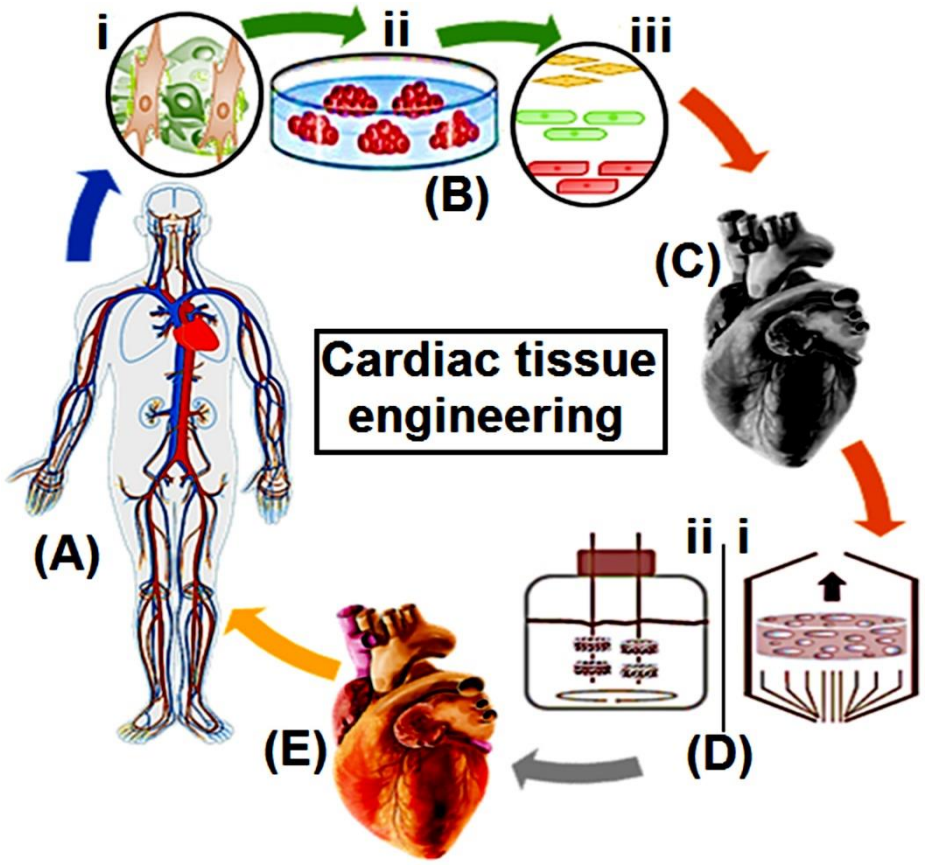

Figure 1-18: Cardiac Tissue Engineering's main approach is to biopsy a A)patients cells B) i) isolate primary cells of interest ii) program IPSC's iii) differentiate into specific cardiac cells C) combine onto a scaffold D) condition in a bioreactor E) create a functional tissue

Paez-Mayorga, J., et al., *Bioreactors for Cardiac Tissue Engineering*. 2019.

1.5.2 Cells in Cardiac Tissue Engineering

The first point of consideration in any tissue engineering construct is the cells used. Regarding myocardial tissue engineering, the CMs comprise the most considerable cell population and are the target cell to replace lost function after MI. Because they are highly

specialized and do not increase, they cannot be isolated and expanded from a biopsy, unlike other native cells. The main target for producing cardiomyocytes has been stem cells' differentiation. Hematopoietic stem cell therapy has been conducted since the 1950s, when it was first used to save the lives of radiation victims.[73] However, it wasn't until later in the 20th century that the possibility of other therapies became available from stem cells. Embryonic stem cells were first derived from mouse blastocysts in 1981, and almost 20 years later, they were harvested from human embryos.[74] Despite these cells' pluripotent nature and the ability to differentiate into virtually any other cell type, ethical concerns have prevented them from being researched further in the field of tissue engineering.[75] The search for other stem cells has led to the discovery of stem cells in almost all body tissues. However, one of the biggest promises for stem cell therapy came from the discovery of induced pluripotent stem cells by Yamanaka and Takahashi in 2006. By utilizing four signaling proteins, Oct-3/4, Sox2, c-Myc, and Klf4, dubbed the Yamanaka factors, fibroblasts could be reprogrammable into cells capable of differentiating into cells from all three germ layers.[76] The advantage of these stem cells lies in their ability to be programmed from easily biopsied tissue such as blood or skin. These cells can be differentiated into cardiomyocytes by utilizing specific pathways critical to cardiovascular development, such as Wnt, Bmp, and Activin/Nodal/TGF-β.[77-79]

While most tissue engineering research is focused on combing cells with scaffolds which will be discussed, cell sheet technology cannot be omitted as a potential source for cardiac therapies. This technology is designed around stacking monolayers of cells to create sheets **(FIG 1-19)**.[80] To perform this, a surface is treated with a temperature-responsive polymer such as poly(N-isopropylacrylamide) that is hydrophobic at a physiological temperature of 37^{o}C. When the temperature drops below 32^{o}C, it transitions into a hydrophilic surface.[81] Cells will

bind to the hydrophobic surface at 37° but then detach when it becomes hydrophilic. Importantly, these cells retain their ECM structure when they separate from the surface with the decrease in temperature, unlike enzymatic processes like trypsinization, leaving them in a monolayer.[82]

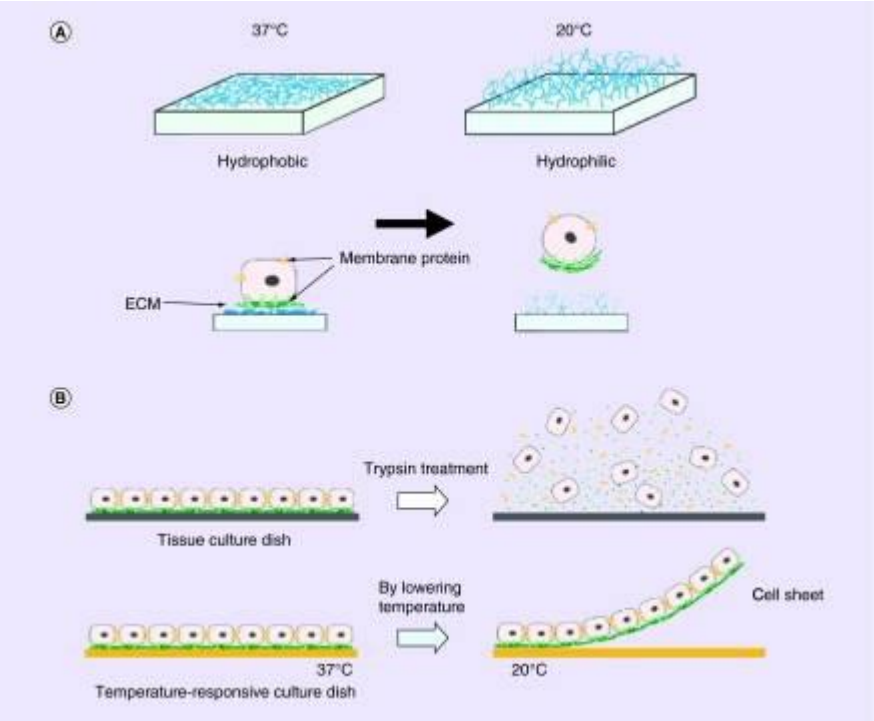

Figure 1-19: Cell Sheet Engineering

Moschouris, K., N. Firoozi, and Y. Kang, *The application of cell sheet engineering in the vascularization of tissue regeneration.* Regen Med, 2016. 11(6): p. 559-70.

1.5.3 Scaffolds

While such scaffold free technologies as cell sheet engineering have displayed some capability in generating cardiac tissue, 3D tissues typically require some form of structure for support. Scaffolds related to tissue engineering come in many forms; however, they all must follow certain criteria to be considered for use. The first and foremost of these is that a scaffold

should be biocompatible to ensure cell viability and integration with the host.[83] Bioresorbable or biodegradable scaffolds are also desired as one of the main effected desires after implantation is that the body should be able to reintegrate the implanted tissue over time into a native configuration. Other criteria related to scaffold preparation are mechanical properties and architecture of the scaffold. Scaffolds should be tissue dependent as tissue of varying mechanical strength and any designed scaffold needs to be strong enough to remain at the point of implantation until it can effectively be reintegrated into the body. Architecture is also important as thick constructs incorporating cells must require some form of porosity to provide the diffusion of nutrients and oxygen.[84]

Scaffolds for cardiac tissue engineering are required to fille all these niches but must specifically modulate the cardiac microenvironment, maintain appropriate substrate stiffness, and have the appropriate electrical conductivity to support healthy cardiac muscle.

One source of scaffolds is the utilization of synthetic materials. These are usually some forms of polymer including poly-lactic acid, poly-glycolic acid, and polyurethane as well as others.[85-87] These polymers are typically researched because of their known biocompatibility and ability to be bioresorbed. Polymers are also typically highly tunable with the ability to make very precise architectures with desired porosity and strength through processes such as electrospinning.[88] Unfortunately, polymer based scaffolds are not the most suited for cardiac tissue engineering as they lack the ability to correctly mimic the native environment of the ECM.

Another source of scaffold is the use of native decellularized(decell). Decell is the process by which a tissue has all of its native cells removed by chemical, temperature, or enzymatic processes.[89] The process by which a tissue is decelled is dependent on its size. Some tissues can be cut then and then undergo and immersion decell but in the instance of

whole organs such as a large mammals heart this is not possible due to thickness of the tissue. In these cases, a perfusion system must be developed that utilized the organs own vasculature to permeate the decell solution though it.[90] This process must be done with some care to remove the cells while also retaining the desired ECM architecture. Considering that decelling a whole heart produces a scaffold that retains the natural SCM, tissue stiffness, and appropriate microenvironment, this scaffold is optimal for cardiac tissue engineering.

1.5.4 Cardiac Patches

While several concepts have been theorized as cardiac patches, the two main branches of this technology are in acellular or cellular cardiac patches. Acellular patches are simpler, easier to produce, and in some cases already exist as potential therapies. One example of this is the CorMatrix Cor^{TM} PATCH, a patch developed from porcine small intestinal submucosa that is designed to be implanted at the time of CABG and ideally will reintegrate with the host tissue and promote cellular repair.[91] Despite these claims the only study analyzing the effectiveness of these patches found that remained compliant at 21 months but exhibited scar formation and no evidence of native cellular ingrowth.[92]

While some autologous epicardial patches have been engrafted such as atrial appendage micrografts, the goal of a translational cardiac patch is a cellulalrized patch that after implantation will form into native cardiac tissue.[93] One proposed method of producing these patches is through the use of bioprinting. Bioprinting is the process by which cells and a scaffold are combined into a 3D structure at the same time. Several bioprinting methods exist including inkjet, pressure assisted, and laser assisted bioprinting.[94] One of the main advantages of bioprinting is the use of biomimetic materials in conjunction with cardiac stem cells. Also depending on the method bioprinting can produce very precise porous scaffolds.[95] The main

drawback of bioprinting is to be able to produce a mechanical strong enough scaffold. Most hydrogels are of low rheological viscosity requiring some form of crosslinker to create a strong scaffold. Most of these crosslinking agents are toxic such as glutaraldehyde or formaldehyde.[96] For this reason bioprinted patches are not currently a suitable pathway for a regenerative patch. Moving on from this the most suitable cardiac patch would come from a combination of the appropriate cardiac stem cells seeded onto a decellularized tissue scaffold. Several studies have concluded that appropriate recellularization of these scaffolds is possible and that this aims to be the best approach to produce a mechanically strong graft.[97-99]

1.5.5 Bioreactors in Cardiac Tissue Engineering

A bioreactor can be simply defined as a vessel that carries out biological reactions and is used to culture aerobic cells for conducting cellular or enzymatic immobilization.[100] At the industrial scale this refers to large spinning flasks or tanks that are used to culture yeasts, bacteria, or other microbes, but concerning tissue engineering, a bioreactor is typically a smaller device capable of fitting into a standard incubator. Bioreactors used in regenerative medicine are custom built depending on specific requirements and conditions designed around the tissue that is to be stimulated. Specifically in the realm of cardiac tissue engineering the three main criteria that are considered when developing one of these bioreactors is mechanical stretch, electrical stimulation, and perfusion. In addition to these conditions, these bioreactors are typically incorporated with some form of ability to change standard conditions to model certain diseases by manipulation of pH, temperature, and biomolecular concentration of certain factors or organic compounds.[101, 102] For example modeling fibrotic conditions could incorporate

TGF-B into the bioreactor media or increasing or decreasing glucose concentrations to model diabetic environments.[103]

Mechanical stimulation of cardiac constructs has a biological basis in the conditioning and development of both CM and CF. Response to change in material stiffness lead to several important biological changes within CM's bolstered by signaling of integrin binding and subsequent activation of receptor tyrosine kinases and GTPases that activate pathways responsible for proliferation, differentiation, and maturation.[104] CFs also respond to mechanical stretch, by activating integrin binding leading to phenotypical changes as well as migration and ECM homeostasis.

Electrical stimulation of CMs leads to improvements in calcium handling, overall contraction force as well as the increase expression of gap junction proteins and cell alignment.[105] While direct stimulation of CFs has not been elaborately studies it is clear that they do have some influence on the modulation of CM activity.[106] A key element of electrical stimulation is the use of electrodes that will not produce a Faradaic redox reaction. For this purpose most bioreactors aiming to have electrical stimulation will have some form of carbon electrode to limit this.[107] Electrical stimulation varies but is typically conducted in a cyclical waveform to simulate the heartbeat and is usually on the range from 1-5V/cm.[108, 109]

One of the first instances of utilizing perfusion in a tissue engineering bioreactor was developed by Radisic et al as a way to combat the diffusion barrier of 100 um.[110] Developing off this several groups have developed perfusion bioreactors to effectively vascularize their tissue constructs. These include bioreactors of porous scaffolds scaling all the way up to whole heart bioreactors.[111, 112]

Chapter 2: Project Motivation, Specific Aims, and Clinical Significance

2.1 Introduction and Clinical Relevance

Cardiovascular disease (CVD) remains the leading cause of death throughout the developed world, frequently due to myocardial infarction and end stage heart failure. Over 600,000 deaths are related to CVD annually in the United States and the economic impact of CVD is expected to rise to 800 billion dollars each year by 2030.[113, 114] Over half of these deaths can be attributed heart failure (HF) which totaled 13% of all US deaths in 2018; 6.2 million Americans are currently living with HF. Myocardial Infarction(MI) is the principle complication leading to HF with over 1 million incidents occurring annually.[115] **It is clear that HF results in a massive concern towards public health as well as an incredible economic burden.**

MI leads to irreversible loss of the specialized muscles cells, cardiomyocytes (CM). As CM's in the affected area die due to ischemia, activated fibroblasts known as myofibroblasts migrate into the area to repair the injury and restore the tissue continuity.[116] These cells will produce a collagenous patch that over time will crosslink into a fibrotic scar.[117] This scar is incapable of replacing the functional cardiac muscle and disrupts the contractility of the remaining muscle tissue, leading to pathological remodeling, ventricular dilation, and wall thinning that is characterized by hypertrophy, fibrosis, reduced ejection fraction, and arrythmias that will lead to HF.[118, 119] **Therapies with the goal of preventing HF should focus on replacing the scar caused by MI with functional cardiac tissue.**

2.2 Current Standards of Care and Limitations:

Current therapies include the administration of medication to reduce stress on the heart, revascularization techniques including coronary artery bypass grafting and percutaneous coronary intervention, as well as ventricular assist devices (VADs) and whole organ transplant. These all have drawbacks: medication does not reverse fibrosis, revascularization only limits the damage done to the tissue, VADs are mechanical and lead to required medications to prevent rejection, as well as chance of failure; organ transplants are limited due to the availability of donors as well as requiring medications. Stem cell therapy has shown to be promising therapy but delivery either through intramyocardial or intracoronary artery injection have only shown slight improvement in cardiac output.[120, 121] The main hypothesis for such outcomes is poor engraftment and integration after delivery, leading to rejection, apoptosis, and lack of differentiation into the required cell phenotypes.[122]

The tissue engineering model can be adapted to address the issue of low cell engraftment after delivery by creating a stable platform and environment for the cells to survive and differentiate appropriately. One of the major problems currently being undertaken within the field is addressing the thickness of tissue constructs. Many engineered tissues are thin (<1mm), as tissues thicker than 100-200um cannot have the appropriate nutrient and oxygen diffusion to prevent cell necrosis.[123] This is fine for disease or drug modeling, but grafts must be thicker (1cm) if they are to replace the transmural infarct scar. Many efforts have been focused on producing vascularized synthetic scaffolds by methods such as bioprinting, but these processes usually produce scaffolds without suitable stiffness to be implanted as well as having errors in adequately reproducing the correct myocardial microenvironment for the proper

differentiation and maturation of cardiac constructs.[124, 125] While many efforts have led to promising results in development of cardiac patches, there are still no clinically available functional cardiac tissues.[126]

Our long-term goal is to develop a biocompatible and highly vascularized cardiac patch, with adequate mechanical and electroconductive properties. To mimic the native ECM, a decellularized porcine myocardial matrix will be used as a scaffold and seeded with mixtures of autologous cardiomyocytes, fibroblasts, and vascular cells.

Our hypothesis is that a perfusion bioreactor, able to provide electrical pacing and mechanical stretch, will contribute to the maturation, alignment, and function of cardiomyocytes and vascular cells seeded onto scaffolds.

2.3 Specific Aims

Three sequential and complementary aims have been prepared with the goal of developing a functional cardiac patch based around the tissue engineering paradigm. The patches will be produced by generating a scaffold, determining optimal cell seeding methods, and conditioning the cell seeded scaffold in a bioreactor under physiological conditions.

AIM 1: To generate a cardiac scaffold that mimics the mechanical properties of the cardiac wall.

Hypothesis: A scaffold with ECM composition similar to the cardiac and vascular wall will maintain the mechanical and biochemical properties of the cardiac wall.

Approach: Cardiac scaffolds will be generated by removal of all cells from porcine hearts. Mechanical properties and matrix composition will be determined using biaxial mechanical testing and histology, respectively.

Innovation: Scaffold technology is centered on producing a scaffold that mimics the native cardiac architecture and the microenvironment that leads to cell differentiation. The fact that our scaffold will not produce an immune response will be confirmed through DNA quantification and histological staining. Histology can also show the retention of vital ECM components; biaxial testing will confirm the appropriate stiffness to mimic the native cardiac ECM.

AIM 2: To fabricate a cardiac patch using cardiac and vascular cells and improving the cell-seeding techniques.

Hypothesis: Cardiac and vascular cells derived from adult stem cells can be optimally seeded onto a scaffold to form a cardiac patch

Approach: Cardiomyocytes, fibroblasts, and endothelial cells derived from adult stem cells, will be optimally seeded into the cardiac scaffold, using perfusion techniques for endothelial cells and injection seeding for cardiomyocytes and fibroblasts.

Innovation: Effectively seeding cells onto scaffolds remains a question to be addressed. Efforts to reseed the endothelial layer of the vasculature will lead to improved cell retention. Injection seeding of myocytes and fibroblasts will be conducted to determine the adequate ratio of these cells as well as the overall cell seeding density.

AIM 3: To develop a perfusion bioreactor for conditioning the engineered cardiac tissue.

Hypothesis: The structure and function of the tissue engineered cardiac patch will be comparable to native myocardium after conditioning in a perfusion bioreactor.

Approach: The cardiac patch will be mounted in a novel bioreactor plate fitted in the FlexCell FX-5000 Compression system. After mechanical and electrical stimulation, the tissue will be analyzed using histological staining and biochemical assays.

Innovation: Stimulation of cardiac constructs is important for tissue development and survival. By customizing our bioreactor with a perfusion element, we will be able to maintain tissue viability, develop thicker tissues, and remove sources of contamination and evaporation of media.

Chapter 3. Aim 1: Generation of a Cardiac Scaffold That Mimics the Mechanical Properties of the Heart Wall

3.1 Introduction

Because of the demonstrated low cell viability in stem cell injections, the concept of pre-seeding cells onto a scaffold mimicking the native ECM to improve viability has been suggested in the field of tissue engineering.[127] An essential consideration in developing scaffolds for implantation is providing the appropriate environment for cells to adhere, proliferate, and differentiate. As well as this, providing adequate mechanical support is paramount to ensuring the stability of the tissue upon implantation. Scaffold stiffness is also essential for cellular differentiation, especially in cardiomyocytes. [128] Considering these requirements, a host of potential scaffold options can be considered, but one of the most promising is the use of decellularized tissues. Decellularization(decell) is a well-studied process typically tissue-dependent and relies on a mixture of chemicals, enzymes, and physical agitation that lyse cells and remove the cellular debris.[89] Notably, the decell process can result in sufficient antigen and nuclear material removal to limit any immunogenic response.[97] The acellular matrix produced by this process acts as a suitable scaffold that retains the requisite environments for cellular engraftment. The remaining structural proteins that comprise the scaffold are typically conserved across mammalian species, so these scaffolds are ideal for allogenic or xenogeneic implantation. In addition to these characteristics, decell can also produce a scaffold that retains the same vascular architecture as the native tissue.[99] The choice of a suitable source of scaffold relies on the ability to closely match the human anatomy with which it is tasked to replicate. For this purpose, we focus on porcine hearts approximately the same size as human

hearts and feature similar anatomical geography.[129] This aim will show that the decellularization of whole porcine hearts can produce a myocardial ECM scaffold that contains the proper microenvironment and architecture for cell engraftment. The scaffold will be free of any remaining cellular or nuclear material, retain a suitable collagenous ECM structure, and retain the mechanical properties of the native cardiac wall.

3.2 Methods

3.2.1 Whole Heart Decellularization

Whole porcine hearts were acquired from a local abattoir immediately after slaughter and transported on ice to the lab for processing. Hearts were examined prior to decell for any incisions from the butchering process that would result in loss of systemic vascular pressure. Upon determination of completely intact hearts, the pericardial sac was removed, and the hearts were prepared by isolation of the aorta and the pulmonary veins. The leaflets of the aortic valved were excised to allow for retrograde flow through the aorta, and then the hearts were weighed for mass loss comparison after decell. The pulmonary veins and aorta were cannulated with a plug, and an inflow tube, respectively, and the hearts were placed in separate decell apparatuses. A reservoir bottle providing the flow into the aorta was placed approximately 1m above the heart containers, and collection reservoirs were placed just below the hearts, which sent the perfusing decell solutions up to the top bottles via a peristaltic pump. The decell regimen consisted of 24-hour perfusion of 30mM EDTA followed by 1% SDS (sodium dodecyl sulfate) with a .02% Sodium Azide additive to prevent microbial growth within the tissue. The total decellularization time within the SDS solution depended on each heart but typically lasted 20-30 days until the heart lost 40% of its initial mass and had turned white. After the decell process was completed, a complete wash of the tissue by perfusion of

distilled/deionized water(ddH20) and 70% ethanol to remove all residual SDS components, and then the final nuclear material was removed by a DNAse/RNAse solution of 720munits. Hearts were then stored at +4°C in PBS with sodium azide and protease inhibitor cocktail to prevent contamination and degradation by endogenous proteases.

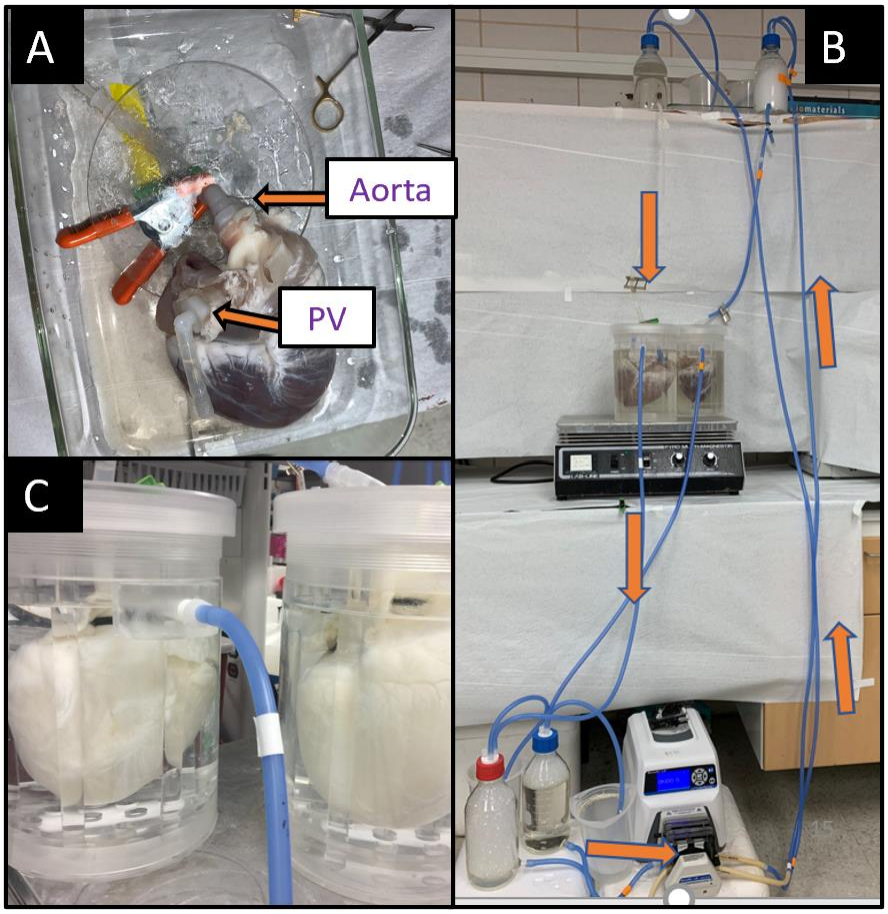

Figure 3-1: A schematic of the whole heart perfusion deceller. A) Recently deceased porcine hearts are cannulated at the aorta and Pulmonary Vein. B) Hearts are placed in custom decell containers that utilize a peristaltic pump to continuously resupply decell solution to upper reservoir bottles. C) After decell, hearts lose approximately 50% of their mass and turn white.

3.2.2 Hydrostatic Pressure Determination

An important point of knowledge for the decell system is the determination of pressure developed by the hydrostatic method. The calculation of the pressure was determined by following the Bernoulli Principle:

$$P_1 + \frac{1}{2}\rho V_1^{\,2} + \rho g h_1 = P_2 + \frac{1}{2}\rho V_2^{\,2} + \rho g h_2$$

Where P1 and P2 are the pressures at two given points in a system, 1/2rho(V^2) is the pressure from kinetic energy, and rho(g)(h) is the pressure determined by the potential energy of the system. Several assumptions can be made to simplify this equation. The kinetic energy component of the system is negligible as the velocity moving through the system is very slow, so this component is negated. We set P1 to the top of the head height where the only pressure is atmospheric and can also be negated. Because we are determining the pressure at P2, the height of the potential energy component is 0, allowing this term to be dropped as well, leaving the equation as this:

$$\rho g h_1 = P_2$$

Where the pressure is solely from the density of the solution, the acceleration of gravity, and the total head height, it was determined that by having an altitude of approximately 1m, the pressure generated at the coronary arteries was approximately 70mmHg.

3.2.3 Tissue Processing and Histology

`To determine the complete decellularization of the whole porcine heart, histology and DNA quantification were used. For histological analysis, sections of the decelled left ventricles and samples from a recently slaughtered porcine heart were excised from the hearts and fixed in 10% phosphate-buffered formalin for a minimum of 48 hours before being processed for paraffin wax embedding. After embedding, 5um sections were prepared by microtomy on glass slides that were allowed to dry overnight in a 56^{o}C oven. After drying, the slides were stored at room temperature for staining.

A standard Hematoxylin and Eosin(H&E) Stain was performed to confirm the removal of the cell nuclei, and other stains were used to characterize the tissue after decell when compared to the fresh tissue. These included Masson's Trichrome for connective tissue and a modified Russell-Movat Pentachrome.

Immunohistochemistry (IHC) was performed to confirm the removal of specific cell markers and any remaining inflammatory markers or other secretory factors. IHC was performed using enzymatic-mediated antigen retrieval (Proteinase K 0.1%) for selected CM markers (Cardiac Troponin(cTnT), Myosin Heavy Chain (MHC), Connexin-43(CX-43)), CF (Vimentin, Heat Shock Protein-47(HSP-47)) and EC (platelet and endothelial cell adhesion molecule 1(CD31), Endothelial Nitric Oxide Synthase (ENOS), E-Selectin, von-Willebrand Factor(vWF)).

3.2.4 DNA Purification

From a fresh and decelled porcine heart, three samples were excised from the septum and ventricular wall each. These samples were then cut to weight (15-20mg). A DNEasy blood and tissue kit from Qiagen (Hilden, Germany) was then used to lyse the tissue overnight and

then purified to pure DNA using mini spin columns and proprietary buffers. After purification, an ethidium bromide/agarose gel electrophoresis was run to detect any resultant DNA using UV light densitometry. The final quantification of DNA was conducted using a Nanodrop Spectrophotometer at an absorbance of 260nm.

3.2.5 Mechanical Properties

The left ventricles of two decelled and two native porcine hearts were isolated. From the native hearts, samples of approximately 1cmx1cm squares were excised based on two anatomical planes, transverse(n=10) and coronal(n=10), to test all three axes. Sections from the decelled heart wall were only taken from the coronal plane(n=10) due to the thinness of the decelled ventricle. The decelled myocardium was isolated by sectioning the decelled ventricle(n=5), freezing the resultant samples overnight, and removing the endocardium and epicardium using a custom tissue slicer and scalpel. All models were stored in PBS, and just before analysis thickness of each sample was measured using a thickness gauge. A biaxial CellScale Biotester was used to test the samples utilizing a specialized program within the companion Labjoy software. Samples were anchored into Cellscale biorakes, and the program was initiated by performing a preload of 100mN to place the sample in tension. After the preload was achieved, a series of 10-second stretch 10-second relax cycles began with one each at 300mN and 500mN before moving to 10 series of 1000mN. The data was then analyzed in Microsoft Excel to produce appropriate stress/strain curves to determine the Elastic Modulus of each sample.

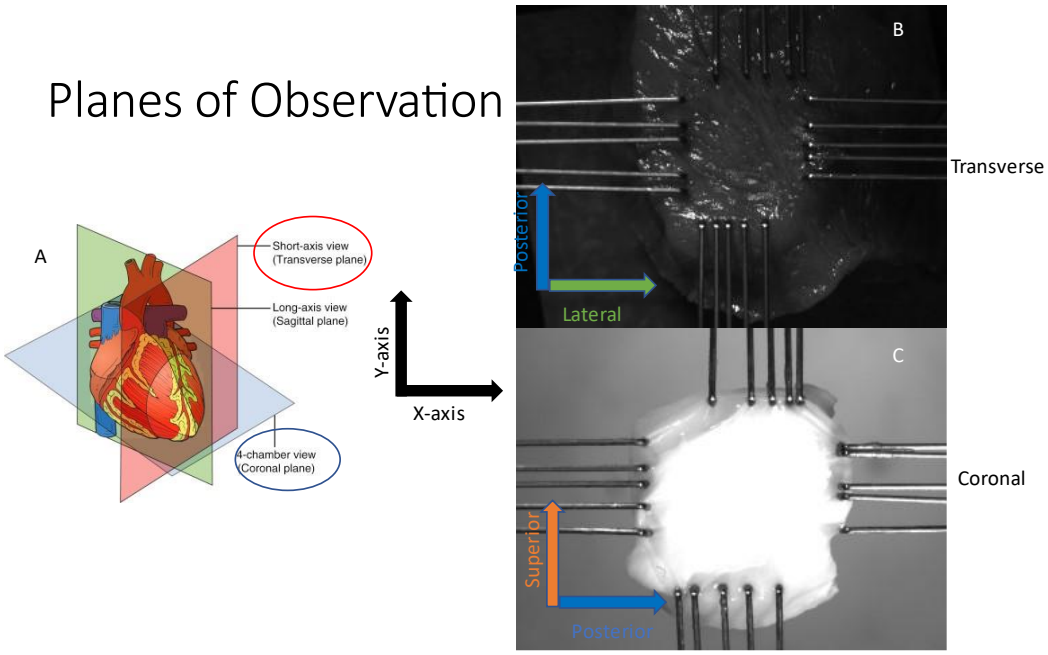

Figure 3-2: Planes of Observation for biaxial mechanical analysis. A) Diagram of anatomical planes concerning the heart wall. B) Fresh myocardial tissue sectioned from transverse plane anchored in Cellscale Biotester with biorakes C) Decelled myocardium sectioned from coronal plane anchored in similar fashion

3.2.6 Statistical Analysis

Quantitative results are reported as mean ± Standard Deviation. Statistical analysis of decell data was conducted using Tukey's student two-tailed t-test within Microsoft Excel. At the same time, all mechanical data groups were completed by one-way analysis of variance (ANOVA) utilizing Minitab Statistical Software. Confidence intervals were set at 95%.

3.3 Results

3.3.1.1 Decellularization Validation

A new group(F) was compared with the two decellularization groups. The first group(A) was performed at a lower pressure of 55-65mmHg, while the second group(B) was at a higher pressure of 70-80mmHg. Fresh tissue was reddish-brown, and as the decell process was

completed, the tissue transitioned into a pale white color. In addition to the color change, mass loss was typically noted at 40-50% of the pre-decelled state, and the tissue went from a rigid to a more malleable consistency **(FIG 3.1)**. Upon completing the decellularization protocol labeled A, tissues were processed for histological analysis and DNA purification. Critically, it was determined that after an H&E stain, all cellular nuclei were not removed from the tissue and the myofibril structure of the myocardium remained partially intact **(FIG 3.3)**. Following an increase in hydrostatic pressure, all cellular nuclei were removed from the tissue.

In addition to the initial histological analysis, DNA was purified and quantified utilizing spectrophotometry. Fresh cardiac samples were estimated at approximately 200-250ng/mg of DNA per weight. While the DNA from Decell A showed a statistically significant decrease compared to the Fresh with samples having less than 100ng/mg of DNA, this was not a low enough concentration to confirm decell **(FIG 3.4A)**. Decell B, on the other hand, showed a significant decrease in the DNA content from Decell A, achieving the <50ng/mg of DNA/sample weight required for decell and over 90% reduction of DNA content from the fresh samples (**FIG 3.4C)**.

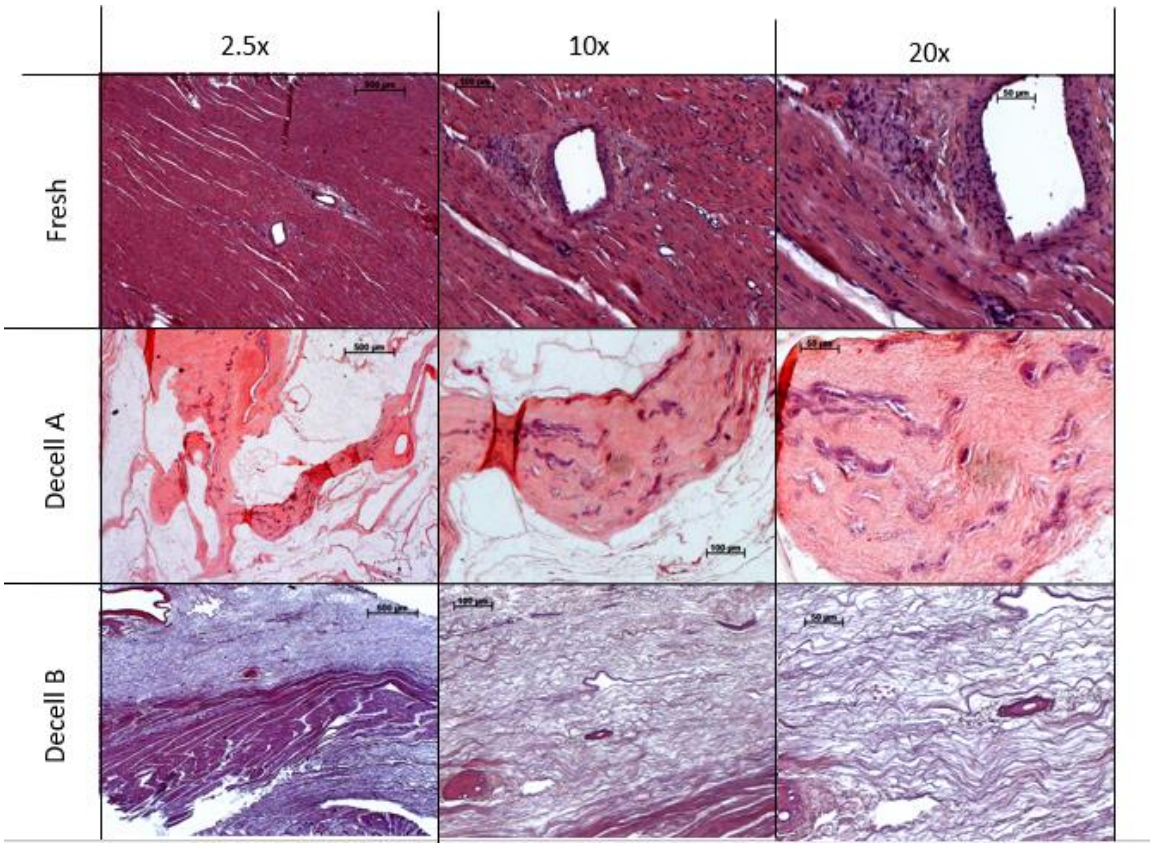

Figure 3-3: Hematoxylin and Eosin stain to confirm cellular removal at 2.5, 10-, and 20-times objective magnification. Fresh Myocardium shows native cell nuclei density. Decell A with lower pressure shows incomplete removal of cell nuclei. Decell B has confirmed the removal of cellular seats.

In addition to DNA quantification of ventricular samples, an ethidium bromide/agarose gel electrophoresis utilizing UV densitometry confirmed the complete removal of DNA content in both ventricular and septum wall samples from decell B **(FIG 3.4C)**. DNA was observed in the fresh cardiac samples as a clear band of non-broken DNA. In the decell B samples, no observed remained DNA would have been displayed as bands of differing base pair length DNA if present.

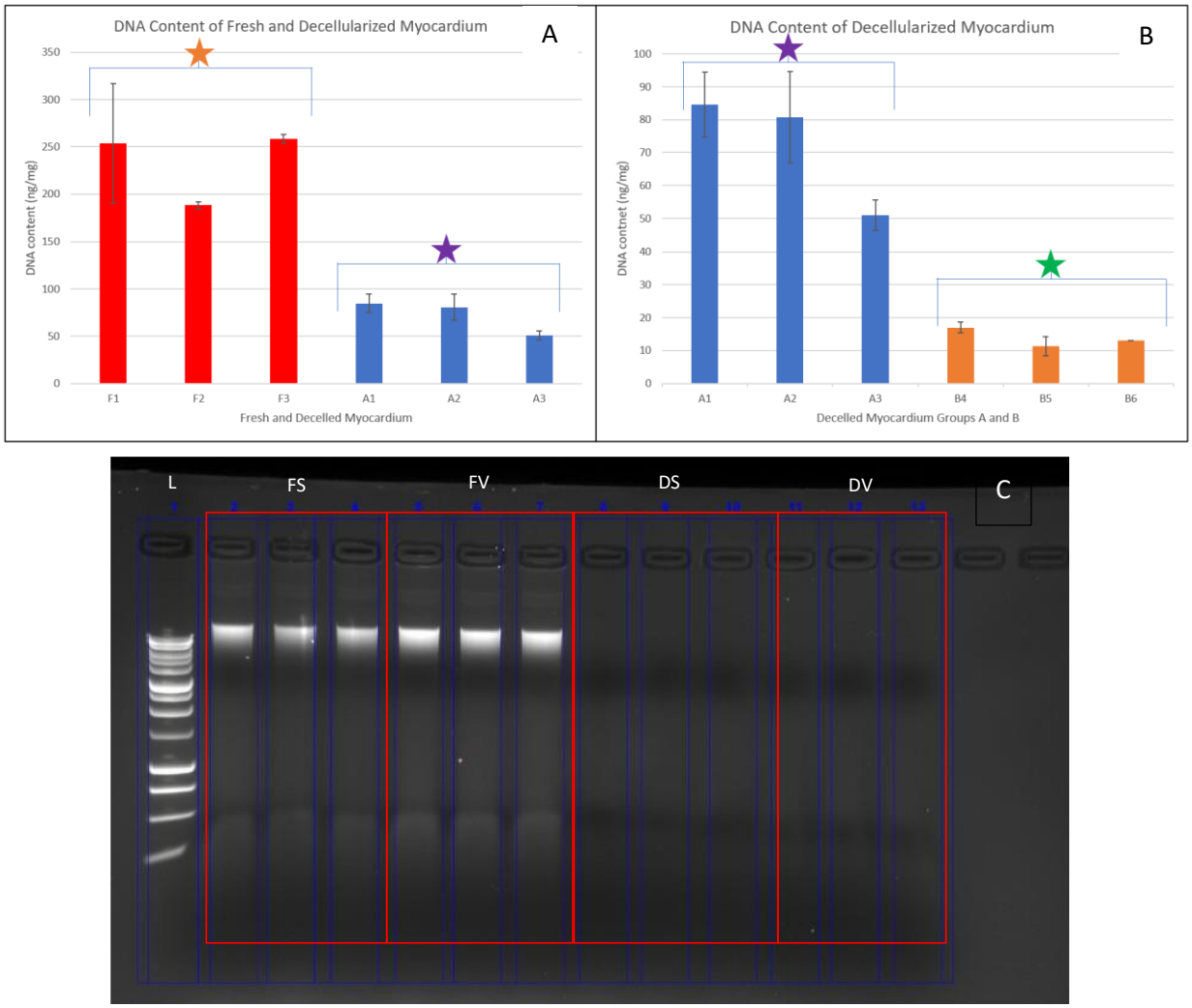

Figure 3-4: DNA characterization of fresh and decellularized samples (units are expressed in ng DNA per weight of the sample. A) DNA is significantly decreased in Decell A (p<.005). B) the decell B method resulted in decreased DNA meeting the threshold for decellularization(p<.04). C) UV densitometry of an ethidium bromide gel displays the non-cleaved DNA of fresh samples of FS-septum and FV-left ventricle. In contrast, no DNA remnants remain in decelled samples of DS-septum and DV-left ventricle.

3.3.2 Histological Analysis

The morphological changes of the decell process could be further identified with the use of Masson's trichrome stain and the Russel-Movat pentachrome stain. Native myocardial tissue is a heterogenous tissue characterized by the vibrant red myofibrils of organized cardiomyocytes with organized ECM collagen and fibrous networks that provide the structural support for the muscle tissue **FIG 3.5**. Also, within the native tissue, the vascular network can be observed. After Decell, the resultant structure displays a deep blue stain of the remaining collagen matrix. Following the trichrome, the pentachrome stain displays the complexity of the ECM of the myocardium before and after the decell **FIG 3.6**.

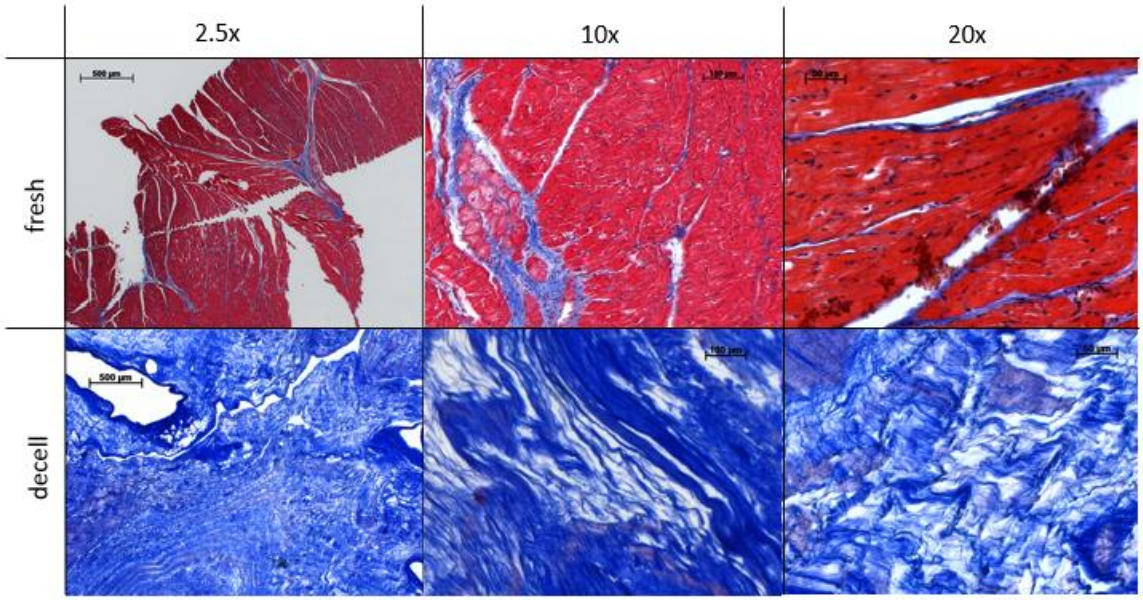

Figure 3-5: Masson's Trichrome Stain of Fresh and decellularized porcine myocardium at 2.5, 10-, and 20-times objective magnification. (KEY: red-muscle, dark blue/black- cell nuclei, blue-ECM/collagen)

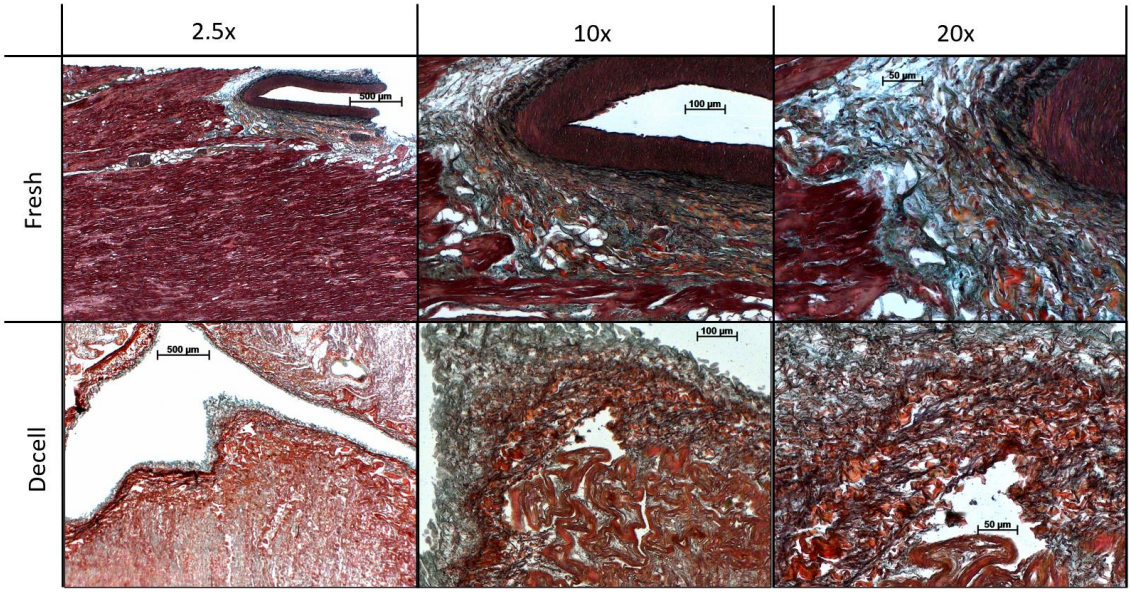

Figure 3-6: Russell-Movat Pentachrome Stain of fresh and decellularized porcine myocardium at 2.5, 10-, and 20-times objective magnification (KEY: dark red-muscle, yellow-collagen/reticular fibers, blue- glycosaminoglycans, black-elastin, dark blue/black-cell nuclei)

Specific cell markers for the primary cardiac cells of interest: CMs, CFs, and ECs, were all observed in the native tissue when conducting Immunohistochemical staining. For CM's, key proteins related to muscle contraction, including MHC and cTnT were observed in the native tissue, and key gap junction marker CX-43 marked the intercalated disk **FIG 3.7**. All three of these proteins were not observed after the decell process. Similarly, HSP-47 and Vimentin, proteins that identify CFs, were present in the native tissue but were also not detected after decell **FIG 3.8.** All endothelial cell markers (CD31, ENOS, E-selectin, vWF) were observed in the native tissue. While no presence of E-selectin or CD31 was detected in the decelled tissue, there was a noticeable presence of ENOS and vWF **FIG3.9.**

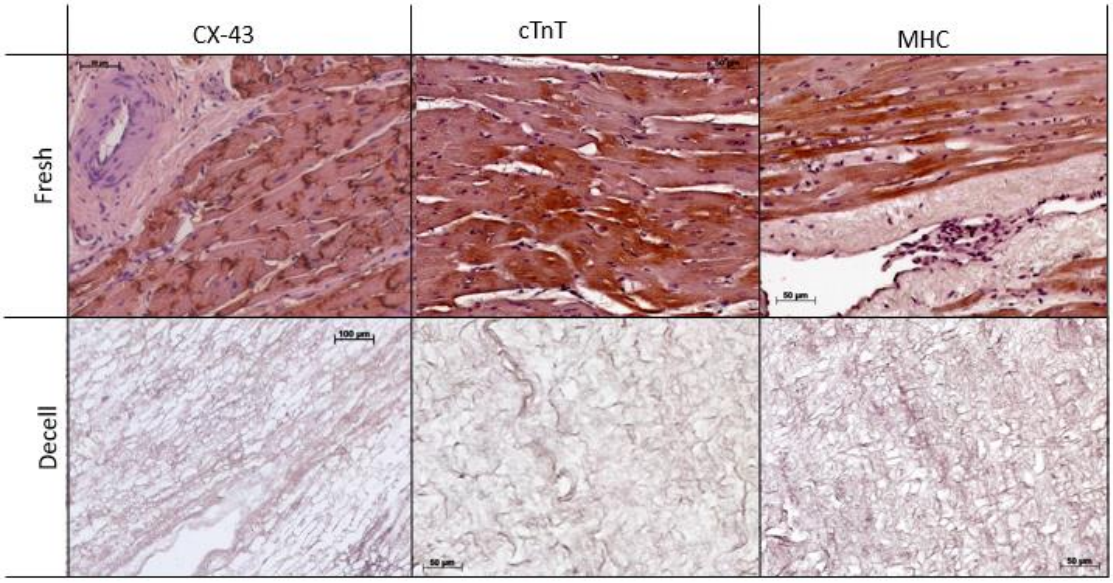

Figure 3-7: Immunohistochemistry for CM positive cell markers at 20 times objective magnification

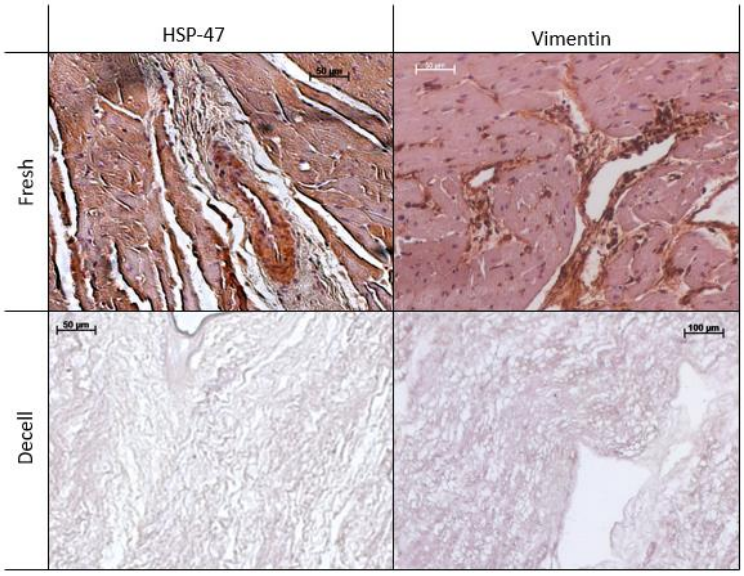

Figure 3-8: Immunohistochemistry for CF positive cell markers at 20 times objective magnification

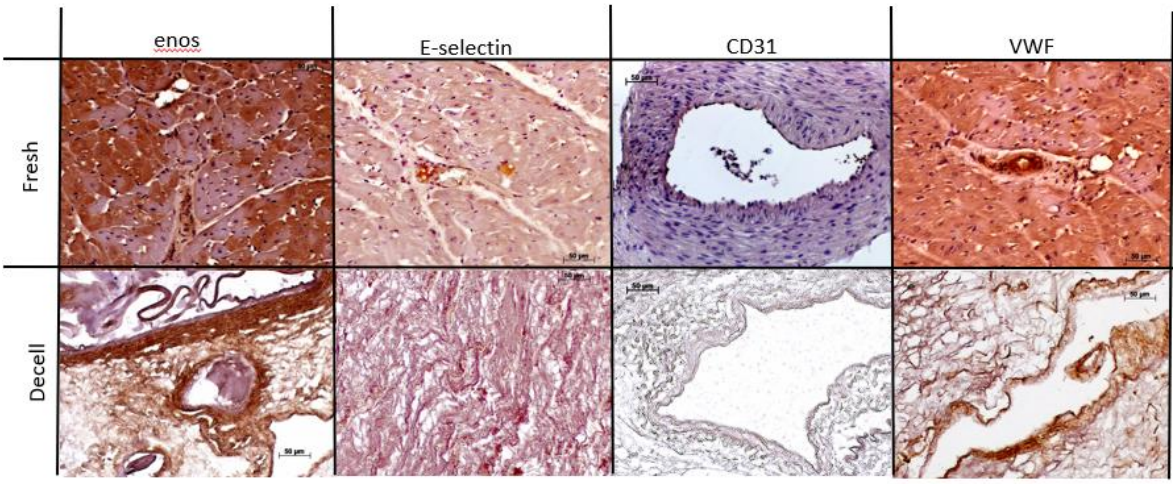

Figure 3-9: Immunohistochemistry for EC positive cell markers at 20 times objective magnification.

3.3.3 Mechanical Characterization

The elastic moduli across all samples reported values in the single digit kPA range **FIG 3.10**. The mean values of the stress/ strain plots display some but not significant variation in either axis of any sample. The shared axis between both transverse and coronal planes was the anterior/posterior axis in the fresh model, resulting in similar values. The stress-strain plots of the decelled tissue were significantly higher in both Superior/Inferior groups and the Y anterior/posterior group but not in the O group **FIG3.11**. The elastic moduli, as reported in **FIG 3.11,** show slightly varied values as they were derived from the slope of the curves from 0-10% elongation, where the stress/strain curves were determined to be in elastic deformation.

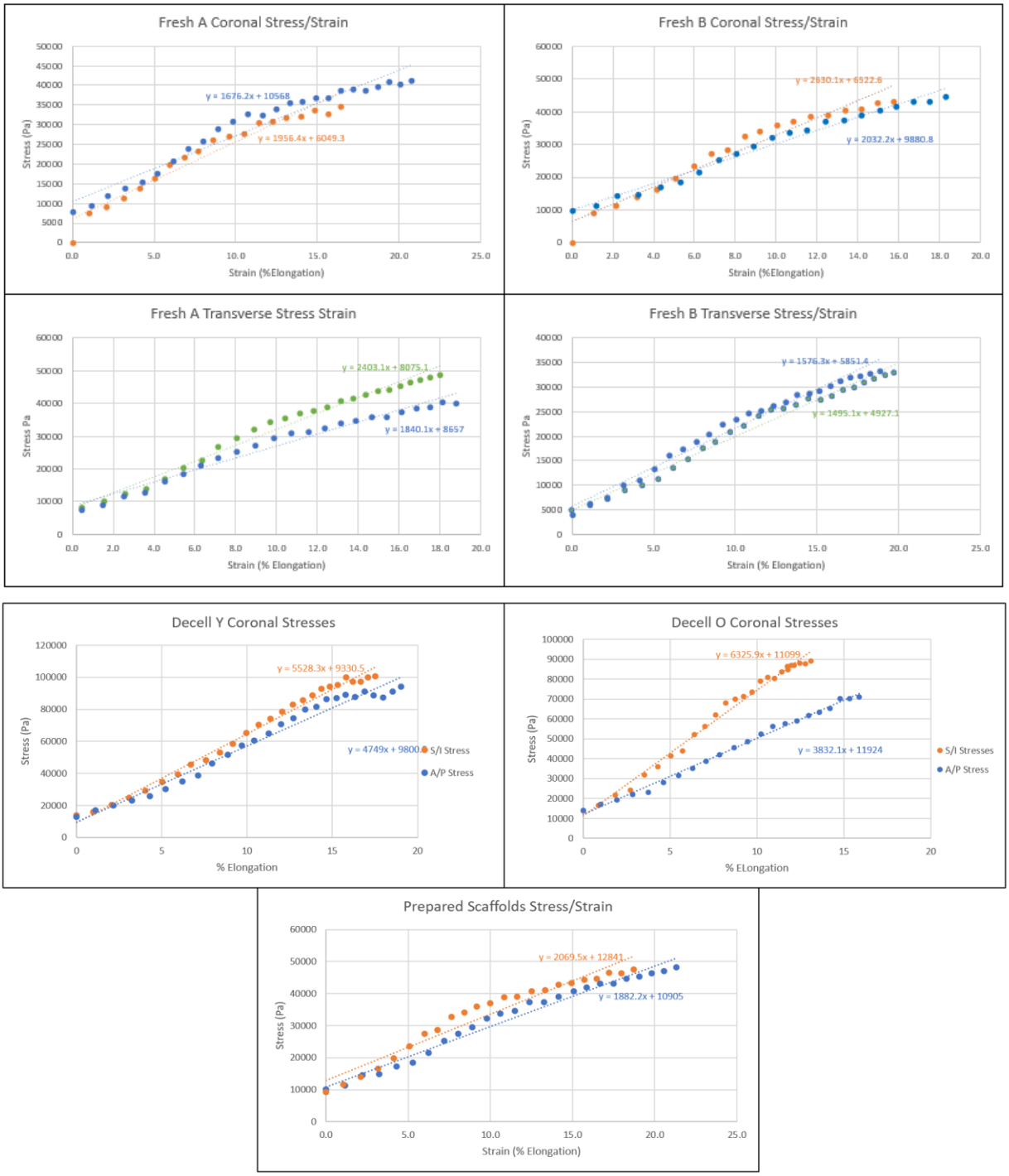

Figure 3-10: Stress/Strain Plots of mean values of biaxial testing of native myocardium, decelled heart wall, and prepared scaffolds. (Orange Superior/Inferior axis, Blue-Anterior/Posterior axis, Green-Lateral/Medial axis)

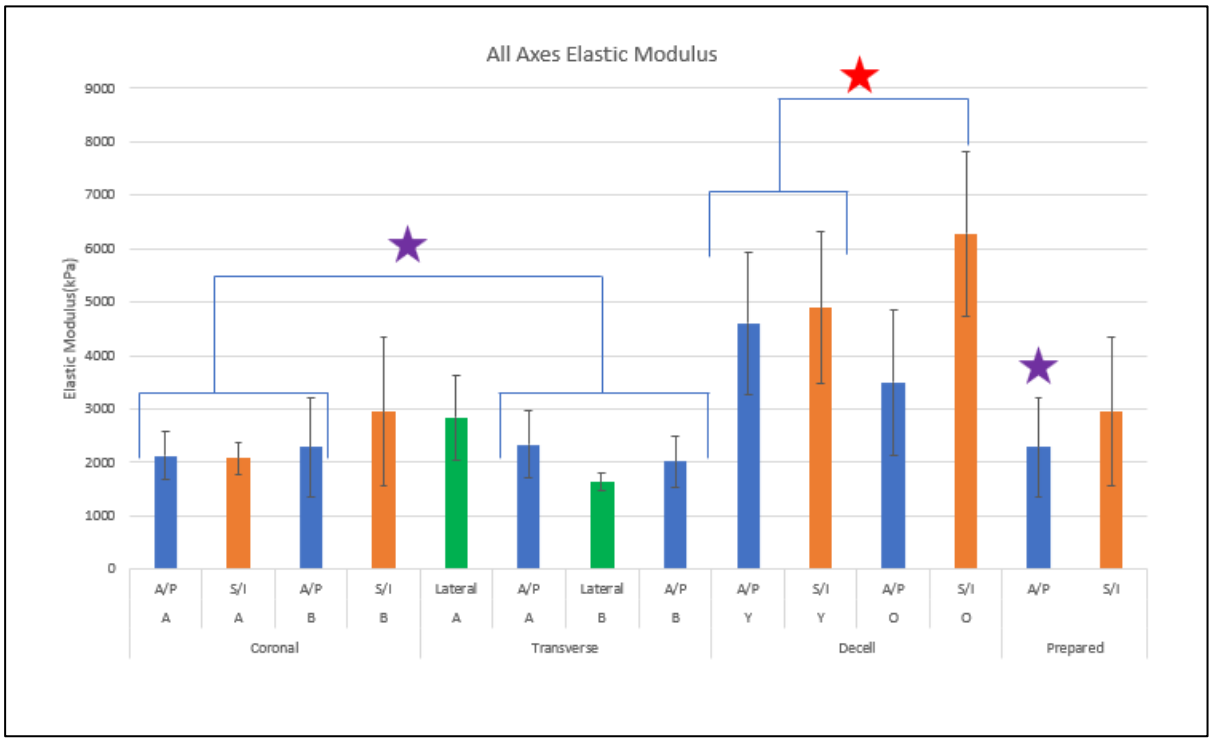

Figure 3-11: Elastic Moduli of Each Sample Axis. Fresh Hearts were designated A and B, Decell Hearts were designated Y and O. A/P refers to the anterior/posterior direction, S/I the superior/inferior, and lateral to the lateral/medial direction. Elastic Moduli are expressed in Pa. Statisical Difference noted between Red and Purple starred groups (p<.05)

3.4 Discussion

This study showed the capability of decellularizing a porcine heart and the suitability of such a construct for use as a Tissue Engineering scaffold. Many pathways to decellularization have been previously researched. However, we have decided on a surfactant-based decellularization protocol utilizing SDS as this is efficacious in removing cells without significant degradation to the underlying matrix.[99] Because the entire ventricular wall is desired to be used as a therapeutic patch, it required the use of a perfusion-based protocol that would use the existing vasculature to decell the heart as the whole wall as immersion-based decell would

not be sufficient to penetrate through the approximately 1-2cm porcine cardiac wall.[130] The one concern using a surfactant-based method is the innate toxicity to living cells, so a thorough wash protocol was used to remove in remaining SDS. Finally, any residual nucleic acids may result in an immune reaction. Therefore the enzymes RNase and DNase were used to clear these remnants. Clearly, the second decell group B resulted in improved cellular and nuclear removal. This can be prescribed to increase the pressure closer to what end-diastolic pressure would be in the native heart; however, the author would like to note that familiarity with the procedure could also have resulted in better outcomes within the decell.

The histological analysis addressed several critical points in determining the appropriateness of the decelled myocardium as a scaffold. The first and foremost of these was to display the complete removal of the native cell population. After this, any morphological changes in the remaining matrix could be identified. As is expected, when large cells such as the CMs are removed, a large volume of the heart is decreased. This can be observed macroscopically as the tissue thins and changes color but becomes even more apparent under the microscope. While some evident fibers do not degrade despite the precise removal of cells, a vast area of void spaces can be observed. This ideal space allows new cells to be injected and have room to migrate through the tissue. Additionally, the histology shows the preservation of vital structural proteins such as collagen and elastin and other basement proteins such as the GAGs, which are crucial in cell signaling roles. The vasculature can also be preserved under the microscope, although thick muscular arterial walls are shown to be degraded by the effects of the decellularization, removing the smooth muscle cells in the medial wall of these vessels. Finally, the immunohistochemistry analysis displayed vital proteins that are expected to be present in the native myocardium. Identifying these markers as potential proteins of interest in

a reseeded tissue is essential and confirming their removal during the decell. As expected, the CM(CX-43, MHC,cTnT) and CF(HSP47, Vimentin) markers were seen in the native tissue and were not identifiable after decell. On the other hand, the EC markers CD31 and E-selectin were not observed after decell, but vWF and ENOS were present. An explanation for vWF is that this is a secretory protein key in the blood coagulation process that can bind to collagen, explaining why it is preserved.[131] Meanwhile, ENOS being conserved could be due to the evidence of the histology showing what appears to be an occluded artery. Hence, the likely explanation for its presence is its expression by platelets that do not contain cell nuclei.[132] Interestingly, despite this occluded artery, the surrounding tissue appears to be decelled, so although there is the possibility of a clot being present, the decell was still effective. One note of consideration regarding the presence of these proteins is the importance in future studies to re-establish the endothelial lining, as it can be expected by the presence of vWF that any graft utilizing the vasculature could be susceptible to thrombus formation and embolism.

Finally, mechanical testing was conducted to ensure that a scaffold produced from a decelled tissue would exhibit the same mechanical characteristics as native tissue. Muscle tissue is anisotropic, having higher stiffness in the cross fiber or transver direction but greater ability to stretch before failure in the longitudinal direction.[133] Still, as opposed to the myofibers of skeletal muscle tissue, the cardiac tissue was observed macroscopically and microscopically to be highly heterogeneous, with muscle fibers' direction being difficult to identify during sample preparation. This led us to believe that axis-dependent stress should be mostly equal due to the organization of these fibers, confirmed in the data collected from the fresh samples. Concerning the decell samples, it was noted that the calculated young's modulus of these samples was significantly higher in three groups than in several of the native tissue. This result most likely

depends on the epicardial layer not being removed before the samples are tested. The epicardium is more fibrous and has greater reported elastic modulus values than the myocaridum.[134] This is confirmed due to the removal of this layer for scaffold preparation resulting in similar results as the native tissues.

3.6 Conclusion

Here we have displayed the ability to completely remove cells from a whole porcine heart and have demonstrated that no remaining cellular or nuclear components remain. In addition, this decelled tissue has the correct mechanical characteristics to be used as a cardiac scaffold. Other examinations of the decelled myocardium showed removal of specfic cell markers of interst in later re-seeding studies as well as appropriate voids for injected cells to integrate into the matrix. With all of these criteria under consideration it has been determined that the decellularized porcine myocardium will create a suitbale scaffold for a cardiac patch.

Chapter 4- AIM 2: Fabrication of a Cardiac Patch Using Cardiac and Vascular Cells and Improving Cell Seeding Methods

4.1 Introduction

Producing an epicardial patch requires combining grafting cells with a chosen scaffold. Acellular matrix scaffolds have the desired mechanical properties and a natural vascular network selected in a patch, but successfully incorporating cells into these patches remains a challenge. While bioprinted or other molded patches can be produced by merging the scaffold and cells at the time of generation, cells seeded onto a decelled scaffold require incorporation by a different method. Injection or cell surface seeding are both methods by which cells have been engrafted onto a scaffold with varying levels of success. Injection seeding is effective at engraftments throughout the thickness of the scaffold but cannot type correctly disperse cells uniformly. On the other hand, cell surface seeding is effective at uniform dispersion of cells onto the surface of the scaffold but then relies on the cells to migrate deeper into the scaffold.

To effectively seed our decelled scaffold, we will look to combine these methods to produce a cardiac patch. Several injection methods will be observed to determine the best engraftment technique for CMs and CFs. In contrast, a custom surface seeding method will be used to reform the endothelial lining of the vasculature. Injection methods will include optimizing the correct cell seeding density and volume and looking at the differences between the engraftment of cells using a standard needle and syringe or a custom-built injection seeder, the Cytoseeder, developed by our lab. To reform the endothelial lining, large patches of the decelled ventricle will be excised from the decelled heart. Using the main coronary arteries, a perfusion seeding will be used to disperse the cells into the vasculature.

4.2 Methods

4.2.1 Scaffold isolation and sterilization

Decelled porcine hearts were removed from their storage solution of PBS with .02% sodium azide and .001% protease inhibitor. The left ventricle was then excised from the decelled heart. Approximately 3cm in diameter rounds were then cut from the ventricle and allowed to freeze overnight. The following day the ventricular discs were set into a custom tissue slicer that removed the endocardium and epicardium of the ventricular wall leaving the decelled myocardium. After isolation of the myocardium, the samples were placed in several washes of PBS to remove any remnants of the storage solution and then placed into a 0.1% peracetic acid solution in PBS that had been titrated to a pH of 7.4 and then sterile filtered for 1 hour. After sterilization, the excess peracetic acid solution was removed via several washes of sterile PBS and stored at 4^{o}C. Forty-eight hours before cell seeding, the myocardial scaffolds were placed in sterile cell culture media (DMEM w/ 10% FBS, 1%ab/am).

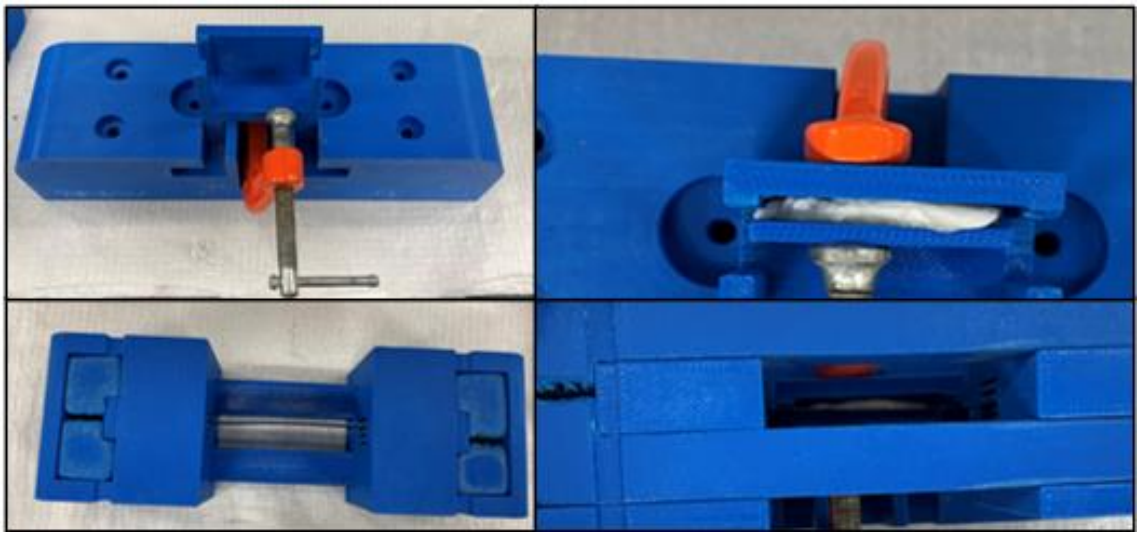

Figure 4-1: The myocardial scaffold slicer. A)The base of the slicer B) The cutting attachment with microtome blade. C) Frozen decell ventricle placed in slicer D) using slicing attachment to isolate myocardium

4.2.2 Ventricular Flap Preparation

After decell, whole hearts were examined to access the coronary artery. After examination, a portion of the left ventricle was removed containing the left descending coronary artery. The artery was cannulated via barbed polypropylene fitting connected to ¼" surgical tubing. A PBS solution containing Red Dye 40 was perfused through the blood vessels to ensure that the vasculature remained patent. Another flap was prepared accordingly and placed into a preliminary endothelialization device consisting of a standard neck 500mL bottle with a ported lid with inflow and outflow tubes connected via Luer fitting. The flap was connected to the bottled inflow tubing, and another line was set higher than the flap to remove excess fluid. The bottle was filled with a PBS solution and then connected in sequence with a barbed 500mL bottle serving as a reservoir connected to a peristaltic pump working to circulate the flow of the solution. Fast Green FCF was then added to the reservoir bottle, and the dye was observed

moving from the reservoir into the vasculature of the flap. Another flap was prepared and then placed into this endothelialization setup and sterilized utilizing several washes of PBS followed by a 1-hour circulation of 0.1% peracetic acid in PBS (pH7.4) followed by several washes of sterile PBS. The flap was then immersed in standard cell culture media (DMEM, 10%FBS, 1%ab/am) 48 hours before cell seeding studies.

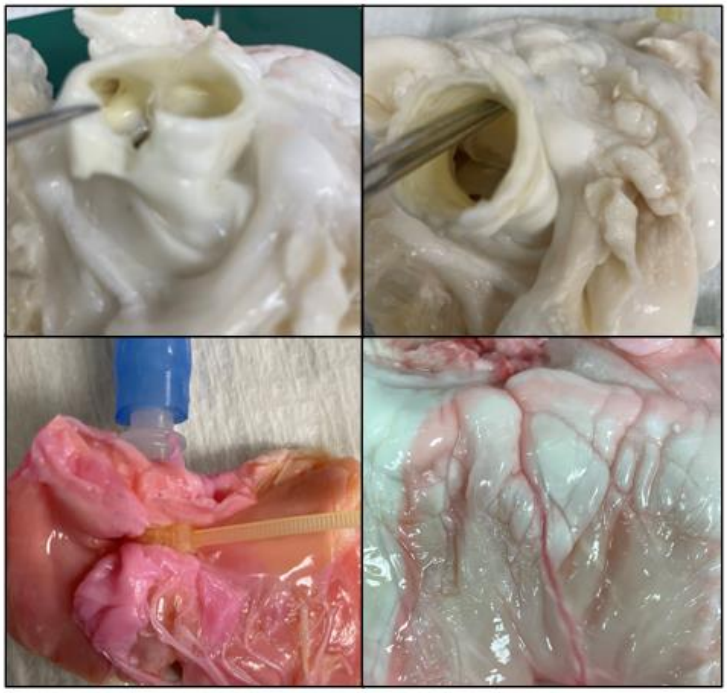

Figure 4-2: Cannulating the coronary artery. A) Observation of coronary artery in decelled heart B) Utilizing tool to follow the path of the artery. C) Utilizing cable ties to anchor hollow bard connected to surgical tubing. D) Perfusion of decelled ventricular wall with a dyed solution.

Figure 4-3: Time lapse of perfusion of dyed solution through the ventricular flap

4.2.3 Mammalian Cell Culture

Cells used in this study were Human Adipose-Derived Stem Cells (ADSC) (Invitrogen), Porcine Valvular Endothelial Cells (pVEC) (Isolated), and Human CMs and CFs (Promocell). The hADSCs and pVECs were removed from LN2 storage and plated at 4000-6000 cells/cm^2 in standard cell culture media (DMEM,10%FBS,1%ab/am). Upon reception of the hCM and hCF, they were expanded using myocyte growth medium or fibroblast growth medium and plated at seeding densities of 10,000-12,000 or 4000-6000 cells/$cm^{2,}$ respectively. Upon reaching 80-90% confluency, the cells were detached from the cell culture flasks using 0.25% Trypsin/0.1% EDTA. The respective cell culture media was then used to neutralize the Trypsin/EDTA, and the cells were aspirated into a centrifuge tube. The cells were spun down in a centrifuge (ThermoFisher) at 200g for 5 minutes, and then the cells were resuspended in media. A sample of 18uL was removed from the cell suspension, which was then taken to be counted using a Luna Fluorescent Cell Counter. 2uL of acridine orange was pipetted into the sample before a 10uL sample was removed to be counted. After the cells were counted, they were replated into the appropriate cell culture flasks at their specified cell seeding density. After expansion, the cells

were either passaged for experimental use or frozen for storage. To freeze the cells once an appropriate number had been expanded, typically 20*10^6, the cells were detached and then combined w/ 5% DMSO for cryopreservation in cryovials before being placed in a Mr. Frosty Freezing container and placed in a -80^{o}C freezer overnight. The next day the vials were moved to a liquid nitrogen tank for long-term storage. For experiments, cells were passaged and counted and then diluted to an appropriate density and plated or injected at study-dependent concentrations.

4.2.4 Immunofluorescence Staining

Human CF and CM were plated in 6 well plates and allowed to reach confluency. The cells were then rinsed in warm PBS and fixed in 4% paraformaldehyde for 30 minutes. The cells were then permeabilized in 0.2% triton for 5 minutes and then rinsed with PBS. Non-specific antibody binding was achieved using a 5% Bovine Serum Albumin in PBS. Primary antibodies for hCF marker (Vimentin) and hCM markers (CX-43, MHC, cTnT) were added to the blocking solution overnight at 4^{o}C. The cells were then rinsed with PBS, and Alexa Fluor secondary antibodies were added for 1 hour at room temperature.

4.2.5 Sterilization and Antiseptic Technique

All stainless steel, glass, and other materials suitable for steam sterilization were placed in sterilization bags and autoclaved for 30 min at 121^{o}C. Other materials unable to be autoclaved were placed into gas permeable sterilization bags, set in an Anprolene Gas Sterilizer, and exposed to ethylene oxide for 24 hours. All sterile studies were conducted inside a biosafety cabinet on a sterile field, and sterile surgical gloves were used to limit the risk of contamination.

4.2.6 Injection Seeding Study

Four myocardial scaffolds were aseptically removed from their media and placed into a sterile petri dish. The Cytoseeder and a syringe fitted with a 27 $^{1/2}$G needle were then used to inject each scaffold with 5x10^5 ADSCs in either a 1mL injection or three separate 1mL injections. After seeding, the scaffolds were placed in a 6-well plate with 2mL of media each and allowed to incubate overnight. The following day PrestoBlue Cell Viability and a Live/Dead Fluorescent stain were used to determine the cells and density in each scaffold.

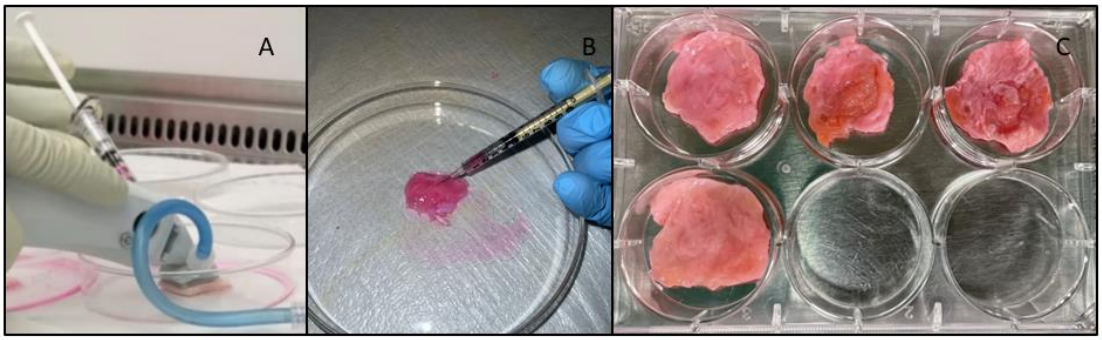

***Figure 4-4: Injection methods with A) Cytoseeder and B) syringe injection. C) Injected scaffolds in* 6-well plate**

4.2.7 Endothelialization Study

An Endothelialization Perfusion Seeder was developed by designing a custom ported lid for a wide mouth 500mL bottle in Solidworks and then 3D printed in nylon on HP's Multi Jet Fusion 3D printer. This wide-mouth bottle was used as the main seeding chamber for the ventricular flap. A double barbed standard 500mL bottle was fitted with a vented cap and used as an upper reservoir to deliver hydrostatic pressure. A peristaltic pump was used to maintain the volume of the ventricular chamber and the media height of the upper reservoir. All tubing and chambers were coated with Sigmacote (Sigma-Aldrich) to prevent cell adhesion to the

setup. A seeding study was conducted by taking a sterile ventricular flap and attaching it to an inner port of the seeding chamber lid before being placed into the chamber. A 5mL injection of bovine fibronectin (200ug/mL) was then administered to improve cell engraftment via Luer lock connected surgical tubing. The chamber was placed in an incubator overnight. The following day, the vasculature was flushed with fresh sterile media, and then an injection of 3x10^6 ADSCs in 1 mL of media was administered. The cells were allowed to attach statically for 2 hours before the upper reservoir was added to begin hydrostatic pressure perfusion. An empty 250mL bottle with a vented cap was added to the final port to prevent pressure buildup and vacuum in the seeding chamber. The perfusion seeding was allowed to continue overnight. The following morning the peristaltic pump was directly attached to the inflow of the main coronary artery, branched, and washed any cell accumulation or blockages for two hours. The flap was removed and sectioned into descending 1cm for analysis by cell viability assays and histology.

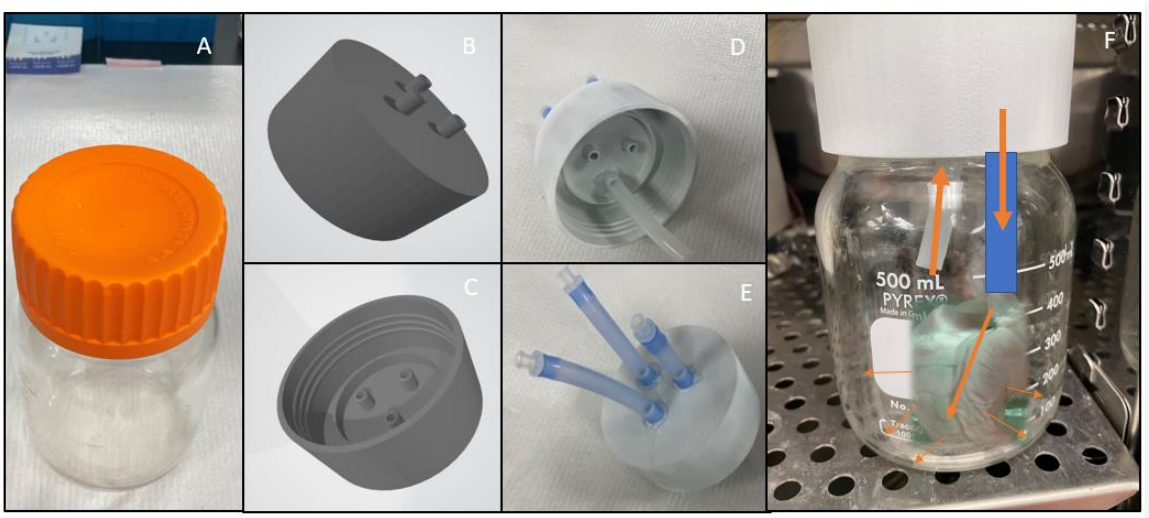

Figure 4-5: Endothelialization system. A) a standard 500mL wide mouth bottle and lid. B-C)3D rendering of the new lid. D-E) 3D printed lid with attached tubing ports. F) New bottle lid fitted to the bottle

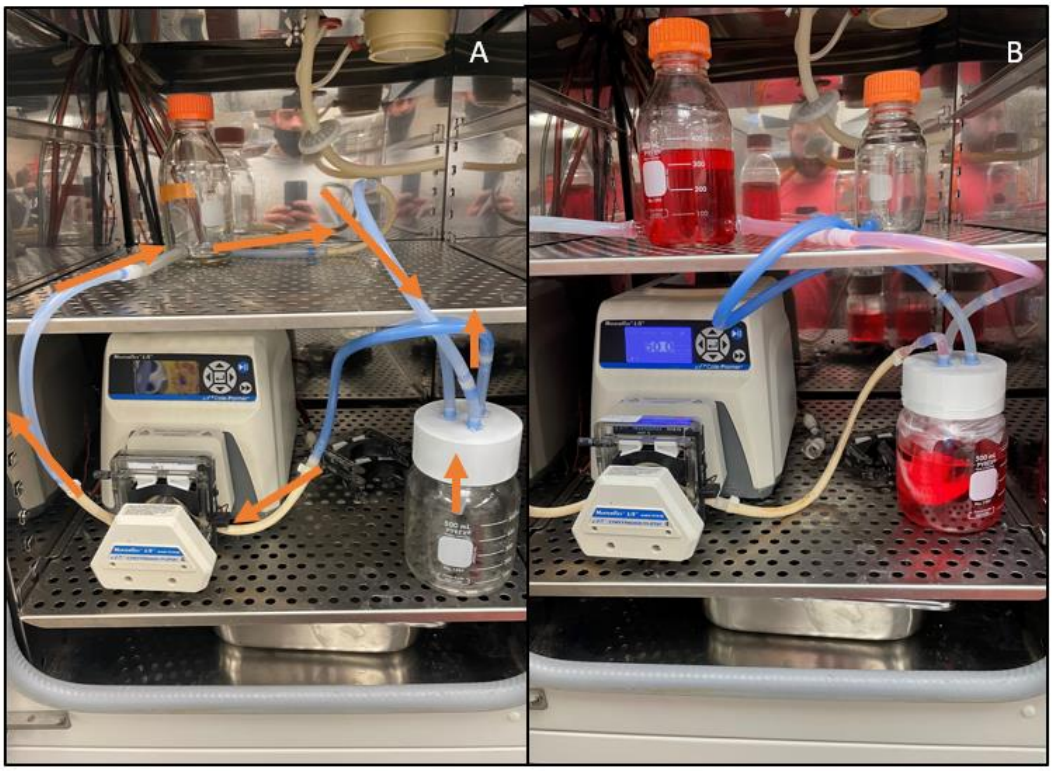

Figure 4-6: Endothelialization Seeder A) path of flow B) full setup with pressure relief bottle

4.2.8 3D Cardiac Patch Injection

Myocardial scaffolds were prepared, and studies were carried out using syringe injections utilizing the 1mL syringe injection. Patches were injected with either CMs or CMs+CFs (n=3 per group). The group of CM+CF patches was seeded at a ratio of 2:1 CF:CM for a total of 3 million cells per patch. The CM patches were seeded with 8 million cells per scaffold to observe the effects of increased cell seeding density. The patches were placed in 6 =-well plates and allowed to sit statically for seven days in an incubator. After seven days, tissues were sectioned for cell viability and processed for histological analysis.

4.2.9 Combined Perfusion and Injection Patch Seeding

Two ventricular patches were prepared as previously described and given a fibronectin treatment overnight in parallel. They were then injected with 25 million pVECs and followed the endothelialization protocol. The following day after the media wash, each scaffold was isolated into 3cm discs and injected with a CM+CF cell injection of 4 million cells with a ratio of 3:1 CM:CF. After one day, the tissues were sectioned for cell viability and processed for histological analysis.

4.2.10 Presto Blue Cell Viability

PrestoBlue cell viability reagent (ThermoFisher) was diluted at 1:10 dilution in DMEM. To create a standard curve, known cell populations (ADSC) were added to a 6-well plate from 5x10^3-1x10^6. 1 mL of the PrestoBlue media solution was added to each well and allowed to incubate for 30 minutes at 37^{o}C 5%CO2. The solution was removed from the wells and read on a fluorescent plate reader at 530nm excitation/590nm emission. A standard curve was then established to determine cell # per unit fluorescence.

4.2.11 Live/Dead Fluorescent Staining

2D cell culture and 3D scaffolds were rinsed with PBS and then immersed in a 4mM Calcein AM/2mM Ethidium homodimer (molecular probes) solutions and incubated for 30 minutes at 37^{o}C. Live images were taken at 488nm, and dead images at 594nm.

4.2.12 Tissue Processing and Histology

Tissue Processing and Histological Staining followed the same protocol in Chapter 3, AIM 1.

4.3 Results

4.3.1 CM and CF cell markers

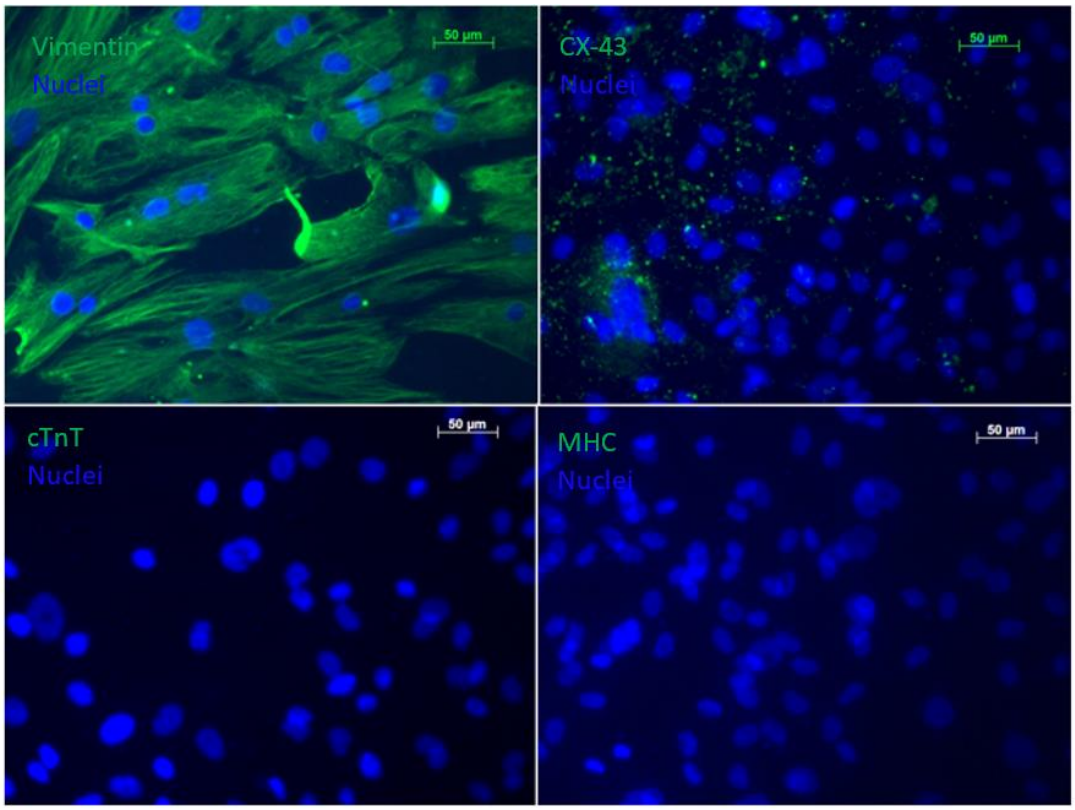

Figure 4-7: Immunofluorescent cell markers were observed for Vimentin(hCF) and CX-43(hCM. cTnT and MHC were not readily observed in the 2D culture of the hCM. (all scale bars 50um)

4.3.2 Cell Injection Validation

In the cell injection study, a higher number of cells was observed for the syringe injection in only 1mL of media with approximately 2x10^5. The Cytoseeder using a total of three 1mL injections had the second highest cell count at 1.75x10^5and the 3mL syringe injection, and 1mL Cytoseeder were at about 1.5x10^5. In the live/dead stain, cells were found alive in each scaffold, but the highest density was observed in the 1mL syringe injection, with smaller cells being kept in the other groups. Groups were labeled S1) syringe injection/1mL, S3)- syringe injection.

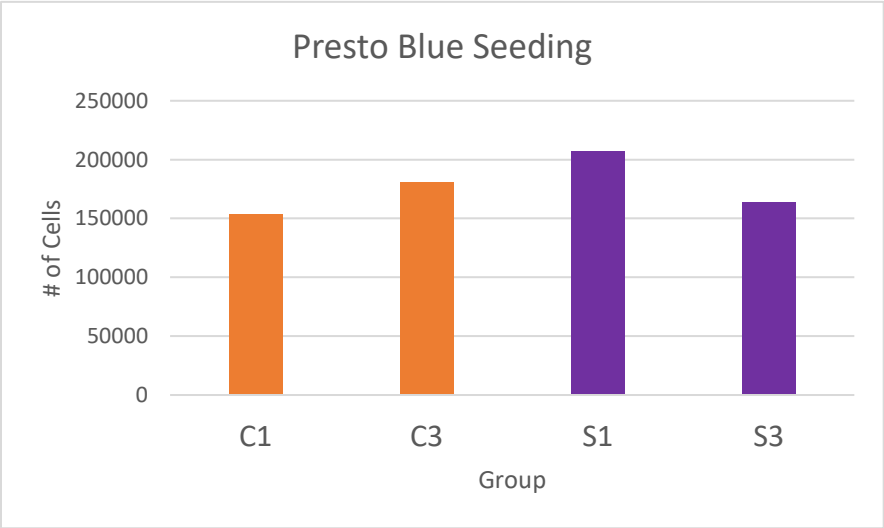

Figure 4-8: PrestoBlue Cell Counting

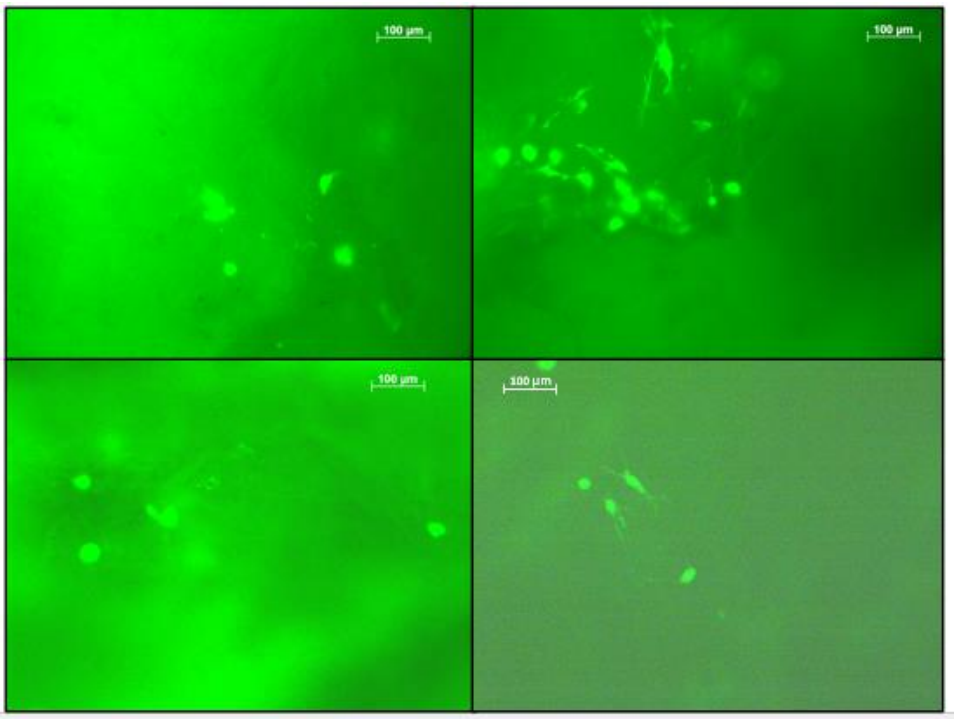

Figure 4-9: Live/Dead Fluorescent images of injection groups (all scale bars 100um)

4.3.3 Endothelialization Study

Live/Dead staining confirmed the presence of living cells with minimal loss of viable cells. Viable cells were noted in the main coronary artery branch and descending sections, each 1cm further down the ventricular flap (**FIG4-10)**. Histological analysis observed cell populations in the descending coronary artery and a branch off this vessel (**FIG 4-11)**. Deeper into the tissue, cells were observed to have adhered to vessels of varying inner diameters from several hundred microns down to <100um **(FIG 4-12)**.

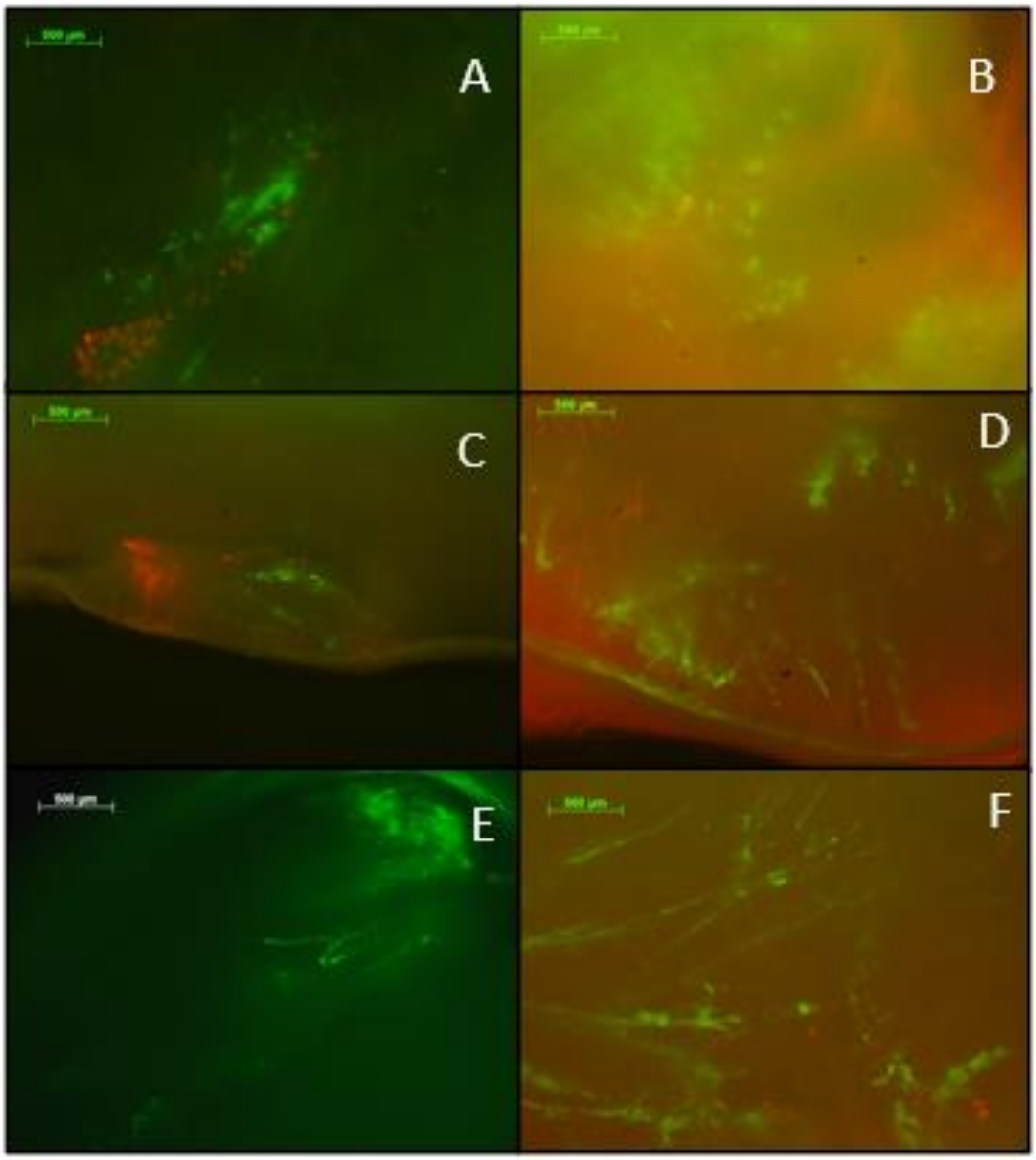

Figure 4-10: Live/Dead staining of the ventricular flap after seeding vasculature with ADSCs. A-C) Images down the main coronary artery D)1cm from the main artery E) 2cm from the main artery F) 3cm from the main artery (all scale bars 500um)

A

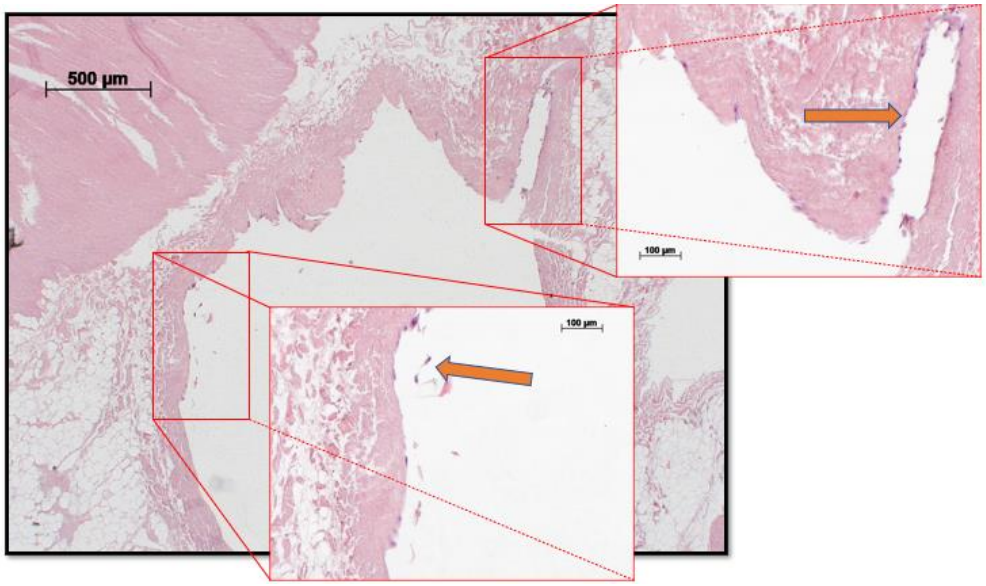

B

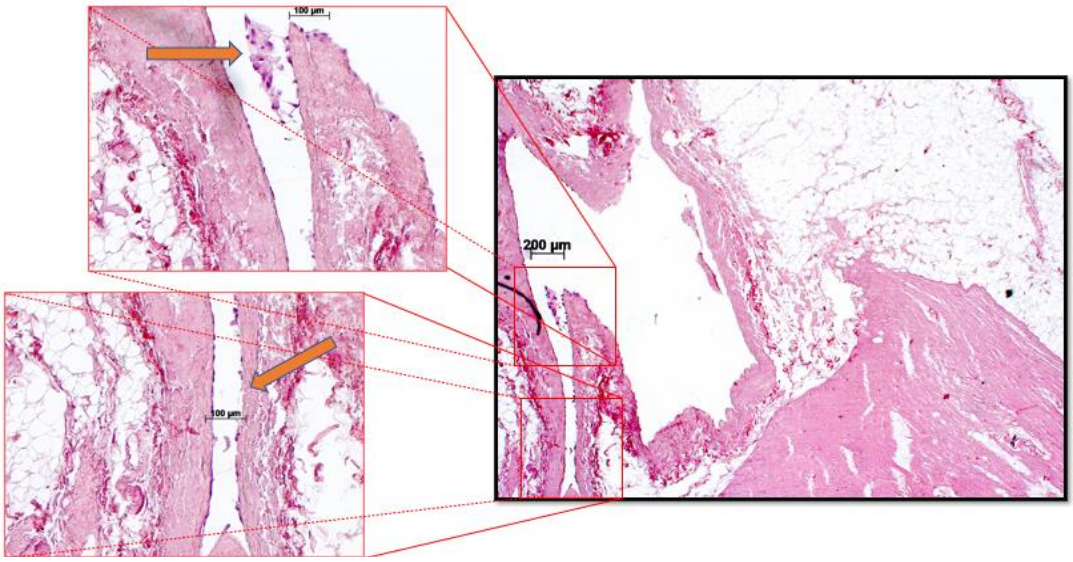

Figure 4-11: H&E stain of A) Descending Coronary Artery B) coronary artery branch. Orange arrows designate observed cells.

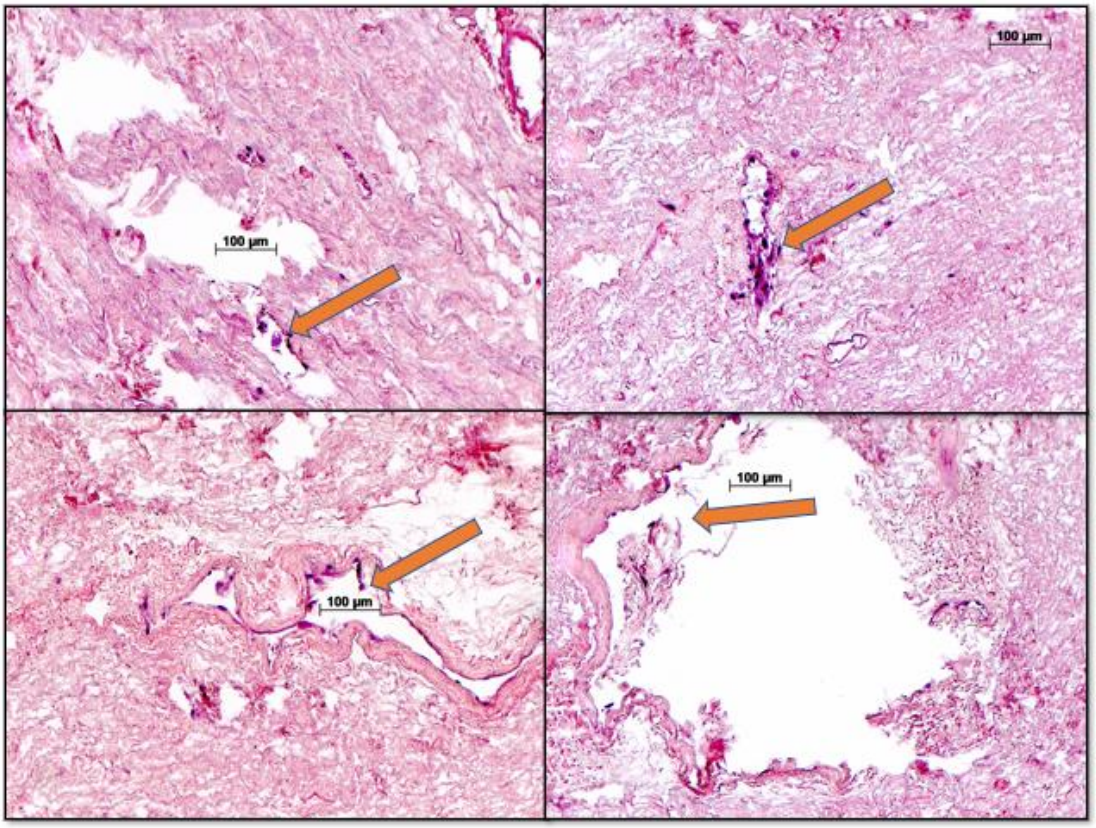

Figure 4-12: H&E Stain of re-endothelialized tissue. A-D) Cells engrafted on various diameters of the vasculature.

4.3.4 Analysis of Injection Cardiac Patches

The cardiac patches injected with a 2:1 ratio of CF:CM and left to remain static for seven days had living and dead cells apparent. However, the histological yielded no large cell pockets in the 2.5x H&E images. Upon higher magnifications, some cell pockets were noted and stained by IHC for vimentin to detect the presence of CFs, CX-43 for CMs, and a-SMA for detecting activated myofibroblasts. All three markers could be seen in these small cell pockets at 20x magnification **(FIG 4-13 C-E)**. The CM group with 8 million cells per scaffold had a significantly higher observation of cells both in live/dead staining and in larger cell pockets that could be seen at lower magnifications **(FIG 4-14).**

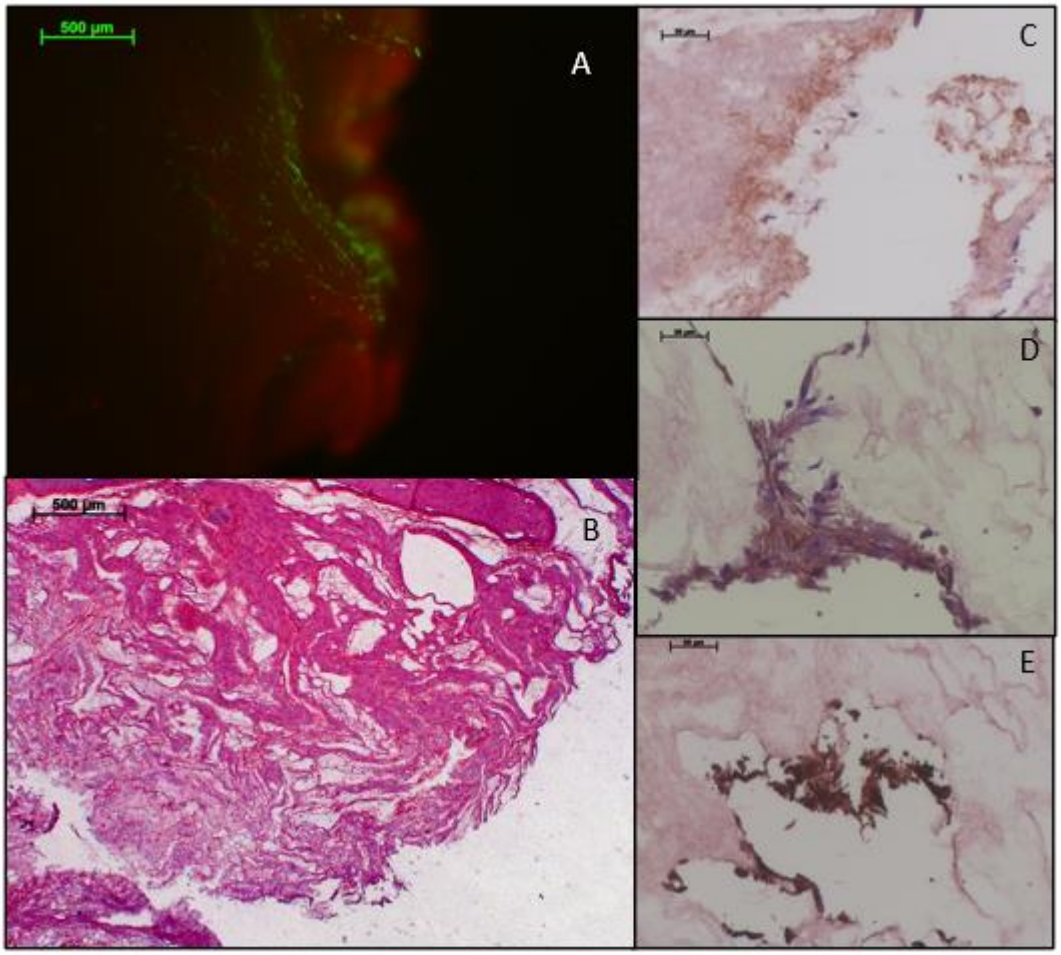

Figure 4-13: 3D cardiac patch A) Live/dead stain B) Macro H&E stain 2.5x objective magnification IHC stains for C) Vimentin D) CX-43 E) α-SMA

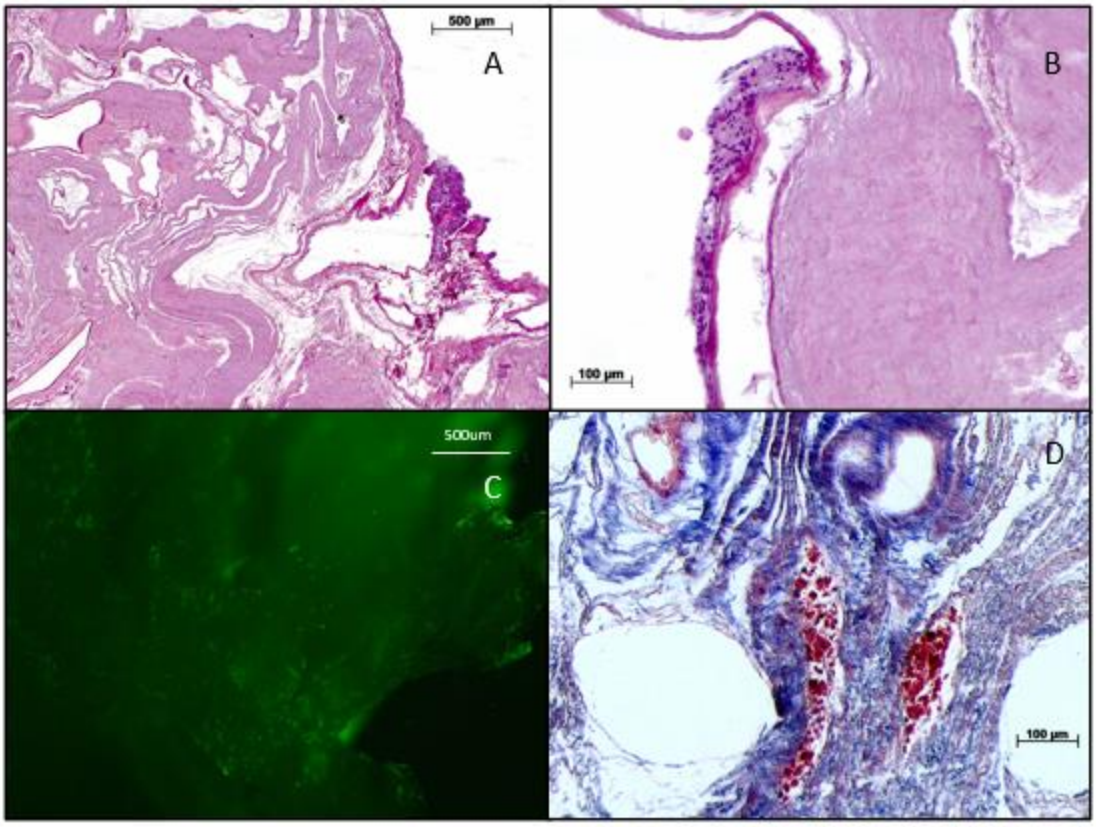

Figure 4-14: Histological images of CM patch with 8 million cells. A) 2.5x objective H&E image B)10x Objective H&E image C)2.5x Objective Live/Dead stain D) 10x objective trichrome stain

4.3.5 Combined Perfusion and Injection Seeding Cardiac Patches

A combination of both seeding methods yielded the most significant density of viable cells in the live/dead staining of any experiment in this study **(FIG 4-15 A-B)**. Cell pockets were noted in various locations in the H&E and Trichrome stain, and apparent endothelial cell-lined vasculature was observed in conjunction with the injection seeded cells. To confirm this observation, IHC stains were positive for CD31 in the vasculature and Vimentin in the cell pockets **(FIG 4-16)**.

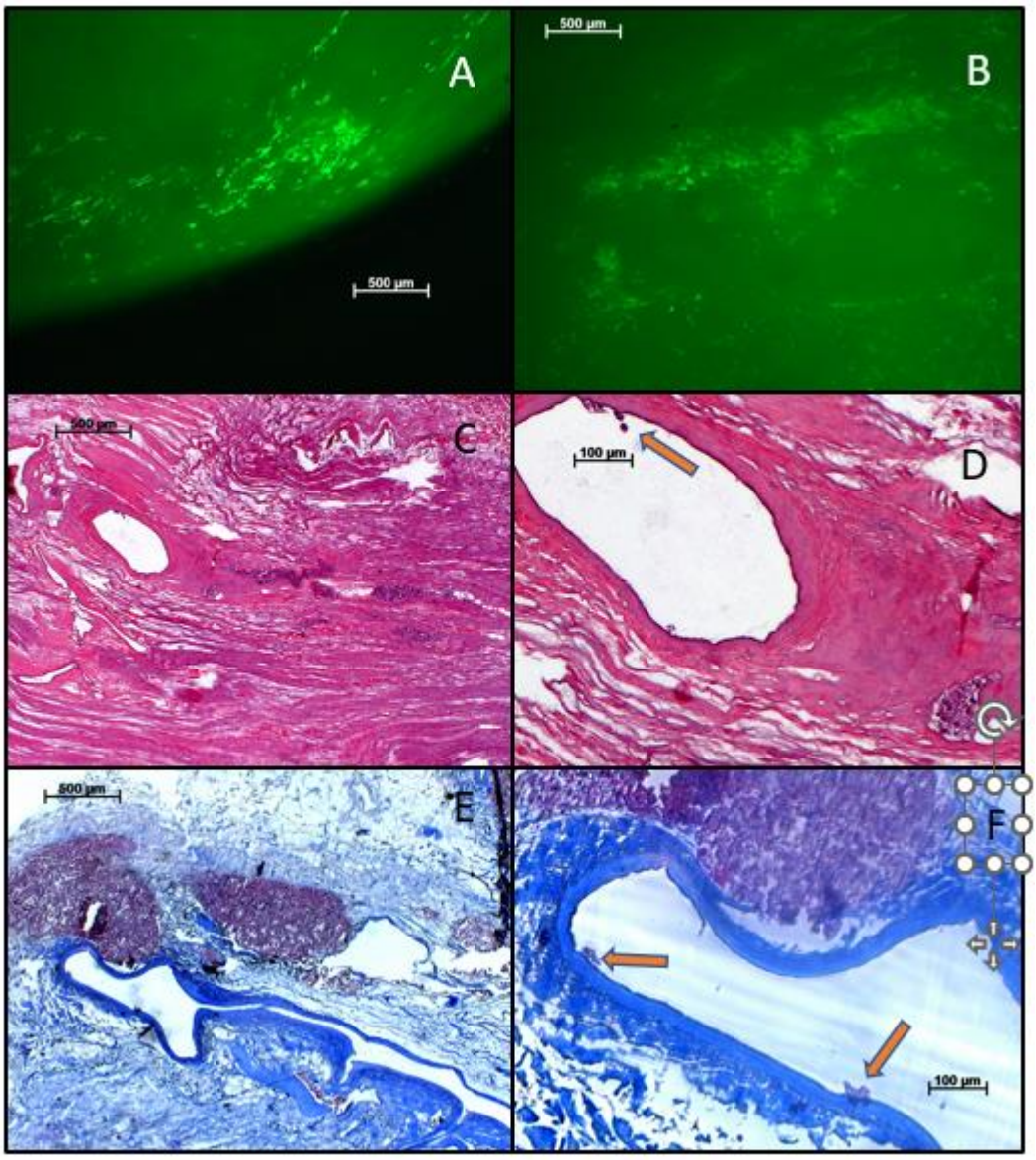

Figure 4-15: Live/Dead and Histological Analysis of Combined Patch. A-B) Live/Dead stain of the patch. H&E stain at C) 2.5x and D)10x magnifications. Trichrome stain at E)2.5x and F) 10x magnification. Arrows denote observed cells

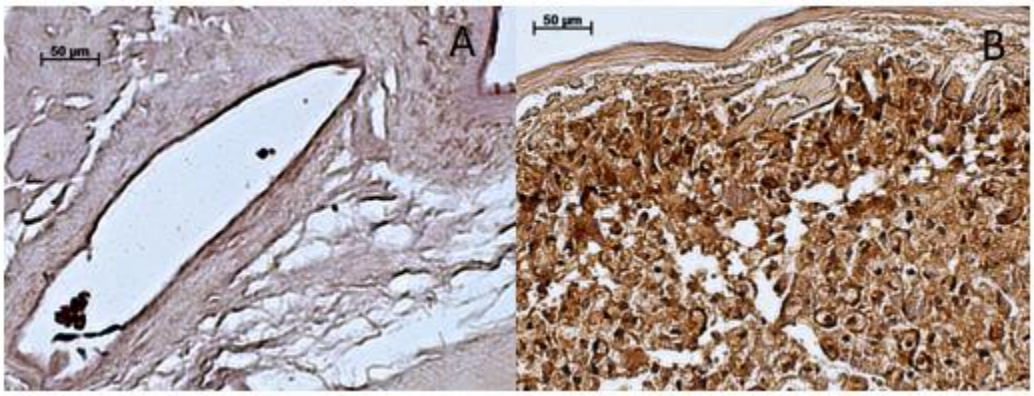

Figure 4-16: IHC stains of A) CD31 and B) Vimentin in the combination seeded cardiac patch

4.4 Discussion

This group of studies was undertaken to prove the efficacy of producing a multicellular cardiac patch. The first experiment within this group was to identify which cell markers were present in our injected cells. As expected, the CFs were positive for Vimentin, a cytoskeletal protein common in cells of mesenchymal origin. Mature CMs are expected to express several proteins that display their ability to contract and organize. For this reason, the critical contractile proteins MHC and cTnT were tested. Surprisingly, these CMs were proliferative, suggesting that they were of an immature phenotype and did not test positive for these proteins. On the other hand, they did test positive for the gap junction protein CX-43, but they did not express a clear intercalated disc suggesting that these myocytes had not yet started to form myofibril. For this purpose, it will be interesting to see how these cells express this protein in further studies after they have been conditioned.

The injection pilot study confirmed the proper cell seeding density and which injection method was preferred in cellular engraftment. While the Cytoseeder's 10x10 needle configuration should have proven optimal cellular dispersion, the material characteristics of the myocardial scaffold made it less than optimal. From a user perspective, the device was simple to

use but did not provide mechanical feedback when the needle penetrated the tissue. Combine this with the slightly gelatinous feel of the decellularized scaffold, and it was difficult to assure when the needles were at the correct depth, an issue that was counter to the observations of using the handheld syringe and needle. While this is the user's experience, it should also be noted that this pilot study lacked a large enough sample size to determine which method was the best.

While some studies have been undertaken utilizing perfusion seeding of decellularized scaffolds, no studies were found that used a combined injection of cardiac cells into the myocardium accompanying this method. Importantly, we could perfuse seed cells down to the microvessel level (<1mm). Along with the seeded vasculature, injected cells close to the vessels that had been reseeded with endothelial cells, which should be beneficial in cell survival and signaling. One last observation from this study was the difference between scaffolds after one and seven days with no stimulation. Observed cell engraftment was significantly lower after seven days which signifies the loss of cells due to lack of stimulation.

4.5 Conclusion

Here we have displayed the ability to form a complex cardiac patch combining the three significant cardiac cell populations with our decelled porcine cardiac matrix. The grafted cells represent a significant portion of the scaffold immediately after seeding but will require conditioning and stimulation to form a more mature patch.

Chapter 5 Aim 3: To develop a perfusion bioreactor for conditioning the engineered cardiac tissue

5.1 Introduction

The combination of cells and a scaffold encompasses the first two tenets of tissue engineering. The third, the stimulation of a tissue-engineered construct was developed as a response to findings that solely grafting cells onto a scaffold did not result in the development of mature tissue. This is seemingly intuitive, as all tissues in the body respond to some form of stimulus during embryonic development through adulthood. It would then follow to create a mature well-differentiated tissue; mimicking these stimuli is an important consideration. Regarding native cardiac tissues, there are several modes of stimuli that affect and condition the tissue. These are the mechanical contraction of the muscle fibers, the electrical signaling to conduct action potentials, the various biochemical stimuli present in secreted cell factors and other bioactive molecules, and the perfusion of blood, allowing for the exchange of nutrients and waste to maintain healthy tissue.

Typically, cardiac tissue constructs are developed in specialized bioreactors built to stimulate tissues with one or multiple stimuli. Mechanical stretch is an essential factor in the overall maturation of cardiac tissues, driving the differentiation of cardiac cells into adult CMs with improved contraction forces and contributing to the effects CFs take on maintaining the ECM. Electrical stimulation also plays a part in the overall maturation of cardiac tissue as these signals regulate the development of voltage gate ion channels in developing tissues. In addition to this, electrically signaling aids in the timing of synchronous cardiac muscle contraction. The development of perfusion in bioreactors has allowed for the ability to develop tissues that are

thicker than early developed tissues that were typically no thicker than 200um to utilize the diffusion of oxygen and nutrients. In addition to thicker tissues, perfusion is also essential in endothelialized tissues as ECs respond to perfusion by secretion of factors important in angiogenesis. Finally, the customized chambers of these bioreactors can include biochemical stimuli to stimulate the tissues or simulate certain physiological conditions or disease states.

Our studies here aim to develop a specialized bioreactor that can combine the conditions of mechanical and electrical stimulation along with perfusion by utilizing cyclical mechanical stretch along with timed electrical pulses to condition our cardiac patches and be able to perfuse them to allow for the viability of thick tissues. This bioreactor will be developed by improving on a current electro-mechanical bioreactor by introducing perfusion and creating a closed system to limit evaporation and contamination

5.2 Methods

5.2.1 Flexcell Bioreactor

The bioreactor system is based on a modified Flexcell FX-5000 Compression system which consists of a baseplate that holds specialized well plates with a flexible silicone membrane that can undergo cyclic stretch with a pump applying and relieving air pressure. This system was modified with a pressure transducer parallel to the outflowing air pressure read by a data acquisition card (DAQ) connected to a computer. A program in LabVIEW interprets the signal and, when proper pressure is registered, send a signal to a second DAQ that times an 80ms electrical pulse of 5V. The pulse is transmitted through a breadboard connected to specialized wiring harnesses soldered with bioinert platinum wire and carbon electrodes. 6-well plates purchased from Flexcell were modified to incorporate this wiring harness with custom inserts that hold the tissue against the plate **(FIG 5-1).**

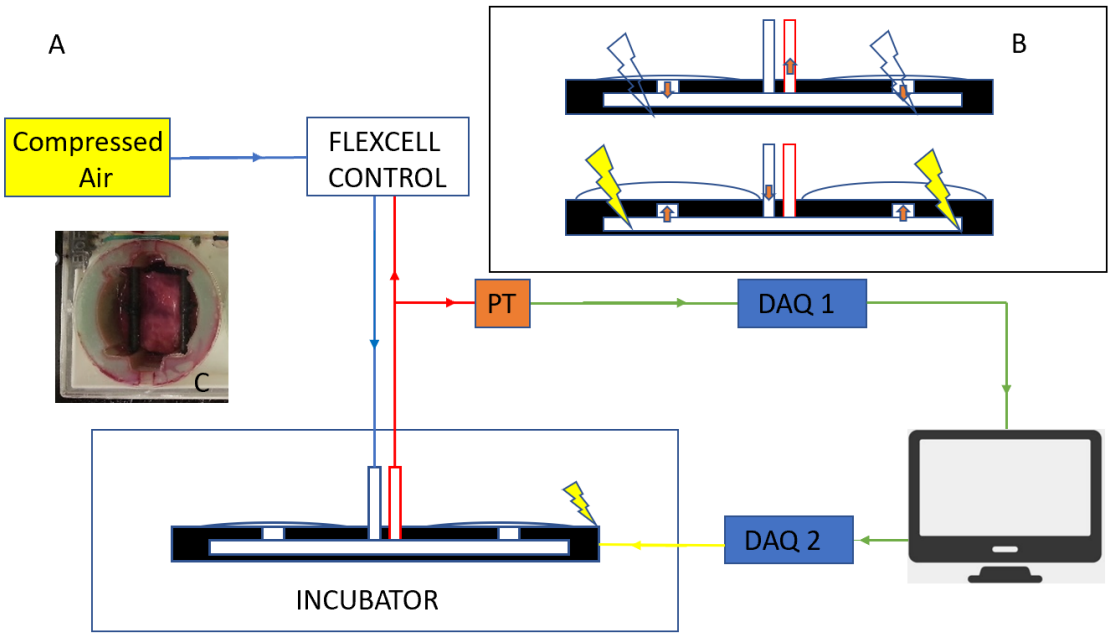

Figure 5-1: Diagram of a Flexcell based bioreactor. A) Schematic of the entire system consisting of a baseplate in an incubator, stimulated by air pressure from the Flexcell Control unit. A DAQ reads outflowing pressure through a pressure transducer that sends a signal to the compute to time an electrical pulse from another DAQ. B) Top- when air pressure leaves the system, the flexible membrane relaxes, and no electrical stimulation occurs. Bottom- Increase in air pressure results in an equibiaxial stretch of the membrane in conjunction with a timed electrical pulse of 5V. C) Image of a 3cm Cardiac Construct in a modified Flexcell plate with a custom insert holding electrodes and tissue against the plate membraned

5.2.2 Flexcell Bioreactor Perfusion Plate 1

A new plate was designed in SOLIDWORKS that would be able to fit into the existing Flexcell baseplate. The dimensions of the plate were 90mmx140mmx40mmH. The plate was designed as a 6-well plate with 30mm diameter wells with two enclosed chambers running

lengthwise, including three wells per chamber. Two 2mmx10mm inserts were designed into each well to hold carbon electrodes. Each chamber had an inflow and outflow nozzle connected to tubing and a reservoir bottle for continuous media flow by a peristaltic pump. A 5mm channel was incorporated down the middle of the plate to accommodate the electrical wiring, and two 1mm holes were designed beside each well along this channel to allow for the wiring to be fed into the chamber **(FIG 5-2)**.

After designing the plate, it was 3D printed in nylon on the HP 3D Fusion Jet Printer **(FIG 5-3A)** Silicone sheeting was acquired of .015" thickness that was identified as the same thickness of membrane on the original Flexcell plates and was used to seal the plate using a silicone adhesive (Loctite). To insert scaffolds into the bottom of the plate, a pronged ring was designed in Solidworks, and 3D printed in nylon **(FIG 5-3A).**

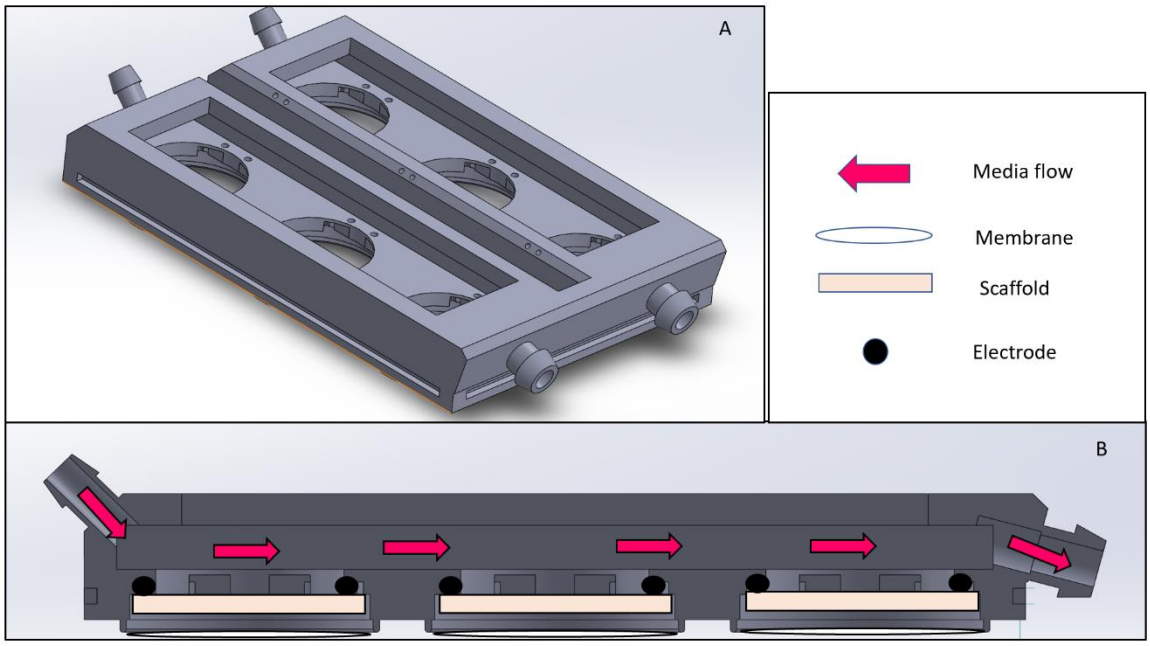

Figure 5-2: Renderings of Perfusion Plate 1. A) Isometric view of the plate in Solidworks. B) Schematic of one chamber with insert scaffolds and path of medial flow

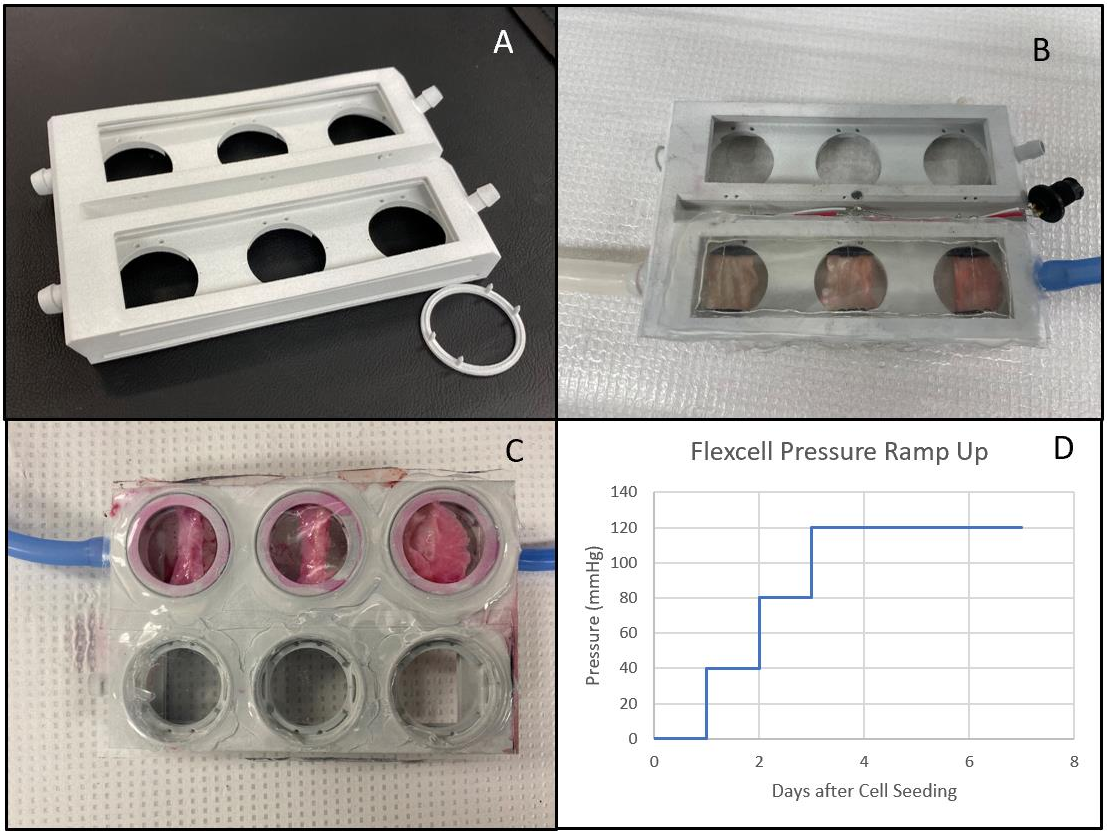

Figure 5-3: 3D Printed Perfusion Plate 1 and Pilot Study

5.2.3 Pilot Study

A pilot study was conducted to determine the effectiveness of Perfusion Plate 1 compared with the original Flexcell plates for one week. All glass and metal instruments were autoclaved for sterility. The perfusion plate with its wiring harness and silicone membrane was sterilized with ethylene oxide for 24 hours and then allowed to off-gas for 12 hours. Six 3cm myocardial scaffolds were prepared and injection seeded with a 2:1 ratio of CF: CM utilizing a 27 ½ Gauge needle. The seeded scaffolds were allowed to rest statically in standard cell culture

media overnight. Three platforms were then placed into the wells of one of the chambers of Perfusion Plate 1**(FIG 5-3 B, C),** and three were placed into the original modified Flexcell plates. The plates were placed into the Flexcell baseplate, and the three-day pressure ramp-up procedure commenced with 1.15 Hz cyclical stretch and 5V electrical pulses beginning at 40mmHg for 24 hours before being increased to 80mmHg the following day and then up to 120mmHg on the 3rd day **(FIG 5-3D).** The bioreactor ran for a total of 7 days, and then the tissues were extracted for Live/Dead fluorescent imaging, tissue processing, and histological analysis.

5.2.4 Flexcell Perfusion Plate 2

A new perfusion plate was designed in SOLIDWORKS with considerations from the pilot study. The new plate was designed around the use of the Flexcell pump to provide cyclical perfusion and stretch **(FIG 5-4)**. The plate departed from the 6-well design, instead favoring the use of 3 enclosed chambers with one scaffold occupying each chamber. The chambers were designed to have a circular chamber that would allow media to flow around the chamber's circumference as the Flexcell pumped. Two nozzles extend out of the top of each chamber. One nozzle above the tissue well is designed to easily add or remove media as needed. The other chamber works in conjunction with a nozzle extending from the base of the chamber across from the tissue well. This nozzle works with a peristaltic pump to infuse incubator air with the media to maintain the proper dissolved oxygen and carbon dioxide to maintain pH. A new clip

was designed to hold the electrode and the tissue that could be inserted into the tissue well **(FIG 5-4C).**

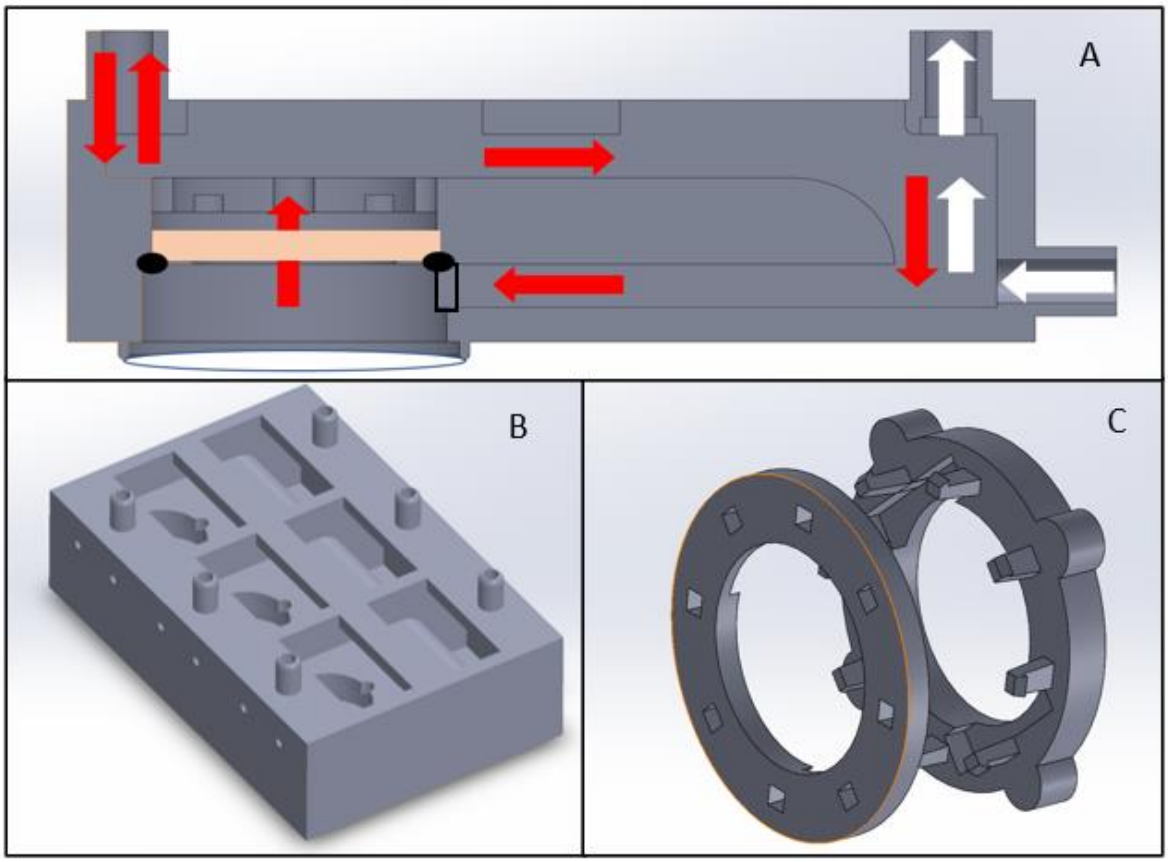

Figure 5-4: Renderings of Perfusion Plate 2(A, B) and a new lock ring (C)

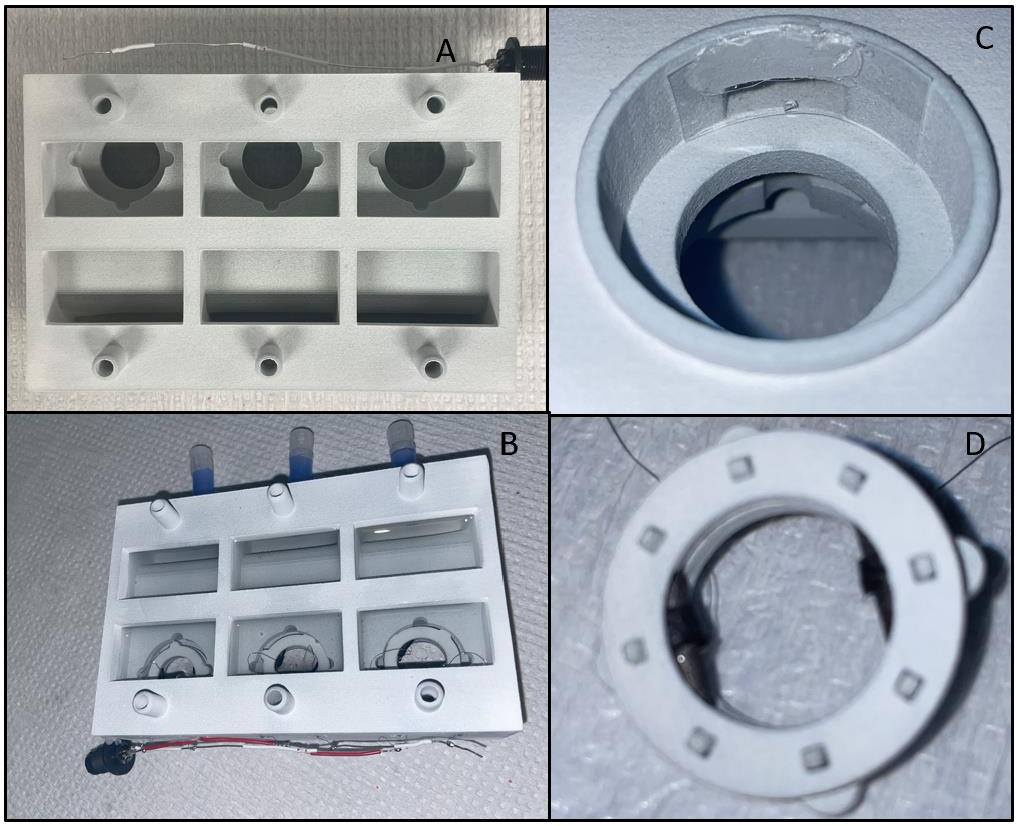

Figure 5-5: 3D Printed Perfusion Plate 2

5.2.5 Bioreactor conditioned cardiac patches

After the development of Perfusion Plate 2, experiments were conducted testing the entire bioreactor system with seeded cardiac patches. All plates and materials unable to be autoclaved were placed in sterilizer bags and placed into an Anprolene Eto Sterilizer on a 24-hour cycle and then allowed to off-gas for 12 hours.

Bioreactor groups consisted of:

CM1: Scaffolds seeded with 3 million CM

CM2: Scaffolds seeded with 8 million CM

CMCF: Scaffolds seeded with 4 million cells in a 3:1 of CM: CF

CMCFEC: Scaffolds endothelialized with 4 million EC and 4 million cells in a 3:1 of CM: CF

Groups CM1, CM2, and CMCF were seeded by 1mL injection of a syringe with a 27 ½ G needle. CMCFEC scaffolds were isolated from endothelialized ventricular patches and then 1mL CM/CF injections with a 27 1/2G needle. After final seeding, all scaffolds were placed in 6 well plates overnight statically. The following day the scaffolds were analyzed with PrestoBlue before being sealed into their respective bioreactor chamber. Bioreactor plates were placed into the Flexcell baseplate, and the electrode harnesses were connected to the breadboard. Vented bottles were connected to the air outflow tubes to prevent any pressure buildup from breaking the seal of the bioreactor. The pressure ramp-up cycle began the same as in the pilot study and the bioreactor was allowed to run for a total of 7 days at 1.15Hz with 5V electrical pulses. After the week's conclusion, tissues were extracted from the bioreactor, analyzed with PrestoBlue, and then sectioned for mechanical, histological, and protein analysis and Live/Dead Fluorescent staining.

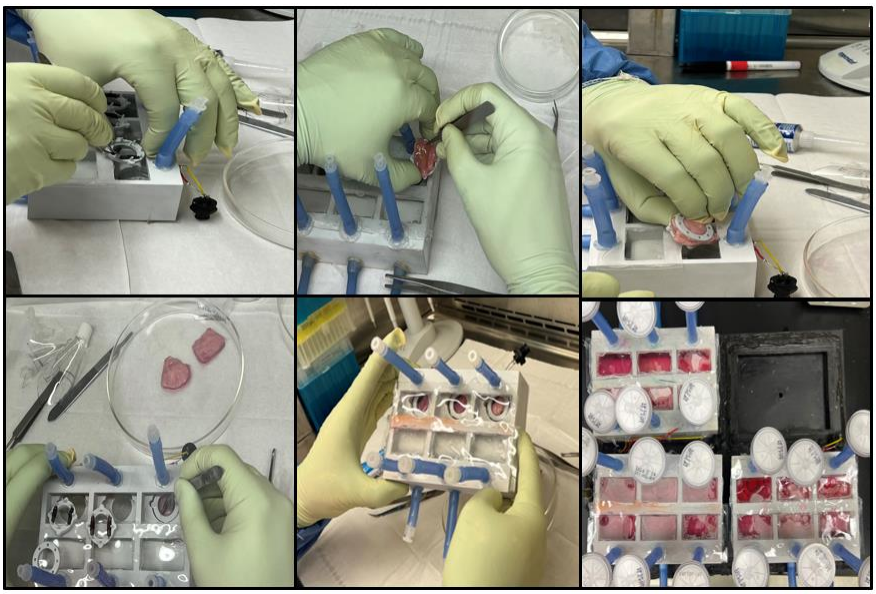

Figure 5-6: Insertion of seeded tissues into perfusion plate 2

5.2.6 Protein Isolation

After experiments were completed, sections of tissue were isolated for protein extraction. Samples were frozen in liquid nitrogen, then pulverized, and then transferred to a glass test tube before being homogenized in RIPA buffer (50mM Tris-HCl, 150mM NaCl, 1mM EDTA, 1% Triton X-100, 1% Sodium Deoxycholate, and 0.1 % SDS) using a TissueRuptor (Qiagen). Homogenized samples were then allowed to rest on ice for at least 15 minutes before being centrifuged to allow for lysis of cells. The samples were centrifuged at 12,000g for 15 minutes at 4^{o}C to pellet large proteins. The supernatant was then collected and frozen at -20^{o}C until protein quantification or assays were needed.

5.2. Protein quantification.

A Bicinchoninic acid assay (BCA) was used to quantify the total protein of isolated protein samples. A series of standard protein concentrations were created using bovine albumin and tested along with unknown protein samples. 20uL of each piece was placed in a 96 healthy plate in duplicates, and then 200uL of the BCA reagent was added before the plate was incubated in the dark at 37^{o}C for 30 minutes. The well plate was then read on a plate reader, measuring absorbance at 562nm. A standard curve was created from the known albumin concentrations and used to determine the total protein concentrations of the unknown samples. These concentrations were then used to calculate the total volume to obtain 20ug of protein for western blotting and gelatin zymography.

5.2.7 Western blotting

Calculated volumes of each protein lysate from the BCA were taken and combined with non-reducing sample buffer (Laemmli) in a 2:1 concentration of buffer to sample to obtain 45uL total volume per well. Samples with low concentrations requiring a high volume per sample

were mixed with 4x Laemmli buffer, samples at approximately 1mg/mL were mixed with 2x Laemmli buffer, and highly concentrated samples were combined with 1x Laemmli buffer. Protein lysates were then reduced by B-mercaptoethanol by placing them in a 95^{o}C water bath for 5 minutes. Samples were then loaded into Bio-Rad mini-protean gels, and proteins were separated by electrophoresis migration at 200V for 35 minutes. Proteins were then transferred onto a prepared PVDF membrane at 90V for 90minutes. Membranes then underwent blocking for one hour in 1%Bovine Serum Albumin in tris buffered saline (TBS) for 1 hour before primary antibodies of CX-43(ab11370) and Vimentin(ab8069) in blocking solution were applied overnight at 4^{o}C. The following day antibodies were washed away using .05% tween-20 in TBS. An HRP secondary in blocking solution was added for one hour at room temperature, followed by another wash of TBS-tween. Finally, the detection reagent, ECL, was added for 5 minutes before blots were imaged using a Chemi-Doc XRS+ from Bio-Rad. Band Intensities were determined using ImageLab software, and values were normalized to the average intensity values of all bands in each group.

5.2.8 Gelatin Zymography (MMP analysis)

Gels for zymography studies were cast utilizing Bio-Rad equipment. A 10% resolving gel with gelatin and 4% stacking gel were prepared with acrylamide/bis, Tris-HCl, and SDS solutions and then crosslinked via ammonium persulfate and TEMED. The resolving gel was poured into the mold and allowed to set with a layer of deionized water over it. After the gel solidified, the water was removed, and the stacking gel was poured with a ten lane comb. Once set, the gels were stored at 4^{o}C before studies being conducted. Protein isolate samples were prepared in western blot samples with volumes containing 20ug of protein combined with a non-reducing sample buffer for a total volume of 40uL. The gels were placed into an electrophoresis chamber,

and the module was run at 90V until the migration was complete, typically from 120-150 minutes. After the migration was finished, the gels were placed in an incubation buffer for 24-48 hours on a shake plate in a 37°C incubator for enzymatic degradation of gelatin. After the digestion of gelatin, the gels were stained with Coomassie brilliant blue for 45-60 minutes and then destained until clear bands appeared. The gels were then imaged in a Chemi-Doc XRS+ from Bio-Rad.

5.2.9 PrestoBlue Cell Viability

The Presto Cell Viability for this aim followed the same protocol for Mechanical Analysis found in Chapter 3(AIM 1), with the addition of tissues being analyzed before insertion into bioreactors and after seven days. Relative viabilities were determined by diving day seven fluorescence by day one fluorescence.

5.2.10 Biaxial Mechanical Analysis

The biaxial mechanical analysis for this aim followed the same protocol for Mechanical Analysis found in Chapter 3(AIM 1) with the change that the axes of observation were in the radial and circumferential directions as opposed to anatomical planes.

5.2.11 Live/Dead Imaging

The Live/Dead Fluorescent Imaging for this aim followed the same protocol for Live/Dead found in Chapter 3(AIM 1)

5.2.12 Tissue Processing and Histological Techniques

Tissue Processing and Histological Techniques followed the same protocol for Tissue Processing in Chapter 3

5.2.13 Statistical Analysis

Results are expressed as mean ± standard deviation. Statistical Analysis for all groups was conducted via one-way ANOVA in Minitab. Some samples were directly compared using Tukey's student two-tailed T-test in Microsoft Excel. Null hypotheses were rejected if p vaules<0.05 at 95% Confidence Intervals. Groups CM1, CM2, and CMCF were all performed at n=3, while CMCFEC was performed at n=6. All Confidence Intervals are reported in the appendices.

5.3 Results

5.3.1 Pilot Study Results

5.3.1.1 Live/Dead Imaging

The original Flexcell group and the perfusion plate 1 group showed dispersed living cells in the scaffolds. Compared to the static seeded group from AIM 2, these tissues had a higher concentration of living cells **(FIG 5-6).**

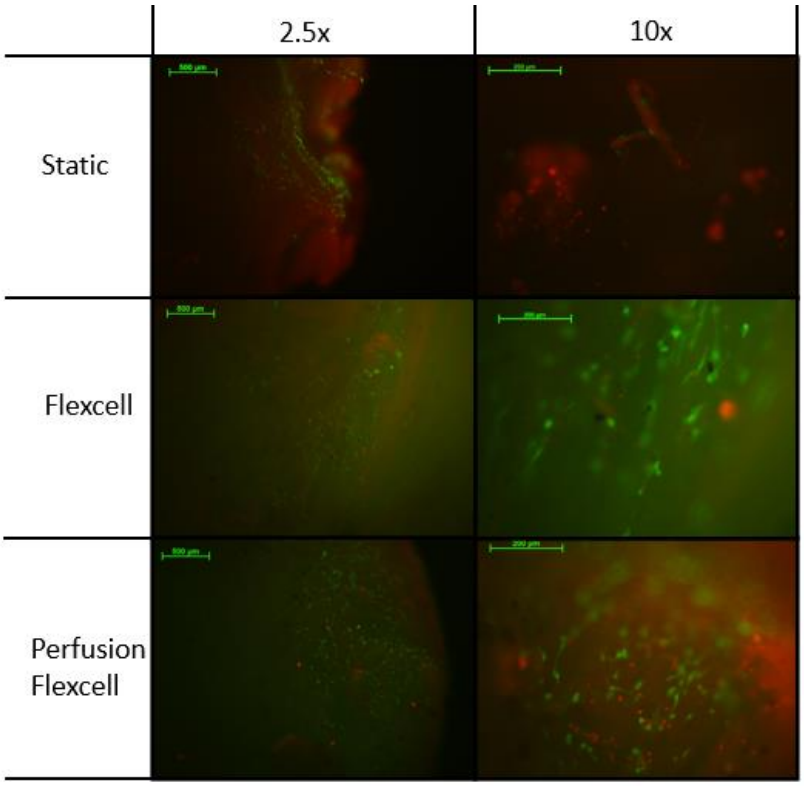

Figure 5-7: Live/Dead Imaging of Static, Flexcell, and Perfusion Plate

5.3.1.2 Pilot Study Histological Analysis

The histological samples from both the Flexcell and the Perfusion Plate did not show widespread pockets of cells; however, the perfusion group had more observed cellular content in the H&E and IHC stains. Both groups showed positive staining for CF marker Vimentin, CM marker CX-43, and a-SMA, indicating a morphological change of the CFs into myofibroblasts.

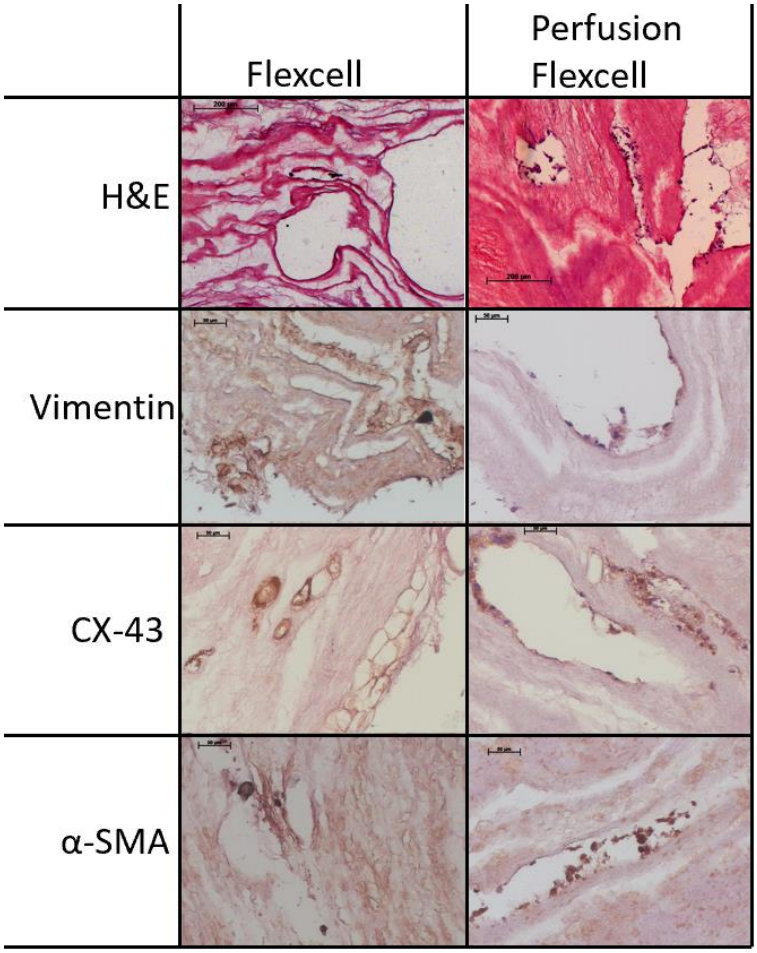

Figure 5-8: Histological Analysis of Flexcell and Perfusion Flexcell Groups. H&E images at 10x magnification. IHC images at 20x magnification

5.3.2 Bioreactor Conditioned Patches

5.3.2.1 Cell Viability Analysis

In live/dead imaging, CM1 had the lowest apparent group of viable cells. The other three groups, CM2, CMCF, and CMCFEC, all had significantly larger living cell populations **(FIG 5-8)**.

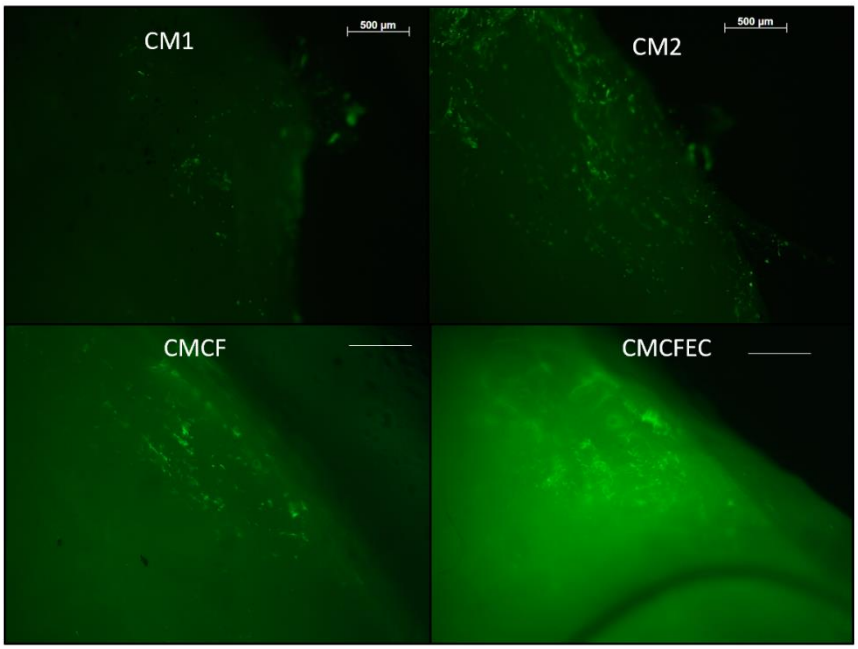

Figure 5-9: Live/Dead Images of Bioreactor Groups

No statistical significance was detected between the groups for 7-day cell viability. The reported mean for CMCFEC was 39%, while the other three groups all had reported means closer to 30% **(FIG 5-10)**.

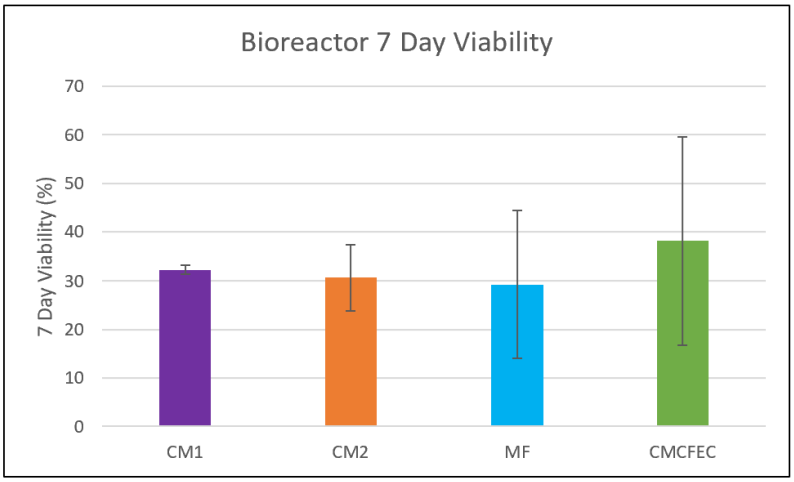

Figure 5-10: Relative 7-day cell viability(p>.05)

5.3.2.2 Bioreactor Histological Analysis

The images below in figure 5-10 show the comparative effects of differing seeding densities in the CM1 and CM2 groups **(FIG 5-11)**. The effect of increased seeding can be observed in the CM2 group by larger and more dispersed cell pockets.

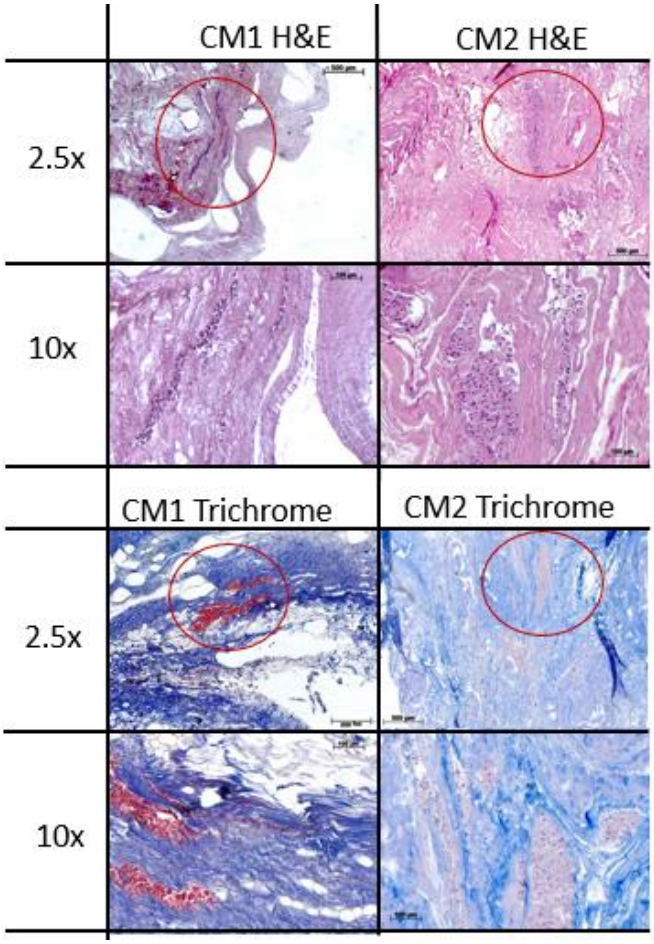

Figure 5-11: H&E and Trichrome Stains of CM1 and CM2. Red circles denote enhanced image areas in 10x magnifications

IHC analysis for specific cardiac protein markers included CX-43, Vimentin, and β-int **(FIG 5-12)**. CX-43 expression was evident in all groups but expressed a deeper stain in the CMCF and

CMCFEC groups. Vimentin was absent from the CM group and was observed in the CMCF and the CMCFEC groups. B-int was also observed in all groups and as the CX-43 expression, displayed increased staining in the CMCF and CMFCEC groups.

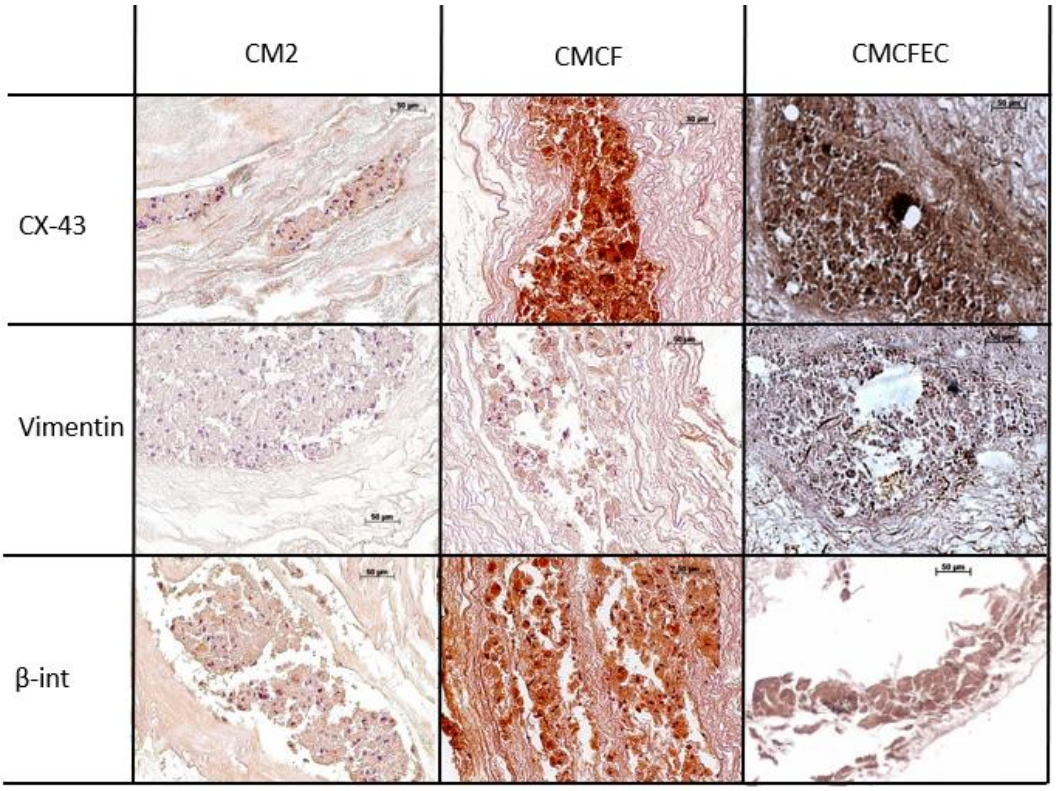

Figure 5-12: Immunohistochemistry Images of Bioreactor Groups

5.3.2.3 Protein and MMP Expression

Western blotting for CX-43 showed statistically significant data, but Vimentin was inconclusive. CMCFEC had the highest expression of CX-43 by more than two times that of the CM2 group. CM1 had almost no expression of CX-43, and the CMCF group had an expression of approximately 1/10 that of the average relative expression of all groups. On the other hand, due to significant variances in the samples, no statistical significance was detected in the groups regarding the expression of Vimentin. Despite this, it ca, n clearly be seen that the groups that

contained CF(CMCF+CMCFEC) both had some expression of Vimentin, while the non-CF groups (CM1+CM2) did not produce bands in the blot **(FIG 5-13)**.

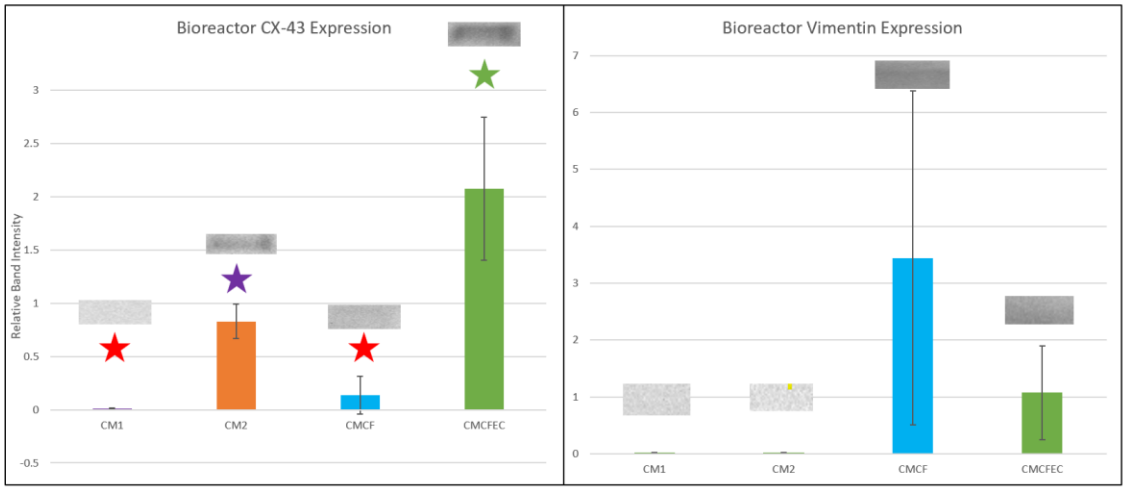

Figure 5-13: Western Blot expression of CX-43 and Vimentin in Bioreactor Groups. No statistical significance observed in Vimentin Groups (p>.05). In CX-43 groups significance observed in CMCFEC-CMCF,CM2,CM1 (p<.001) and CM2-CMCF,CM1(p<.001)

MMP analysis conducted by gelatin zymography showed clear expression of MMP-9 at 92kD and MMP-2 at 72kD in all groups but CMCF, which expressed MMP-2 but not MMP-9. There was no statistical significance in the overall expression of the group due to the variance but groups CM2 and CMCFEC had relative densitometry means higher than one. In contrast, the other groups, CM1 and CMCF, expressed means below 1 **(FIG 5-14)**.

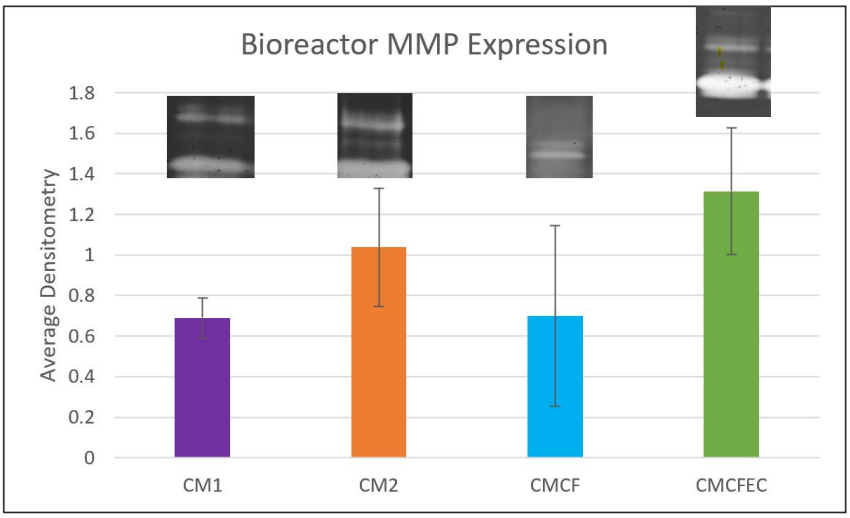

FIG 5-14: MMP expression of Bioreactor groups (p>.05)

Upper band: MMP-9 92kD, Lower band: MMP-2 72kD

5.3.2.4 Mechanical Analysis of Bioreactor Tissues

Samples from bioreactor tissues were analyzed in the radial and circumferential directions. Measured moduli ranged from approximately 4-9 kPa across the groups with the only significance detected from the CM1 radial group and a group including the CM2, CMCF, CMCFEC circumferential, and CMCFEC radial **(FIG 5-15)**. Compared to the pre-conditioned groups the bioreactor samples all trended to have higher related stiffnesses.

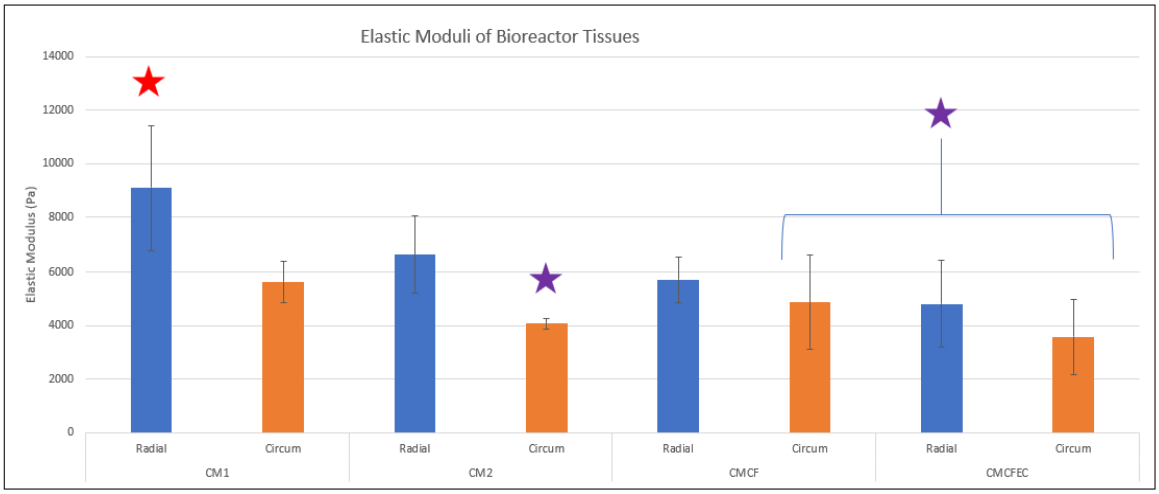

Figure 5-15: Biaxial Mechanical Data of Bioreactor Groups. Significance between (CM2 Circum, CMCF Circum, CMCFEC)-(CM1 Radial) ($p<.05$)

5.4 Discussion

Development of a bioreactor is complicated as in most cases they are built from the ground up with the considerations of each specific group taken into account with their design. We tried to take advantage of modifications to an existing system, and this had its benefits as well as it's challenged. The Flexcell FX-5000 Compression system is an adequate tool in the development of a bioreactor as it provides a system that was observed to execute >10,000 cycles over multiple experiments without any observed failure of the device. This is an essential tool in any cardiac system that has the intention of adequately conditioning cardiac tissues. Contrary to this, the Flexcell itself is a relatively simple system only providing pressure against a flexible membrane to produce a stretch force. We have developed the system to include an electrical stimulation unit to transform this system into a mechanoelectrical bioreactor. From there it was observed that the standard housing with original well plates resulted in quick evaporation of media and opened the entire system to the risk of contamination. To combat this, we have developed here a perfusion plate capable of retaining media and being an

effectively closed system. This new bioreactor is not without its own issues. The plates are built to hold enough media for an entire experiment resulting in a reduction of total number of tissues capable of being conditioned to 12 across 4 plates instead of the original 24 in the Flexcell 6-well plates. In addition to this the material used to print the plates is robust yet porous leaving concerns of effective sterilization. Finally, because we were unable to find a clear material to print our plates in, we had to leave ports open for observation that had to be sealed with silicone membrane prior to placement in the bioreactor. This left a possible point of failure open as pressure was increased within the chamber. Despite these concerns we have shown remarkable ability in the conditioning and preservation of cardiac tissue conditioned within our bioreactor.

Our pilot study was used to compare the effectiveness of our new plate when compared to our original Flexcell modifications. From this study we determined that there were similar viabilities in the tissues after a weeklong study, however the original Flexcell modifications required multiple media changes a day and constant observation to ensure tissues were not compromised, and while perfusion plate 1 was constantly observed no leaks were detected and required significantly less maintenance. This histological analysis was not completely conclusive as cell populations were hard to detect but the observed protein expression appeared higher in the perfusion plate tissues.

From this plate we moved onto our final plate design and began experimenting with the conditioning of cardiac patches from various cell sources. The cell viability analysis confirmed that groups with higher initial cell seeding had higher density of cell engraftment over 1 week. Considering the PrestoBlue cell viability assay all groups had effective viability of 30% after 1 week. While this does not seem like an ideal result, when compared to studies that have

injected cells directly for cardiac repair, the bioreactor conditioned tissues result in higher cell survivability rates.[135] It should also be noted that despite the lack of statistical significance the reported mean of the CMCFEC groups was several percentage points higher than the other groups, alluding to a positive effect of the inclusion of the ECs and CFs when compared to the CMS alone.

From the histology we could once again see the result from an increased number of cells injected between the CM1 and CM2 groups, identifying much larger cell pockets within the CM2 tissues. Moving on from this, we compared the expression of proteins indicative of a healthy tissue. CX-43 was expressed in all IHC samples indicative of the presence of the CMs in the tissue. When comparing this result to the western blots, it was noted that the highest expression of CX-43 was in the CMCFEC group with significant increase of expression over CM2. CM2 being seeded with 8 million cells and the CMCFEC group with only 3 million CMs clearly displays that the presence of a multicellular patch drives the maturation of the cells over CMs solely. Compared to the CX-43, Vimentin, as expected, was not present in either CM group but was present in the CMCF and CMCFEC group. Notably no significant difference was observed in these groups from the western blots due to high variance. β-int was observed in all the bioreactor groups indicating successful cellular engraftment to the scaffold. It appears that the CMCF and CMCFEC groups stain more noticeably for this adhesion molecule, another indication that the communication between CMs and CFs is beneficial to the maturation of the tissue.[136] Finally, MMP analysis shows that the tissues with the highest cell seeding, CM2 and CMCFEC, also exhibited the highest expression of MMPs. While MMPs are commonly referenced for the activity in pathologic matrix remodeling, they also exhibit in beneficial matrix turnover and the inhibition of MMP activity can be associated with decreased cell migration and

angiogenesis.[137, 138]. It has also been determined that incorporation of electrical pulses induce MMP activation.[139]

Finally, the mechanical analysis shows us reported mean stiffnesses that were slightly higher than what was reported for the prepared scaffolds from Chapter 3 Aim 1. Despite this increase statistical analysis of the groups showed that only radial groups from the CM1 and CM2 groups were significantly higher. This result does display that conditioning in a bioreactor does influence stiffness but that the presence of CF in the scaffold resulted in a tissue of approximately the same stiffness as the before the conditioning, indicating the CF influenced homeostasis of the ECM.

5.5 Conclusion

Our studies here have shown that we have produced a bioreactor capable of successfully conditioning tissues in a weeklong study. Furthermore, we have displayed the positive effects of incorporating various cell types into our scaffold driving the maturation of the tissue.

Chapter 6: Conclusions and Future Work

6.1 Conclusion

As the population of the developed world continues to age, the prevalence of CVD can only expect to increase. While the overall survivability of MI and its resultant disease states of ventricular remodeling, cardiac fibrosis, and HF has become more favorable over the years, there still exists no one size fits all therapy to treat these diseases, and while developments in pharmaceuticals, mechanical devices, and donor heart availability give more positive prognoses, there still exists a gap in the treatment of these diseases. This research was aimed towards finding a tissue engineering solution that can help fill this void and provide a regenerative approach that will effectively render a therapy as a native tissue, dispensing of the risks associated with implanted devices and the required immunosuppressive drugs required for those with transplants. In that regard we have made a great stride towards a regenerative therapy that consists of a cardiac patch consisting of the three major cell types of the myocardium, seeded onto a proper scaffold containing the requisite mechanical properties, and conditioned in a custom bioreactor that provides the adequate stimulation to drive this construct into a mature tissue.

6.2 Future work

The bioreactor platform developed here was ideal in the conditioning of the 3cm tissues that were developed however some modifications can be made. The main issue of note is the nylon material of the 3D printer. One key issue here is the porosity of the material resulting in

difficulty sealing the plate. This required the use of a silicone sealant that while bioinert once set, was possibly cytotoxic while curing. Efforts to use clamping methods failed resulting in fluid loss and contamination. Also, the nylon was opaque resulting in the inclusion of two ports to visibly see the tissues while in the bioreactor. There exist newer 3D printed materials that are clear, less porous, and should have enough strength to withstand the forces of the Flexcell. A new plate of this material could only have one opening at the membrane for the Flexcell. Tissues could be set into the plate from the bottom and then clamped into place so that no sealant is required.

Once a new plate is made it will be ideal for more mature tissues. These size tissues would be ideal for the next step in the project of *in vivo* testing. In the case of a rodent model, the tissues can be seeded with rat primary or stem cells and then conditioned as normal in the bioreactor. The tissues are large enough to then be cut to size at the time of implantation and grafted onto the epicardium. While it may be difficult to graft the vasculature of the patch to the rat heart, engraftment on the heart over a multiple week study will show the ability of the patch to absorb into the native tissue of the heart. The effects of angiogenesis of the patch could also analyzed.

Following on this a new bioreactor plate should be designed to accommodate a whole ventricular flap. Effectively this plate could be simpler than the multi tissue plates currently used. The cannulated coronary artery of the ventricular flap can be used to perfuse media through the entire tissue which should result in higher engraftment rates and long-term cell survivability. In addition to this anchoring to one large membrane (10cm) will allow for stimulation of the entire flap. A flap this size would be ideal to continue the work into larger

animal models. Hopefully, this is the path that will be taken to reach the goal of regenerative cardiac patch.

Chapter 7: Appendix

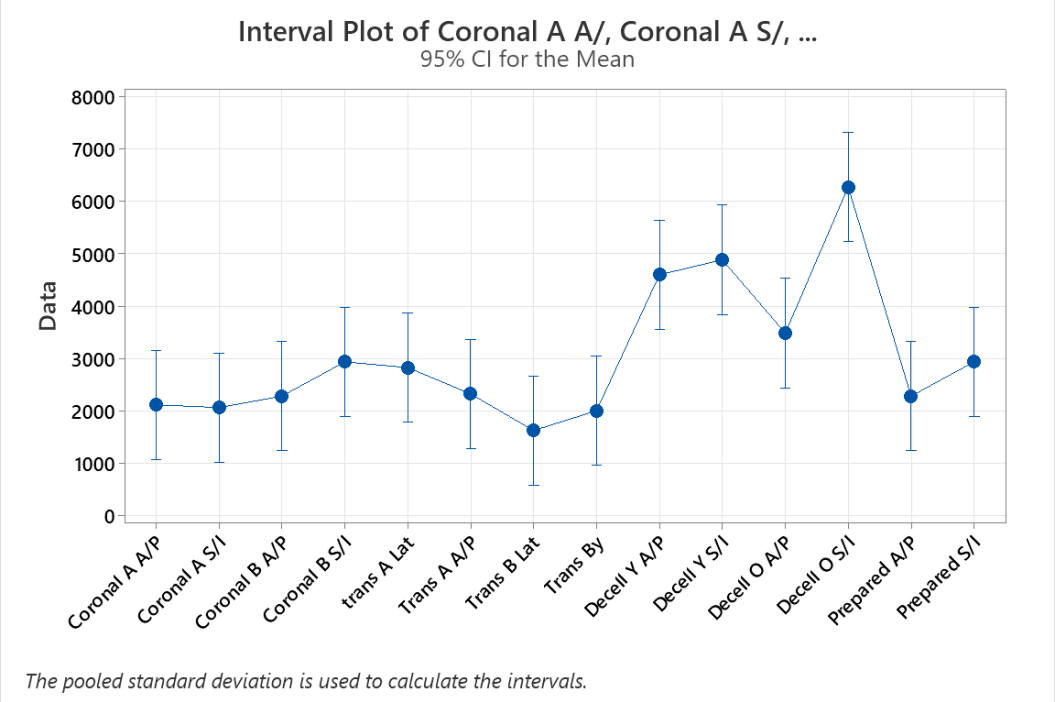

A-1: Confidence Intervals for biaxial mechanical testing groups

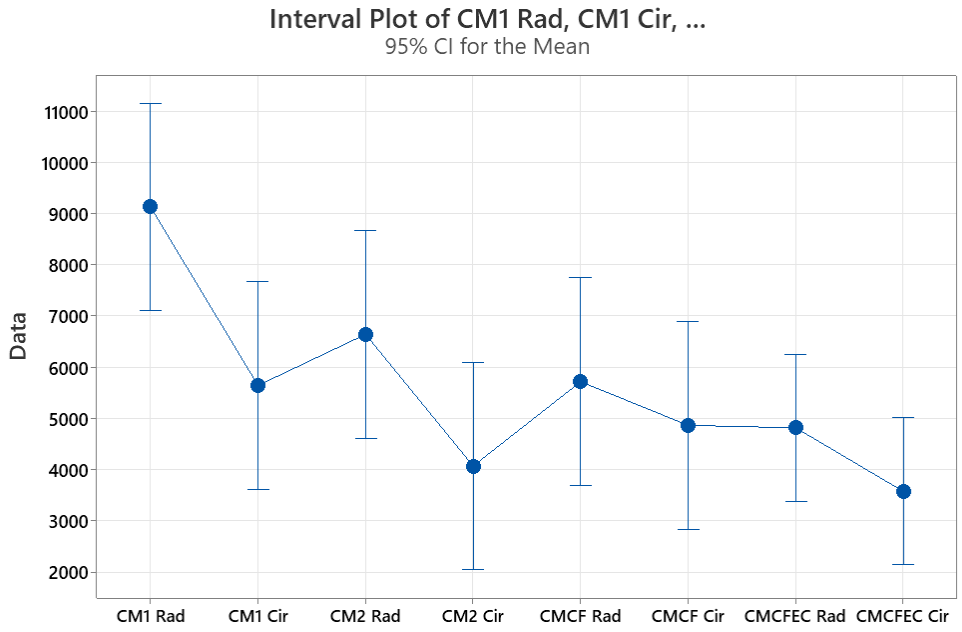

The pooled standard deviation is used to calculate the intervals.

A-2: Confidence Intervals for Bioreactor Biaxial mechanical analysis

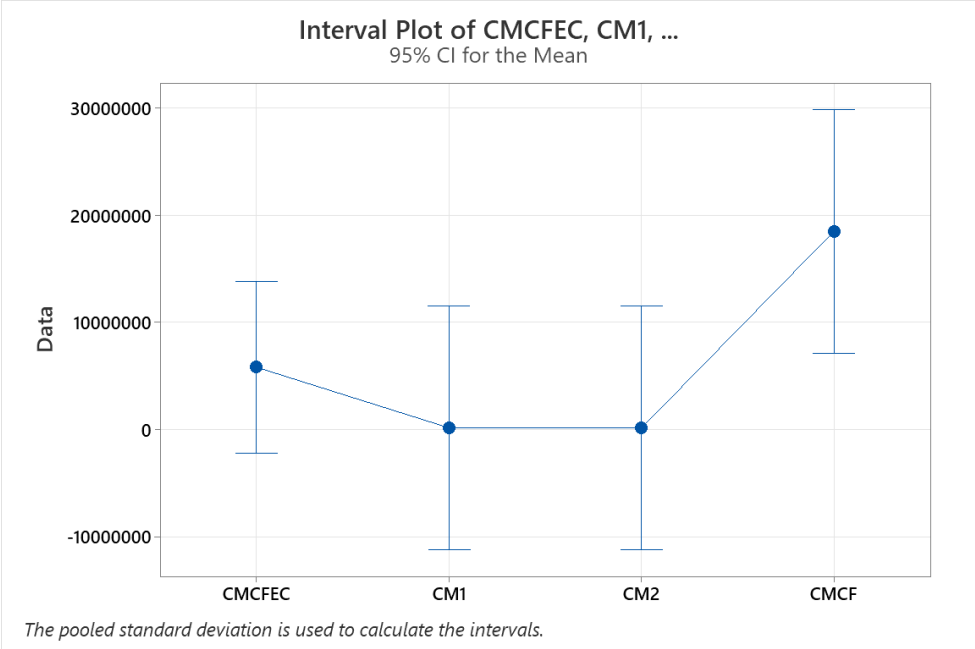

A-3: Confidence Intervals for Vimentin Expression

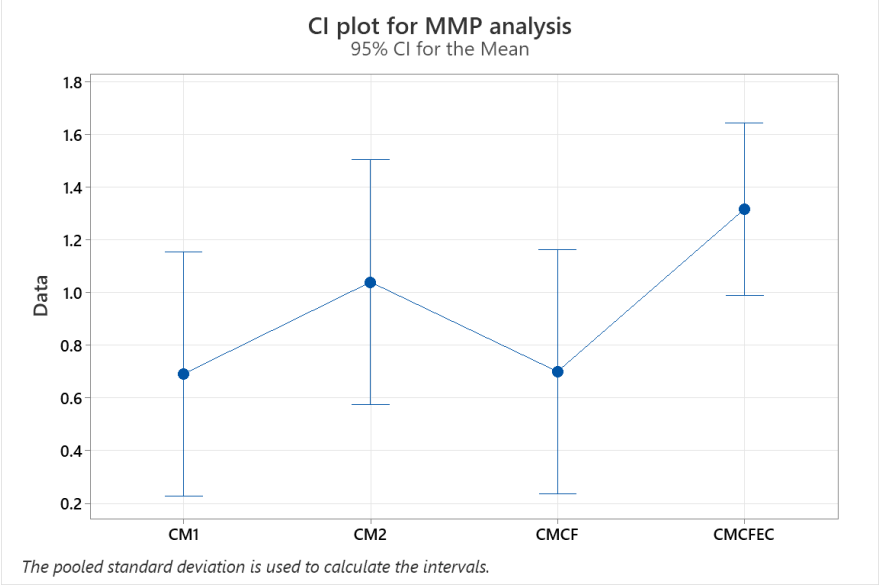

A-4: Confidence Intervals for MMP analysis

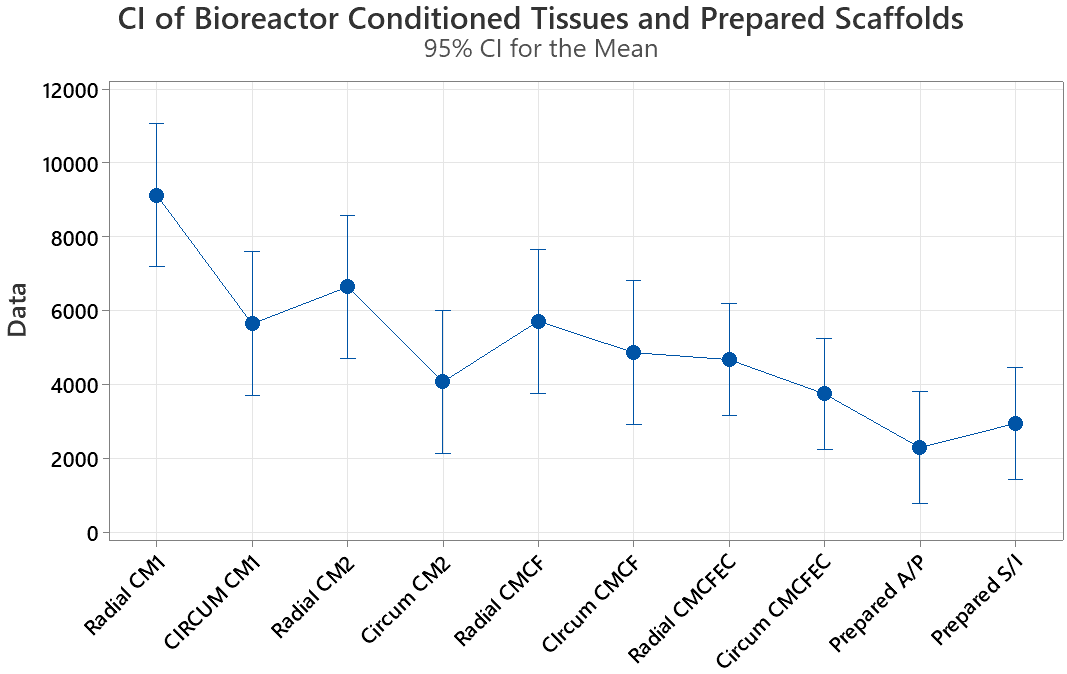

The pooled standard deviation is used to calculate the intervals.

A-5: Confidence Intervals for Bioreactor and Scaffold Mechanics

References

1. Rehman, I. and A. Rehman, *Anatomy, Thorax, Heart*, in *StatPearls*. 2022: Treasure Island (FL).
2. Iqbal, A.M. and S.F. Jamal, *Essential Hypertension*, in *StatPearls*. 2022: Treasure Island (FL).
3. Foale, R., et al., *Echocardiographic measurement of the normal adult right ventricle.* Br Heart J, 1986. **56**(1): p. 33-44.
4. Walpot, J., et al., *Left Ventricular Mid-Diastolic Wall Thickness: Normal Values for Coronary CT Angiography.* Radiol Cardiothorac Imaging, 2019. **1**(5): p. e190034.
5. Iaizzo, P.A., ed. *Handbook of the cardiac anatomy, physiology, and devices, third edition*. 2015.
6. Saremi, F., et al., *Fibrous Skeleton of the Heart: Anatomic Overview and Evaluation of Pathologic Conditions with CT and MR Imaging.* Radiographics, 2017. **37**(5): p. 1330-1351.
7. Zhou, P. and W.T. Pu, *Recounting cardiac cellular composition*. 2016.
8. Litvinukova, M., et al., *Cells of the adult human heart.* Nature, 2020. **588**(7838): p. 466-472.
9. Guo, Y. and W.T. Pu, *Cardiomyocyte Maturation: New Phase in Development.* Circ Res, 2020. **126**(8): p. 1086-1106.
10. Lampe, P.D. and A.F. Lau, *The effects of connexin phosphorylation on gap junctional communication.* Int J Biochem Cell Biol, 2004. **36**(7): p. 1171-86.

11. Periasamy, M. and A. Kalyanasundaram, *SERCA pump isoforms: their role in calcium transport and disease.* Muscle Nerve, 2007. **35**(4): p. 430-42.

12. Nakao, K., et al., *Myosin heavy chain gene expression in human heart failure.* J Clin Invest, 1997. **100**(9): p. 2362-70.

13. Sasse, S., et al., *Troponin I gene expression during human cardiac development and in end-stage heart failure.* Circ Res, 1993. **72**(5): p. 932-8.

14. Tan, C.M.J. and A.J. Lewandowski, *The Transitional Heart: From Early Embryonic and Fetal Development to Neonatal Life.* Fetal Diagn Ther, 2020. **47**(5): p. 373-386.

15. Karbassi, E., et al., *Cardiomyocyte maturation: advances in knowledge and implications for regenerative medicine.* Nat Rev Cardiol, 2020. **17**(6): p. 341-359.

16. Bergmann, O., et al., *Evidence for cardiomyocyte renewal in humans.* Science, 2009. **324**(5923): p. 98-102.

17. Hashmi, S. and H.R. Ahmad, *Molecular switch model for cardiomyocyte proliferation.* Cell Regen, 2019. **8**(1): p. 12-20.

18. Harvey, P.A. and L.A. Leinwand, *The cell biology of disease: cellular mechanisms of cardiomyopathy.* J Cell Biol, 2011. **194**(3): p. 355-65.

19. Li, M.X. and P.M. Hwang, *Structure and function of cardiac troponin C (TNNC1): Implications for heart failure, cardiomyopathies, and troponin modulating drugs.* Gene, 2015. **571**(2): p. 153-66.

20. Ghosh, S., et al., *Insights on the impact of mitochondrial organisation on bioenergetics in high-resolution computational models of cardiac cell architecture.* PLoS Comput Biol, 2018. **14**(12): p. e1006640.

21. Ivey, M.J. and M.D. Tallquist, *Defining the Cardiac Fibroblast.* Circ J, 2016. **80**(11): p. 2269-2276.

22. Fan, D., et al., *Cardiac fibroblasts, fibrosis and extracellular matrix remodeling in heart disease*. 2012.

23. Chen, W. and N.G. Frangogiannis, *Fibroblasts in post-infarction inflammation and cardiac repair*. 2013.

24. Tallquist, M.D. and J.D. Molkentin, *Redefining the identity of cardiac fibroblasts*. 2017.

25. Nakashima, Y., T.N. Wight, and K. Sueishi, *Early atherosclerosis in humans: role of diffuse intimal thickening and extracellular matrix proteoglycans.* Cardiovasc Res, 2008. **79**(1): p. 14-23.

26. Brutsaert, D.L., *Cardiac endothelial-myocardial signaling: Its role in cardiac growth, contractile performance, and rhythmicity*. 2003.

27. Mitchell, J.A., et al., *Role of nitric oxide and prostacyclin as vasoactive hormones released by the endothelium.* Exp Physiol, 2008. **93**(1): p. 141-7.

28. Hsieh, P.C., et al., *Endothelial-cardiomyocyte interactions in cardiac development and repair.* Annu Rev Physiol, 2006. **68**: p. 51-66.

29. Rienks, M., et al., *Myocardial extracellular matrix: an ever-changing and diverse entity.* Circ Res, 2014. **114**(5): p. 872-88.

30. Shoulders, M.D. and R.T. Raines, *Collagen structure and stability.* Annu Rev Biochem, 2009. **78**: p. 929-58.

31. Wang, K., X. Meng, and Z. Guo, *Elastin Structure, Synthesis, Regulatory Mechanism and Relationship With Cardiovascular Diseases.* Front Cell Dev Biol, 2021. **9**: p. 596702.

32. Casale, J. and J.S. Crane, *Biochemistry, Glycosaminoglycans*, in *StatPearls*. 2022: Treasure Island (FL).

33. Zhao, X., et al., *Left Ventricular Wall Stress Is Sensitive Marker of Hypertrophic Cardiomyopathy With Preserved Ejection Fraction.* Front Physiol, 2018. **9**: p. 250.

34. Badeer, H.S., *Contractile Tension in the Myocardium.* Am Heart J, 1963. **66**: p. 432-4.

35. Gsell, M.A.F., et al., *Assessment of wall stresses and mechanical heart power in the left ventricle: Finite element modeling versus Laplace analysis.* Int J Numer Method Biomed Eng, 2018. **34**(12): p. e3147.

36. Emig, R., et al., *Passive myocardial mechanical properties: meaning, measurement, models.* Biophys Rev, 2021. **13**(5): p. 587-610.

37. Huyer, L.D., et al., *Biomaterial based cardiac tissue engineering and its applications.* Biomed Mater, 2015. **10**(3): p. 034004.

38. Buckberg, G., et al., *Ventricular torsion and untwisting: further insights into mechanics and timing interdependence: a viewpoint.* Echocardiography, 2011. **28**(7): p. 782-804.

39. Biswas, M., et al., *Two- and three-dimensional speckle tracking echocardiography: clinical applications and future directions.* Echocardiography, 2013. **30**(1): p. 88-105.

40. Buckberg, G., et al., *Cardiac mechanics revisited: the relationship of cardiac architecture to ventricular function.* Circulation, 2008. **118**(24): p. 2571-87.

41. Salvo, G.D., et al., *Strain Echocardiography and Myocardial Mechanics: From Basics to Clinical Applications.* J Cardiovasc Echogr, 2015. **25**(1): p. 1-8.

42. Nerbonne, J.M. and R.S. Kass, *Molecular physiology of cardiac repolarization.* Physiol Rev, 2005. **85**(4): p. 1205-53.

43. Klabunde, R.E., *Cardiac electrophysiology: normal and ischemic ionic currents and the ECG.* Adv Physiol Educ, 2017. **41**(1): p. 29-37.

44. Lin, J. and J.P. Keener, *Ephaptic coupling in cardiac myocytes.* IEEE Trans Biomed Eng, 2013. **60**(2): p. 576-82.

45. Fruchart, J.C., et al., *New risk factors for atherosclerosis and patient risk assessment.* Circulation, 2004. **109**(23 Suppl 1): p. III15-9.

46. Taimor, G., et al., *Induction of necrosis but not apoptosis after anoxia and reoxygenation in isolated adult cardiomyocytes of rat.* Cardiovasc Res, 1999. **41**(1): p. 147-56.

47. Kumar, V., A.K. Abbas, and J.C. Aster, *Robbins & Cotran Pathologic Basis of Disease*. 2014: Elsevier Health Sciences.

48. Robbins, S.L., V. Kumar, and R.S. Cotran, *Robbins and Cotran pathologic basis of disease*. 8th ed. 2010, Philadelphia, PA: Saunders/Elsevier. xiv, 1450 p.

49. Wajant, H. and D. Siegmund, *TNFR1 and TNFR2 in the Control of the Life and Death Balance of Macrophages.* Front Cell Dev Biol, 2019. **7**: p. 91.

50. Volpe, E., et al., *Fas-Fas Ligand: Checkpoint of T Cell Functions in Multiple Sclerosis.* Front Immunol, 2016. **7**: p. 382.

51. Yellon, D.M. and D.J. Hausenloy, *Myocardial Reperfusion Injury.* New England Journal of Medicine, 2007.

52. de Oliveira, S., E.E. Rosowski, and A. Huttenlocher, *Neutrophil migration in infection and wound repair: going forward in reverse.* Nat Rev Immunol, 2016. **16**(6): p. 378-91.

53. Saadat, S., et al., *Pivotal Role of TGF-beta/Smad Signaling in Cardiac Fibrosis: Non-coding RNAs as Effectual Players.* Front Cardiovasc Med, 2020. **7**: p. 588347.

54. Bochaton-Piallat, M.L., G. Gabbiani, and B. Hinz, *The myofibroblast in wound healing and fibrosis: Answered and unanswered questions*. 2016.

55. Travers, J.G., et al., *Cardiac Fibrosis: The Fibroblast Awakens.* Circ Res, 2016. **118**(6): p. 1021-40.

56. Paulus, W.J. and M.R. Zile, *From Systemic Inflammation to Myocardial Fibrosis: The Heart Failure With Preserved Ejection Fraction Paradigm Revisited.* Circ Res, 2021. **128**(10): p. 1451-1467.

57. Ahmed, I. and S. Yandrapalli, *Internal Mammary Artery Bypass*, in *StatPearls*. 2022: Treasure Island (FL).

58. Tam, D.Y., et al., *Long-Term Survival After Surgical or Percutaneous Revascularization in Patients With Diabetes and Multivessel Coronary Disease.* Journal of the American College of Cardiology, 2020. **76**(10): p. 1153-1164.

59. Jeong, D., et al., *Matricellular Protein CCN5 Reverses Established Cardiac Fibrosis.* J Am Coll Cardiol, 2016. **67**(13): p. 1556-1568.

60. Tao, H., et al., *Histone deacetylases in cardiac fibrosis: current perspectives for therapy.* Cell Signal, 2014. **26**(3): p. 521-7.

61. Du, X.J., et al., *Reversal of cardiac fibrosis and related dysfunction by relaxin.* Ann N Y Acad Sci, 2009. **1160**: p. 278-84.

62. Shanmugam, G. and I.S. Ali, *Surgical Ventricular Restoration: An Operation to Reverse Remodeling - Clinical Application (Part II).* Curr Cardiol Rev, 2009. **5**(4): p. 350-9.

63. Starling, R.C., et al., *Sustained benefits of the CorCap Cardiac Support Device on left ventricular remodeling: three year follow-up results from the Acorn clinical trial.* Ann Thorac Surg, 2007. **84**(4): p. 1236-42.

64. Ghanta, R.K., et al., *Adjustable, physiological ventricular restraint improves left ventricular mechanics and reduces dilatation in an ovine model of chronic heart failure.* Circulation, 2007. **115**(10): p. 1201-10.

65. Wilhelm, M.J., *Long-term outcome following heart transplantation: Current perspective.* Journal of Thoracic Disease, 2015. **7**(3).

66. Sliwa, K. and P. Zilla, *50th Anniversary of the first Human Heart Transplant-How is it seen today?* Eur Heart J, 2017. **38**(46): p. 3402-3404.

67. Dharmavaram, N., et al., *National Trends in Heart Donor Usage Rates: Are We Efficiently Transplanting More Hearts?* J Am Heart Assoc, 2021. **10**(15): p. e019655.

68. Bottle, A., et al., *Five-year outcomes following left ventricular assist device implantation in England.* Open Heart, 2021. **8**(1).

69. Health Quality, O., *Left Ventricular Assist Devices for Destination Therapy: A Health Technology Assessment.* Ont Health Technol Assess Ser, 2016. **16**(3): p. 1-60.

70. Varshney, A.S., et al., *Trends and Outcomes of Left Ventricular Assist Device Therapy.* Journal of the American College of Cardiology, 2022. **79**(11): p. 1092-1107.

71. Fernandez-Ruiz, I., *Breakthrough in heart xenotransplantation.* Nat Rev Cardiol, 2019. **16**(2): p. 69.

72. Langer, R. and J.P. Vacanti, *Tissue engineering.* Science, 1993. **260**(5110): p. 920-6.

73. Weissman, I.L. and J.A. Shizuru, *The origins of the identification and isolation of hematopoietic stem cells, and their capability to induce donor-specific transplantation tolerance and treat autoimmune diseases.* Blood, 2008. **112**(9): p. 3543-53.

74. Eguizabal, C., et al., *Two decades of embryonic stem cells: a historical overview.* Hum Reprod Open, 2019. **2019**(1): p. hoy024.

75. Wang, F. and J. Guan, *Cellular cardiomyoplasty and cardiac tissue engineering for myocardial therapy.* Adv Drug Deliv Rev, 2010. **62**(7-8): p. 784-97.

76. Takahashi, K. and S. Yamanaka, *Induction of pluripotent stem cells from mouse embryonic and adult fibroblast cultures by defined factors.* Cell, 2006. **126**(4): p. 663-76.

77. Peischard, S., et al., *From iPSC towards cardiac tissue-a road under construction.* Pflugers Arch, 2017. **469**(10): p. 1233-1243.

78. Bylund, J.B., et al., *Coordinated Proliferation and Differentiation of Human-Induced Pluripotent Stem Cell-Derived Cardiac Progenitor Cells Depend on Bone Morphogenetic Protein Signaling Regulation by GREMLIN 2.* Stem Cells Dev, 2017. **26**(9): p. 678-693.

79. Nusse, R., et al., *Wnt signaling and stem cell control.* Cold Spring Harb Symp Quant Biol, 2008. **73**: p. 59-66.

80. Moschouris, K., N. Firoozi, and Y. Kang, *The application of cell sheet engineering in the vascularization of tissue regeneration.* Regen Med, 2016. **11**(6): p. 559-70.

81. Matsuura, K., et al., *Cell sheet approach for tissue engineering and regenerative medicine.* J Control Release, 2014. **190**: p. 228-39.

82. Yang, J., et al., *Cell sheet engineering: recreating tissues without biodegradable scaffolds.* Biomaterials, 2005. **26**(33): p. 6415-22.

83. O'Brien, F.J., *Biomaterials & scaffolds for tissue engineering*. 2011.

84. Loh, Q.L. and C. Choong, *Three-dimensional scaffolds for tissue engineering applications: role of porosity and pore size.* Tissue Eng Part B Rev, 2013. **19**(6): p. 485-502.

85. Gorna, K. and S. Gogolewski, *Biodegradable porous polyurethane scaffolds for tissue repair and regeneration.* J Biomed Mater Res A, 2006. **79**(1): p. 128-38.

86. Gui, L., et al., *Development of novel biodegradable polymer scaffolds for vascular tissue engineering.* Tissue Eng Part A, 2011. **17**(9-10): p. 1191-200.

87. Gregor, A., et al., *Designing of PLA scaffolds for bone tissue replacement fabricated by ordinary commercial 3D printer.* J Biol Eng, 2017. **11**: p. 31.

88. Suh, T.C., A.Y. Amanah, and J.M. Gluck, *Electrospun Scaffolds and Induced Pluripotent Stem Cell-Derived Cardiomyocytes for Cardiac Tissue Engineering Applications.* Bioengineering (Basel), 2020. **7**(3).

89. Gilpin, A. and Y. Yang, *Decellularization Strategies for Regenerative Medicine: From Processing Techniques to Applications.* Biomed Res Int, 2017. **2017**: p. 9831534.

90. Guyette, J.P., et al., *Perfusion decellularization of whole organs.* Nat Protoc, 2014. **9**(6): p. 1451-68.

91. Vasanthan, V., et al., *The CorMatrix Cor PATCH for epicardial infarct repair.* Future Cardiol, 2021. **17**(8): p. 1297-1305.

92. Nelson, J.S., et al., *Evaluation of Explanted CorMatrix Intracardiac Patches in Children With Congenital Heart Disease.* Ann Thorac Surg, 2016. **102**(4): p. 1329-35.

93. Nummi, A., et al., *Epicardial Transplantation of Autologous Cardiac Micrografts During Coronary Artery Bypass Surgery.* Front Cardiovasc Med, 2021. **8**: p. 726889.

94. Li, J., et al., *Recent advances in bioprinting techniques: approaches, applications and future prospects.* J Transl Med, 2016. **14**: p. 271.

95. Pati, F., et al., *Printing three-dimensional tissue analogues with decellularized extracellular matrix bioink.* Nat Commun, 2014. **5**: p. 3935.

96. GhavamiNejad, A., et al., *Crosslinking Strategies for 3D Bioprinting of Polymeric Hydrogels.* Small, 2020. **16**(35): p. e2002931.

97. Guyette, J.P., et al., *Bioengineering Human Myocardium on Native Extracellular Matrix.* Circ Res, 2016. **118**(1): p. 56-72.

98. Wang, B., et al., *Fabrication of cardiac patch with decellularized porcine myocardial scaffold and bone marrow mononuclear cells.* J Biomed Mater Res A, 2010. **94**(4): p. 1100-10.

99. Schulte, J.B., A. Simionescu, and D.T. Simionescu, *The acellular myocardial flap: A novel extracellular matrix scaffold enriched with patent microvascular networks and biocompatible cell niches.* Tissue Engineering - Part C: Methods, 2013. **19**(7).

100. Bhatia, S. and T. Bera, *Chapter 7 - Classical and Nonclassical Techniques for Secondary Metabolite Production in Plant Cell Culture*, in *Modern Applications of Plant Biotechnology in Pharmaceutical Sciences*, S. Bhatia, et al., Editors. 2015, Academic Press: Boston. p. 231-291.

101. Plunkett, N. and F.J. O'Brien, *Bioreactors in tissue engineering.* Technol Health Care, 2011. **19**(1): p. 55-69.

102. Paez-Mayorga, J., et al., *Bioreactors for Cardiac Tissue Engineering*. 2019.

103. Marsh, S.e.a., *Dynamic Bioreactor Model to Mimic Early Cardia Fibrosis in Diabetes.* Journal of Mechanics in Medicine and Biology, 2021. **Vol .21**(No. 06, 2150047).

104. Stoppel, W.L., D.L. Kaplan, and L.D. Black, *Electrical and mechanical stimulation of cardiac cells and tissue constructs*. 2016.

105. Baumgartner, S., et al., *Electrophysiological and morphological maturation of murine fetal cardiomyocytes during electrical stimulation in vitro.* J Cardiovasc Pharmacol Ther, 2015. **20**(1): p. 104-12.

106. Yue, L., J. Xie, and S. Nattel, *Molecular determinants of cardiac fibroblast electrical function and therapeutic implications for atrial fibrillation.* Cardiovasc Res, 2011. **89**(4): p. 744-53.

107. Tandon, N., et al., *Design of electrical stimulation bioreactors for cardiac tissue engineering.* Annu Int Conf IEEE Eng Med Biol Soc, 2008. **2008**: p. 3594-7.

108. Tandon, N., et al., *Electrical stimulation systems for cardiac tissue engineering.* Nat Protoc, 2009. **4**(2): p. 155-73.

109. Berger, H.J., et al., *Continual electric field stimulation preserves contractile function of adult ventricular myocytes in primary culture.* Am J Physiol, 1994. **266**(1 Pt 2): p. H341-9.

110. Radisic, M., et al., *Cardiac tissue engineering using perfusion bioreactor systems.* Nat Protoc, 2008. **3**(4): p. 719-38.

111. Weymann, A., et al., *Bioartificial heart: a human-sized porcine model--the way ahead.* PLoS One, 2014. **9**(11): p. e111591.

112. Sakaguchi, K., et al., *In vitro engineering of vascularized tissue surrogates.* Sci Rep, 2013. **3**: p. 1316.

113. Virani, S.S., et al., *Heart disease and stroke statistics—2020 update: A report from the American Heart Association*. 2020.

114. Heidenreich, P.A., et al., *Forecasting the future of cardiovascular disease in the United States: A policy statement from the American Heart Association.* Circulation, 2011.

115. Mechanic, O.J., M. Gavin, and S.A. Grossman, *Acute Myocardial Infarction*, in *StatPearls*. 2022: Treasure Island (FL).

116. van den Borne, S.W., et al., *Myocardial remodeling after infarction: the role of myofibroblasts.* Nat Rev Cardiol, 2010. **7**(1): p. 30-7.

117. Voorhees, A.P., et al., *Building a better infarct: Modulation of collagen cross-linking to increase infarct stiffness and reduce left ventricular dilation post-myocardial infarction.* J Mol Cell Cardiol, 2015. **85**: p. 229-39.

118. Richardson, W.J., et al., *Physiological implications of myocardial scar structure.* Comprehensive Physiology, 2015.

119. Rockey, D.C., P.D. Bell, and J.A. Hill, *Fibrosis--A Common Pathway to Organ Injury and Failure.* N Engl J Med, 2015. **373**(1): p. 96.

120. Collins, J.M. and B. Russell, *Stem cell therapy for cardiac repair.* J Cardiovasc Nurs, 2009. **24**(2): p. 93-7.

121. Orlic, D., et al., *Bone marrow cells regenerate infarcted myocardium.* Nature, 2001. **410**(6829): p. 701-5.

122. Sharif, F., J. Bartunek, and M. Vanderheyden, *Adult stem cells in the treatment of acute myocardial infarction.* Catheter Cardiovasc Interv, 2011. **77**(1): p. 72-83.

123. Thomlinson, R.H. and L.H. Gray, *The histological structure of some human lung cancers and the possible implications for radiotherapy.* Br J Cancer, 1955. **9**(4): p. 539-49.

124. Alonzo, M., et al., *3D Bioprinting of cardiac tissue and cardiac stem cell therapy.* Transl Res, 2019. **211**: p. 64-83.

125. Roche, C.D., et al., *Current challenges in three-dimensional bioprinting heart tissues for cardiac surgery.* Eur J Cardiothorac Surg, 2020. **58**(3): p. 500-510.

126. Mei, X. and K. Cheng, *Recent Development in Therapeutic Cardiac Patches.* Front Cardiovasc Med, 2020. **7**: p. 610364.

127. Muschler, G.F., C. Nakamoto, and L.G. Griffith, *Engineering principles of clinical cell-based tissue engineering.* J Bone Joint Surg Am, 2004. **86**(7): p. 1541-58.

128. Ribeiro, A.J., et al., *Contractility of single cardiomyocytes differentiated from pluripotent stem cells depends on physiological shape and substrate stiffness.* Proc Natl Acad Sci U S A, 2015. **112**(41): p. 12705-10.

129. Crick, S.J., et al., *Anatomy of the pig heart: comparisons with normal human cardiac structure.* J Anat, 1998. **193 (Pt 1)**: p. 105-19.

130. Remlinger, N.T., P.D. Wearden, and T.W. Gilbert, *Procedure for decellularization of porcine heart by retrograde coronary perfusion.* J Vis Exp, 2012(70): p. e50059.

131. Brondijk, T.H., et al., *Implications for collagen I chain registry from the structure of the collagen von Willebrand factor A3 domain complex.* Proc Natl Acad Sci U S A, 2012. **109**(14): p. 5253-8.

132. Radziwon-Balicka, A., et al., *Differential eNOS-signalling by platelet subpopulations regulates adhesion and aggregation.* Cardiovasc Res, 2017. **113**(14): p. 1719-1731.

133. Takaza, M., et al., *The anisotropic mechanical behaviour of passive skeletal muscle tissue subjected to large tensile strain.* J Mech Behav Biomed Mater, 2013. **17**: p. 209-20.

134. Jacot, J.G., J.C. Martin, and D.L. Hunt, *Mechanobiology of cardiomyocyte development.* J Biomech, 2010. **43**(1): p. 93-8.

135. Hou, D., et al., *Radiolabeled cell distribution after intramyocardial, intracoronary, and interstitial retrograde coronary venous delivery: implications for current clinical trials.* Circulation, 2005. **112**(9 Suppl): p. I150-6.

136. Civitarese, R.A., et al., *Role of integrins in mediating cardiac fibroblast-cardiomyocyte cross talk: a dynamic relationship in cardiac biology and pathophysiology.* Basic Res Cardiol, 2017. **112**(1): p. 6.

137. Webb, A.H., et al., *Inhibition of MMP-2 and MMP-9 decreases cellular migration, and angiogenesis in in vitro models of retinoblastoma.* BMC Cancer, 2017. **17**(1): p. 434.

138. Yabluchanskiy, A., et al., *Matrix metalloproteinase-9: Many shades of function in cardiovascular disease.* Physiology (Bethesda), 2013. **28**(6): p. 391-403.

139. Gouarderes, S., et al., *Pulsed Electric Fields Induce Extracellular Matrix Remodeling through Matrix Metalloproteinases Activation and Decreased Collagen Production.* J Invest Dermatol, 2022. **142**(5): p. 1326-1337 e9.